P53 GENES ACT TO RESTRAIN MOBILE ELEMENTS

APPROVED BY SUPERVISORY COMMITTEE

John M. Abrams, Ph.D. (Mentor)

James F. Amatruda, M.D, Ph.D. (Chair)

Helen Hobbs, M.D.

Sean Morrison, Ph.D.

DEDICATION

This is dedicated to my parents, Heide and Larry Butler.

ACKNOWLEDGEMENTS

First and foremost, I thank my mentor, Dr. John M. Abrams. You helped me find my voice. You are an incredible mentor and brilliant scientist. I admire your intuition, patience, and love of science and I am lucky to have been mentored by you.

I also thank my thesis committee members: Dr. James Amatruda, Dr. Helen Hobbs, and Dr. Sean Morrison. I am grateful for your continued guidance. You have pushed me to become a better scientist. I also thank the many collaborators for teaching me new approaches to a problem. These people include: Drs Michael Buszczak, James Amatruda, Dinesh Rakheja, John V. Moran, Sarah Comerford, and Bob Hammer.

In addition, I acknowledge former and current members of the Abrams lab. You make science fun. These people include: Wan-Jin Lu, Nikki Link, Melissa O'Neal, Alex D'Brot, Paula Kurtz, Amanda Jones, Po Chen, Sam Glaves, Erin Regan, Gianell Garcia-Hughes, Daniew Hwang, Corey Timmermann and Jessica Alatorre.

I thank my family for their encouragement and loving support. You inspire me each and every day.

Finally, I thank my one and only: Layne. You are my rock and constant source of laughter and happiness.

P53 GENES ACT TO RESTRAIN MOBILE ELEMENTS

by

ANNIKA WYLIE

DISSERTATION / THESIS

Presented to the Faculty of the Graduate School of Biomedical Sciences

The University of Texas Southwestern Medical Center at Dallas

In Partial Fulfillment of the Requirements

For the Degree of

DOCTOR OF PHILOSOPHY

The University of Texas Southwestern Medical Center at Dallas

Dallas, Texas

December, 2015

P53 GENES ACT TO RESTRAIN MOBILE ELEMENTS

Publication No._____

Annika Wylie, Ph.D.

The University of Texas Southwestern Medical Center at Dallas, Graduation Year

John M. Abrams, Ph.D.

Oncogenic stress provokes tumor suppression by p53 but the extent to which this regulatory axis is conserved remains unknown. Using a biosensor to visualize p53 action, we find that *Drosophila* p53 is selectively active in gonadal stem cells after exposure to stressors that destabilize the genome. Similar p53 activity occurred in hyperplastic growths that were triggered either by the Ras^{V12} oncoprotein or by failed differentiation programs. In a model of transient sterility, p53 was required for the recovery of fertility after stress, and entry into the cell cycle was delayed in $p53^{-}$ stem cells. Together, these observations establish that the stem cell compartment of the *Drosophila* germline is selectively licensed for stress-induced activation of the p53

regulatory network. Furthermore, the findings uncover ancestral links between p53 and aberrant proliferation that are independent of DNA breaks and predate evolution of the ARF/Mdm2 axis. While exploring the role of p53 in this context, we made a series of observations that justify a comprehensive examination of the relationship between p53 and transposon biology. Using *Drosophila*, zebrafish, and mouse models, we found that p53 functions to restrict the activity of retrotransposons. Furthermore, *Drosophila* p53 genetically interacted with components of the piRNA pathway and, in complementation studies, normal human p53 alleles restrained these mobile elements, but mutant p53 alleles from cancer patients could not. Consistent with these results, we also found patterns of unrestrained retrotransposons in p53-driven human cancers. Together, these observations indicate that ancestral functions of p53 operate through conserved mechanisms to suppress retrotransposons. Furthermore, since human p53 mutants are disabled for this activity, our findings raise the possibility that p53 mitigates oncogenic disease, in part, by restricting retrotransposon mobility.

TABLE OF CONTENTS

PRIOR PUBLICATIONS

1. Wylie, A., Fleming, J.A., Whitener, A. and Lekven, A.C. (2014) Post-transcriptional regulation of wnt8a is essential to zebrafish axis development. **Developmental Biology** 386: 53–63.
2. Wylie, A., Lu, WJ., D'Brot, A., Buszczak, M. and Abrams, J.M. (2014) p53 activity is selectively licensed in the *Drosophila* stem cell compartment. **eLife**: 3, e01530.
3. Wylie, A., Jones, A., D'Brot, A., Lu, WJ., Kurtz, P. Moran, J.V., Rakheja, D., Chen, K., Robert E. Hammer, Sarah Comerford, Amatruda, J.F. and Abrams, J.M. (2015) p53 Genes Act to Restrain Mobile Elements. **Genes and Development** (accepted manuscript 2015)

LIST OF FIGURES

LIST OF TABLES

LIST OF DEFINITIONS

17kT – 17K T antigen

ARE – Antioxidant Response Element

ARF – Alternate Reading Frame

Aub – Aubergine

ATR – Ataxia Telangiectasia and Rad3 related

bam – bag of marbles

BMP – bone morphogenic protein

BrdU – 5-Bromo-2'-deoxyuridine

Caspase – Cysteinyl aspartate-specific protease

CB – cystoblast

Chk2 – Checkpoint Kinase 2

Cuff – cutoff

CycE – Cyclin E

cyt – cytoplasmic

DBD – DNA binding domain

ddPCR – droplet digital polymerase chain reaction

DNA – Deoxy-ribo nucleic acid

Dp53 – *Drosophila* p53

DSBs – Double stranded DNA breaks (DSBs)

EGFP – Enhanced Green Fluorescent Protein

FBS – Fetile Bovine Serum

FISH – Fluorescent in situ hybridization

GB – gonioblasts

GFP – green fluorescent protein

GSCs – germline stem cells

HCC – hepatocellularcarninoma

Hp53 – Human p53

hr – hour

IHC – immunohistochemistry

IAP – intracisternal A particle

iPSCs – induced pluripotent stem cells

IR – ionizing radiation

krad – kilo-rad

ng – nanogram

L1_Hs – Human Specific Long interspersed nuclear element 1

LINE-1 – long interspersed nuclear element 1

nL – nanoLiter

Lsd1 – lysine-specific demethylase 1

LT – large T antigen

LTR – long terminal repeat

Mdm2 – transformed mouse 3T3 cell double minute 2

nls – nuclear localization signal

ORF – open reading frame

piRNA – piwi-associated RNA piRNA

pH2Av – phosphoHistone 2.Av

PIWI – element induced wimpy testis

qRT-PCR – quantitative reverse transcriptase polymerase chain reaction

Rb – Retinoblastoma

RNA – ribonucleic acid

RNAi – RNA interference

RNAseq – ribonucleic acid sequencing

ROS – reactive oxygen species

RT-PCR – reverse transcriptase polymerase chain reaction

SV40 – Simian Virus 40

TCGA – Cancer Genome Atlas (TCGA)

TP53 – Tumor suppressor p53

UAS – upstream activating sequence

WT – Wild Type

Chapter 1:

Ancestral p53 functions: a route to understanding p53 cancer mysteries

The p53 tumor suppressor is mutated in over half of human cancers. This extensively studied protein is a transcription factor that is acutely responsive to stress and activates effector genes to mediate appropriate responses [1-3]. Despite a large body of literature describing p53 functions, many mysteries remain. This chapter provides a brief review of the major questions in the p53 field and how ancestral p53 functions are a route to uncovering the answers.

A p53 mystery: How does p53 suppress tumor formation?

The precise mechanism for how p53 suppresses tumor formation is not known. Underscoring this point, no single target – or combination of targets - has replicated p53 cancer phenotypes when genetically tested in mice. Conventionally it is thought that p53 restricts oncogenesis by promoting apoptosis through transcriptional induction of Puma and Noxa, or by promoting cell cycle arrest through induction of p21 (Figure 1-1). However, whereas p53 null mice are highly tumor prone by 6 months of age, p21 deficient mice remain tumor free for over 16 months [4,5]. Similarly, neither *Puma*$^{-/-}$ nor *Noxa*$^{-/-}$ mice develop tumors[6]. To test whether these three effectors collaborate to prevent oncogenesis, *Puma*$^{-/-}$ *; Noxa*$^{-/-}$*; p21*$^{-/-}$ triple knockout mice were tested for tumor development. Strikingly, these mice were tumor free, despite exhibiting severe

defects in cell cycle arrest, apoptosis, and senescence (Figure 1-1) [7]. These studies indicate that the tumor suppressive effects of p53 remain incompletely defined (Figure 1-1).

A p53 mystery: Gain of Function Activities in Human Cancers

In human cancers, tumor suppressor genes normally have loss of function mutations that involve deletions or premature stop codons. However, the majority of TP53 mutations in human cancers produce missense alleles with single amino-acid changes [8].These missense mutations are predominantly found in the p53 DNA binding domain (DBD) and occur at 'hotspot' residues suggesting a strong selective advantage [8]. These residues are normally involved in making contacts with the DNA or support the structure of the DNA binding surface [8]. *p53* knockout mice are highly cancer prone but the tumor spectrum is largely restricted to lymphomas and occasional sarcomas but carcinomas are rare in p53 null mice [4,9]. Thus, to model p53 hotspot mutations in human cancers, several labs have generated mouse strains with missense mutations at the endogenous p53 locus [10,11]. Unlike the p53 null mice, mice harboring p53 'hotspot' mutations commonly develop invasive and metastatic carcinomas, thus mimicking the tumor spectrum in human cancer patients. A hallmark of cancer is the nuclear stabilization and accumulation of mutant p53 protein [12]. Surprisingly, in mice harboring p53 missense alleles, the p53 protein is undetected in normal tissue [10,11]. Instead, p53 protein accumulates in transformed tissue and

correlates with more malignant histology in both human cancers and mouse models [10,11]. These data suggest that the p53 missense proteins are not inherently more stable than WT p53 protein and that stabilization is likely due to secondary events associated with oncogenesis. Therefore, genetic studies in mouse models provide strong evidence that p53 missense mutations in human cancers confer not only a loss of function but also a 'gain of function' activity. However, the precise 'gain of function' activity of p53 cancer alleles remains elusive.

To summarize, despite extensive research for over 30 years, we still do not fully understand how p53 suppresses tumors or how p53 cancer alleles confer gain of function activities. To develop appropriate cancer therapies, these questions need to be answered.

p53 genes are conserved across the animal kingdom

The p53 gene family is highly conserved among vertebrates and invertebrate systems. Initially, it was thought that p53 arose during the emergence of multicellular organisms. However, p53 genes have recently been documented in unicellular protists (*Monosiga brevicollis*) [13], Furthermore, since p53 is present in short-lived organism these data demonstrate that the emergence of the p53 gene family preceded the need for tumor suppression. Since tumor suppressor functions were most likely co-opted from ancient p53 functions, elucidating the

primordial activities of p53 may help elucidate how p53 acts as a tumor suppressor [14]. The remainder of this chapter reviews the literature on ancient p53 genes.

Conserved Roles of p53 in Reproduction

p53 genes have been described in numerous organisms including sea anemones [15], clams [16], *C. elegans*, *Drosophila* [17-19], frogs [20], zebrafish [21] and mice [22]. One unifying theme among these diverse organisms is that p53 function is intimately linked to reproduction.

In *Drosophila*, the process of genetic recombination triggers p53 activity [23]. Specifically, meiotic double stranded breaks formed by the topoisomerase, Spo11, provoke p53 activity and this is evolutionarily conserved in mice [23]. Furthermore, $p53^{-/-}$ mice exhibit implantation defects [24], giant-cell degenerative syndrome in testis [25],and altered kinetics of gametogenesis [26]. Other organisms show similar p53 links to reproduction. For example the p53-like protein in *C. elegan*, CEP-1, mediates proper chrosomomal segregation during meiosis [27] Furthermore, CEP-1 is essential for radiation-induced apoptosis in germ cells which is similar to the *M. musculus* p53 gene [27,28]. The p53 like-protein in the sea anemone (nvp63) is highly expressed in the germ cells and promotes apoptosis in gametes after UV radiation [15]. Together, these data indicate p53 genes play a role in promoting germline integrity. Furthermore, these observations suggest

that p53 tumor suppressor functions may have been co-opted from activities related to meiotic recombination.

Dissertation Objectives:

The general aim of my thesis is to use the power of the *Drosophila* genetic model to uncover primordial functions of p53 and determine the extent to which these play roles in human health and disease. The following aims are presented in subsequent dissertation chapters:

1) Characterizing p53 functions in *Drosophila* Germline Stem Cells (GSCs)

Wan-Jin Lu, a previous graduate student in the lab, generated a p53 biosensor that allowed us to study p53 activity *in vivo*. Using this biosensor, she found that after Ionizing radiation, p53 was selectively activated in the GSCs despite widespread damage to the entire animal. When I joined the Abrams lab, my goal was to elucidate the function of p53 in GSCs and uncover p53 effectors required for this selectivity. This is presented in Chapter 2 of this dissertation.

2) Uncovering unappreciated functions of p53 as a tumor suppressor

While trying to understand p53 function in GSCs, I discovered that *Drosophila* p53 acts to restrain retrotransposons. This ancient p53 function is evolutionarily conserved and p53-driven tumors exhibit transposon dysregulation. This work is presented in Chapter 3 of this dissertation.

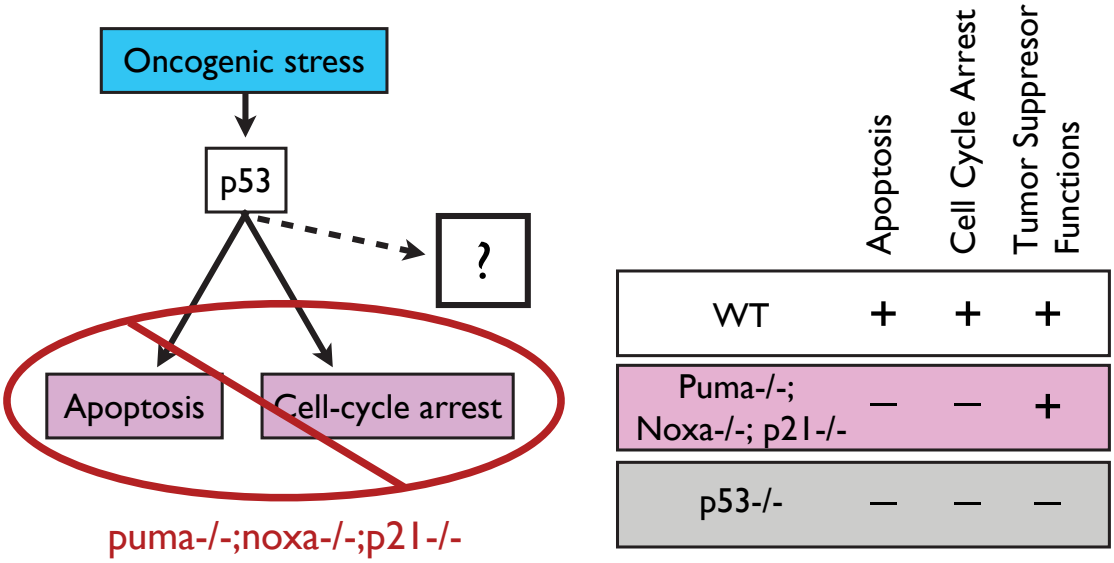

Figure 1-1 Combined removal of canonical p53 effectors does not account for tumor suppression in mice

Conventionally it is thought that p53 restricts oncogenesis by promoting apoptosis or cell cycle arrest through three canonical effectors: Puma, Noxa, and p21. $p53^{-/-}$ mice (grey bar) are highly tumor prone. Conversely, $Puma^{-/-}$;$Noxa^{-/-}$,$p21^{-/-}$ triple knockout mice (pink bar) retained tumor suppressor functions (+) despite severe defects in apoptosis and cell cycle arrest (-) [7]. These studies indicate that effectors of p53 remain to be discovered. This Figure was adapted from data presented in [7].

Chapter 2:

p53 activity is selectively licensed in the *Drosophila* stem cell compartment

This chapter is adapted from the following publication:

Annika Wylie*, Wan-Jin Lu*, Alejandro D'Brot, Michael Buszczak, and John M. Abrams. p53 activity is selectively licensed in the *Drosophila* stem cell compartment. *eLife* 3: e01530 (2014).

The initial discovery presented in this chapter was made by Wan-Jin Lu, a previous graduate student in the Abrams lab. When I joined the lab, Wan-Jin and I undertook a collaborative effort to extend and explore the implications of this discovery.

SUMMARY

Oncogenic stress provokes tumor suppression by p53 but the extent to which this regulatory axis is conserved remains unknown. Using a biosensor to visualize p53 action, we find that *Drosophila* p53 is selectively active in gonadal stem cells after exposure to stressors that destabilize the genome. Similar p53 activity occurred in hyperplastic growths that were triggered either by the Ras^{V12} oncoprotein or by failed differentiation programs. In a model of transient sterility, p53 was required for the recovery of fertility after stress, and entry into the cell

cycle was delayed in p53^{-} stem cells. Together, these observations establish that the stem cell compartment of the *Drosophila* germline is selectively licensed for stress-induced activation of the p53 regulatory network. Furthermore, the findings uncover ancestral links between p53 and aberrant proliferation that are independent of DNA breaks and predate evolution of the ARF/Mdm2 axis.

INTRODUCTION

Throughout the animal kingdom, p53 occupies a central position within conserved stress response networks. The protein integrates diverse signals associated with DNA damage and uncontrolled proliferation to govern adaptive downstream responses such as increased DNA repair, arrested cell cycle, and apoptosis [2]. Where examined, the genes encoding p53 are not essential for viability but have been implicated as regulators of aging [29-32]. It is now well appreciated that ancestral roles for this gene family must have predated functions in tumor suppression. In support of this, members of the p53 gene family are present in unicellular protists and short-lived multicellular organisms [13,14,33]. Furthermore, cancer was probably a negligible source of selection pressure during the course of human evolution [34] and the combined removal of canonical p53 effectors (p21, Puma, and Noxa) does not account for tumor suppression in mice [7]. These and other observations suggest that tumor suppressive roles for the p53 family were co-opted from primordial functions, some of which may have been linked to meiotic recombination [23].

In recent years, considerable evidence has surfaced linking p53 action to stem cell biology. For example, in mammary stem cells p53 promotes asymmetric division and cell polarity, thereby helping to limit the population of stem cells in the mammary gland [35]. Furthermore, reprogramming of somatic cells into induced pluripotent stem cells (iPSCs) is greatly increased in p53 deficient cells, suggesting that p53 may act as a "barrier for induced pluripotency" [36]. Consistent with this, several labs have shown that p53 induces embryonic stem cell differentiation to maintain genomic stability after DNA damage [37-39]. Together with recent studies in planaria, these observations indicate that an ancestral focus of p53 action could operate in stem cells [40]. We directly tested this possibility using a p53 biosensor to visualize *Drosophila* germline stem cells and their progeny. When DNA breaks were exogenously imposed or intrinsically engineered, *Drosophila* p53 (Dp53) was activated selectively in germline stem cells (GSCs) and their immediate daughters, indicating that these cells are uniquely licensed for p53 action. Furthermore, in various germline tumor models Dp53 was constitutively hyperactivated, suggesting that ancient links between p53 and inappropriate growth predate canonical effectors that connect these regulatory networks (e.g. ARF and MDM2).

MATERIALS AND METHODS

Fly stocks and genetics

All fly stocks were maintained at 22-25°C on standard food media. We obtained *rad54*, *aubergine* and *cutoff* mutants: *rad54*^{RU}, *rad54*^{AA}, *aub*^{HN}, *aub*^{QC}, *cuff*^{WM}, and *cuff*^{QQ} from T. Schupbach (Princeton University, Princeton, NJ, USA); *c587*-GAL4, UAS-*dpp*, UAS- *Lsd1*^{KD} [41] homozygous viable allele of *bam*$^{\Delta 86}$ [42] *nanos*-GAL4VP16, and UASp-*tkvCA* [43] have been described previously. The gstD1-GFP reporter was obtained from Dirk Bohman [44]. All other stocks were obtained from Bloomington Stock Center (Indiana University, Bloomington, IN, USA). The Dp53 rescue strain was engineered by ϕC31 integration of a 20kb genomic fragment BAC containing the Dp53 locus into an attP site on the X chromosome of the PBac{y+-attP-9A}VK00006 line (Bloomington #9726). The parent BAC CH322-15D03 was obtained from the P[acman] resource library [45] and Rainbow Transgenic Flies performed the injection and screening for recombinants. The I-SceI endonuclease strain was generated by K. Galindo [46] which was crossed to p53R-GFPnls(STI150); HS-(70Flp)(70 I- Sce I)/TM6 for heat-inducible I-SceI endonuclease expression. Adult females were fattened for 2-3 days after eclosion and then subjected to heat shock in a circulating water bath at 37°C for 90 min and repeated for 3 consecutive days. 24 hours after the last heat shock, ovaries were dissected for immunostaining. For forced proliferation assays, two GAL4 lines were used: *nanos*-GAL4VP16 was used to achieve overexpression in the germline with UAS constructs for Ras^{V12}, CyclinE, and Thickveins [47]. *c587*-

GAL4 was used to achieve overexpression of UAS constructs of *Dpp* or *Lsd1-RNAi* in the somatic cells of the ovariole tip [48]. For cyclinE overexpression, stocks were maintained in 25ºC and female virgins were collected upon eclosion, shifted to 29ºC for 4-5 days then subjected to immunostaining. For the Ras^{V12} studies, female virgins were shifted to 29ºC for 1 day and then shifted down to 25ºC for 3 days prior to immunostaining. The Gal4-UAS system (adapted from yeast) often produces optimal expression at temperatures higher than 25C. Since the UAS-Rasv12 and UAS-CyclinE constructs were not optimized for expression in the germline we applied these temperature shifts to produce more penetrant phenotypes.

Irradiation Assay

Well-fed flies were exposed to ionizing radiation using a Cs-137 Mark 1-68A irradiator (J.L. Shepherd & Associates, San Ferando, CA, USA) at a dose of 4 krad unless otherwise noted. When irradiating several genotypes, each genotype was placed in an individual vial, and all vials were exposed to IR at the same time on a rotating turntable inside the irradiator. For visualizing reporter activation after IR, flies were dissected 24hrs post-IR to allow for stable GFP expression.

Immunostaining of fly tissue

3-5 days old well-fed females were dissected in PBS and fixed in 4% EM-grade formaldehyde (Polysciences) diluted in PBS-0.1% tween-20, with three times the

volume of heptane. After washing, tissues were blocked in 1.5% BSA, then incubated with primary antibodies at 4°C overnight. Antibodies used: rabbit α-GFP (Invitrogen); rabbit α-pH2Av (kindly provided by K. McKim with specific staining protocols), rabbit α-cleaved caspase 3 (Asp175) (Cell Signaling); mouse α-Armadillo, mouse α-BrdU (BD Biosciences), mouse α-HTS clone 1B1 (Developmental Studies Hybridoma Bank), and rat α-Vasa (DSHB). For fluorescence visualization, Alexa-488, 568 (Invitrogen) and DyLight 649 (Jackson ImmunoResearch) secondary antibodies were used and 0.1μg/ml of DAPI (Invitrogen) for DNA staining was added in the first wash step. After three washes, ovaries were further hand dissected and mounted in VECTASHIELD (Vector Laboratories) for microscopy imaging. For validating stimulus dependent p53 action as visualized by the reporters, we routinely confirmed absence of GFP expression using flies null for Dp53. We note that p53R-GFPnls shows constitutive expression independent of p53 in a subset of gut cells and in the region of the testis containing elongated spermatids, reflecting position effects upon this transgene.

Fertility tracking and proliferative arrest assay

In fertility assays, two *p53* null alleles, 238H (ns) and 5A-1-4 (k1) were used in trans-combination to reduce genetic background influences. Two wild type strains, *yw* and w^{1118} were used for comparison. p53 rescue transgenes were tested in a transheterozygous $p53^{-/-}$ background (A1; ns/k1 and A2; ns/k1) to

exclude contributions from background modifiers. Five to seven day-old females were irradiated at desired doses (11.5 krad for Figure 2-8 and 9 krad for Figure 2-9) and fertility was tracked over time in groups. Each group contained ten females and five unirradiated wild type Canton-S males. The animals were transferred to a new vial at designated time points, and fertility was scored by presence of larvae ten days after the parents were removed. Each trial contained 2 to 15 replicates per genotype. For Figure 2-8 percentages of fertile samples are plotted based on 5 trials. In the proliferative arrest assay, ovaries were dissected and immersed in Grace's media containing BrdU (10μM) for 1hr at room temperature. After fixation, ovaries were treated with 2N HCl for 30min then 100mM of borax was added for 2 minutes to neutralize the pH. Tissues were then processed for blocking and regular IHC.

Statistical Analysis

For all statistical analysis, data was placed into GraphPad Prism software. For statistics on the IR and Isce-I reporter activation (Figure 2-1), one-way ANOVA test was performed on all genotypes with a Tukey's Multiple Comparison post-test. Reporter activation in *aubergine*, *cutoff*, and *rad54* mutants (Figure 2-5) was analyzed using a two-tailed unpaired t-test comparing the transheterozygous mutant to the heterozygous control. The same analysis was carried out for region 3 and stage 2-8 (Table 3-2). For statistical analysis on fertility and BrdU incorporation assays (Figure 2-8), one-way ANOVA test was performed for each

time point with a Dunnett post-test in which $p53^{-/-}$ data was the control. For cleaved-caspase 3 analysis (Figure 2-6), the data was analyzed using a two-tailed unpaired t-test. In cases where replicates produce identical values incompatible with the prism two-tailed unpaired t-test tool, one value was negligibly revised to enable computation by this software (e.g. when both values were 0, one value was changed to 1.0^{e-12}).

Microarray and Gene Expression Commons (GEXC) analysis

About 200 ovaries from bam or bamp53 adult females were dissected in batches and pooled together to extract total RNA using Trizol (Invitrogen). After verifying RNA integrity using Bioanalyzer (Agilent 2100), whole-genome expression of each genotype was analyzed using Affymetrix *Drosophila* Genome 2.0 Array at UTSW Genomics & Microarray core facility. Microarray datasets were uploaded to Gene Expression Commons (https://gexc.stanford.edu) and analyzed with 17 other public available datasets. In Gene Expression Commons, raw microarray data is individually normalized against a large-scale common reference (for *Drosophila* genome, n=2687 as of Nov 2013), mapped onto the probeset meta profile. This strategy enables profiling of absolute expression levels of all genes on the microarray, instead of conventional methods where differences in gene expression are compared only between samples within an individual experiment [49].

RESULTS

Damage-induced Dp53 activity in the germline is restricted to stem cells

The *Drosophila* gonad is a classic system for studying the stem cell compartment since stem cells, their immediate daughters, and the surrounding niche are easily identified. In the ovary, germline stem cells (GSCs) undergo self-renewing divisions that typically produce a GSC and a cystoblast (CB). These GSCs support egg production throughout the lifespan of female adults (see Figure 2-1B). We used *in vivo* biosensors [23] to visualize p53 activity as GSCs responded to various sources of stress (Figure 2-1A). To exclude technical artifacts, two GFP reporters were used- one is localized to the nucleus (p53R-GFPnls) and the other does not (p53R-GFPcyt). As previously described [23], programmed p53 activity triggered by meiosis was only observed in region 2 (Figure 2-1B). After exposure to ionizing radiation (IR) stress, p53 activity was induced in virtually all germaria. However, despite widespread damage to the organ (Figure 2-7), this unprogrammed response was remarkably restricted to germline stem cells (GSCs) and their immediate progeny (CBs) (Figure 2-1C, 2-1E). Furthermore, as seen in Table 2-1, this response was highly penetrant. Since we rarely observe reporter activation only in CBs, the signal seen in CBs probably reflects GFP perduring from the parental stem cells. Furthermore, post-irradiation levels of GFP were noticeably more robust than the programmed activity during meiosis (compare solid arrows to open arrows in Figure 2-1C and 2-1D) [23]. As expected, p53 biosensor activity was not observed within the ovary of $p53^{-/-}$ animals and

was also absent from ovaries lacking the upstream Chk2 kinase (Figure 2-1E, Table 2-1).

Double stranded DNA breaks (DSBs) are responsible for many of the biological effects associated with IR [50]. Therefore, to determine whether DSBs are sufficient to induce the p53 reporter, we ubiquitously expressed the I-SceI endonuclease in the germline of flies engineered to harbor a single I-SceI recognition site in each nucleus. As seen with IR exposure, p53 activity occurred only in GSCs/CBs when DSBs were induced (Figure 2-1D, 2-1E, Table 2-1). Furthermore, it is notable that a single DSB was sufficient to provoke robust p53 activity in GSCs/CBs. Therefore, whether exogenously imposed or intrinsically engineered, DSBs triggered p53 selective activation that was confined to GSCs and their immediate progeny. Furthermore, this stem cell restricted response is clearly under genetic control. For example, in directed tests of chosen mutants we identified a class of lesions that exhibit non-selective p53 action throughout the ovary only after IR challenge (see Figure 2-2, Table 2-1). Therefore, although p53 is present and potentially functional in all cells of the ovary, under normal conditions its action is somehow confined to GSCs and their immediate progeny.

To ask whether this pattern might reflect a general property of germline stem cells we similarly examined the male gonad. As seen in the ovary, we observed selective p53 reporter activation in GSCs and their immediate progeny

(gonioblasts) in irradiated testis (Figure 2-3). Likewise, stimulus-dependent activity required p53 and was not seen in unchallenged testis (Figure 2-3C, Figure 2-4). Occasionally, the biosensor was also present in early spermatogonial cysts, perhaps reflecting perduring GFP and/or independent activation associated with dying cells (Figure 2-3D-D" and Figure 2-4D-E"). Collectively, the observations in Figure 2-1 and Figure 2-3 demonstrate that selective p53 activation in the stem cell compartment is a general property of germline tissues exposed to genotoxic stress. We note that perturbation-dependent induction of the p53 biosensor in gonadal stem cells was highly penetrant (Figure 2-1E, Figure 2-3C). However, like all stress responses, the strength of signal and the number of responding cells were variable from animal to animal (Figure 1C, 1D and Figure 2D) perhaps reflecting distinct cell cycle dynamics occurring in GSCs at the time of challenge.

Genome instability provokes p53 action in the stem cells

We tested whether other genome destabilizing factors elicited similar p53 activity in stem cells. To examine the effect of deregulated retrotransposons, we introduced the p53 biosensor into *cutoff* or *aubergine* mutant animals. These genes encode essential components of the piwi-associated RNA (piRNA) pathway, acting to silence retrotransposons in the germline [51]. The corresponding mutants exhibit disregulated retrotransposition, reduced fecundity, and egg shell ventralization [51]. Figure 2-5A shows that in *cutoff* mutants induction of p53R-

GFP occurs exclusively in GSCs and their progeny at a penetrance comparable to irradiated wild type animals (Table 2-3). Frequent p53 activation in the germline was similarly observed in the GSCs of *aubergine* mutants (Figure 2-5B) and *rad54* mutants defective for DNA repair (Figure 2-5C). However, in contrast to *cutoff* mutants, the p53 biosensor was not entirely restricted to GSCs/CBs in these mutants (Table 2-2) perhaps reflecting differences in the kinetics of repair that may occur in these different backgrounds [52].

p53 enables recovery from stress-induced sterility and proper exit from proliferative arrest

In somatic cells, Dp53 promotes stress-induced apoptosis [32]. Therefore we examined the germarium for evidence of cell death by detecting cleaved caspase-3. In the 24hr period post challenge, over 90% of GSCs induce the reporter but the average incidence of apoptosis was less than 4% (Figure 2-6). Furthermore, we did not observe an obvious role for p53 in regulating stem cell numbers in the *Drosophila* ovary in the presence or absence of stress (Table 2-1 and Table 2-3). We also used α-pH2Av immunostaining, the *Drosophila* counterpart of mammalian pH2AX [53], to follow the repair of DSBs after IR and found that resolution of these lesions was unaffected in the germaria of p53 mutants (Figure 2-7). Similarly, in BrdU incorporation studies, the rates at which wild type and $p53^{-/-}$ GSCs/CBs entered proliferative arrest were also indistinguishable (Figure 2-8A). However, in the post-stress period, we did

observe that p53 mutants were significantly delayed for re-entry into the cell cycle (Figure 2-8A, Table 2-3). Furthermore, this defect is reversed in p53 genomic rescue strains confirming an assignment of this phenotype to the p53 locus.

To examine how the action of p53 might coordinate adaptive stress responses in GSCs, we developed a fertility recovery assay. Here, females were irradiated to induce transient sterility and the recovery of fertility was scored over time (see methods). Figure 2-8B shows that wild type females recovered from infertility within one week post-exposure to IR at a dose of 11.5 krad. In contrast, females lacking p53 remained permanently infertile even when tracked over two weeks after IR (Figure 2-8B). To confirm that p53 gene function is responsible for this phenotype, we tested $p53^{-}$ females carrying a genomic rescue fragment spanning the p53 gene (see methods). We tested two rescue strains and in both cases the sterility defect was reversed (Figure 2-8B). However, neither rescue strain fully restored fertility to wild type levels, possibly reflecting incomplete restoration of wild type regulation in the transgenes.

To test whether we could link the fertility defect (Figure 2-8B) to the cell cycle defects observed at a lower dose (Figure 2-8A), we examined fertility and cell cycle kinetics at an intermediate dose (9 krad) of IR. After this challenge, $p53^{-/-}$ females exhibit impaired fertility while WT flies remained fertile (Figure 2-9A,B).

We performed BrdU incorporation studies over 7 days with females irradiated at 9 krad and assayed the number of germaria that had BrdU positive cells in region 1. Under these conditions, we observed persistently reduced proliferative activity in $p53^{-/-}$ stem cells even 7 days after IR (Figure 2-9C). This result is consistent with the possibility that fertility defects seen in $p53^{-/-}$ flies are linked to the impaired cell cycle kinetics found in GSCs. Furthermore, the data in Figure 2-8B and Figure 2-9A suggest that radiosensitivity associated with the $p53^{-/-}$ genotype, previously documented for larval stages [32], also applies to germline tissue.

Exposure to ionizing radiation is thought to lead to elevated reactive oxygen species (ROS) and ROS signaling pathways are, in turn, activated to combat these oxygen radicals [54]. To test if GSCs differ in ROS signaling, we utilized a ROS reporter (gstD1-GFP) whereby cells express GFP upon activation of the ROS signaling pathway (Figure 2-10A) [44]. As shown in Figure 2-10B, in unchallenged ovaries we did not observe gstD1-GFP reporter activity in the stem cell compartment. However, we did observe persisting GFP in the germline beginning in the first egg chamber (Figure 2-10B). Upon ionizing radiation, the gstD1-GFp reporter was strongly activated in the somatic follicle cells but the GSCs and CBs remained unresponsive (Figure 2-10C). These data suggest that the germline stem cells differ in their ROS response upon IR stress. We are currently testing whether p53 influences this signaling pathway.

Uncontrolled Stem Cell proliferation activates p53

Oncogenic properties are thought to simulate 'stemness' and oncogenic signals frequently result in p53 activation [2]. However, it is not known whether this regulatory axis is conserved beyond mammals. To test whether inappropriate growth triggers *Drosophila* p53 function, we examined the p53 biosensors in various germline tumor models. First, we expressed an oncogenic form of RAS commonly found in human cancers together with the p53 biosensor [55]. Transient expression of the *Drosophila* Ras^{V12} counterpart provoked robust p53 activation mainly in the GSCs and CBs (Figure 2-11B and Table 2-4). Figure 2-11E shows that another oncoprotein, Cyclin E, produced similar results. We also examined these biosensors in *bam* mutants where a block in differentiation causes extensive hyperplasia [42] and in these tumors extensive reporter activity was also seen (Figure 2-11C, D). Likewise, expanded BMP (bone morphogenic protein) signaling [43] or reduced *Lsd1* (lysine-specific demethylase 1) activity [41] in neighboring somatic cells can also cause inappropriate growth and robust p53 activity was similarly observed in these germline tumors as well (Figure 2-11 F, G, H). Therefore, whether caused by forced oncoprotein expression (panels B, E), failed differentiation programs (panels C, D) or expansion of the stem cell niche (panels F-H), inappropriate growth of *Drosophila* tissues was consistently accompanied by p53 activity. As seen with genotoxic stress, biosensor responses seen in these contexts was somewhat variable, perhaps reflecting complex signaling and/or cell cycle dynamics that occur in these tumor models.

Technical sources of variation linked the UAS-Gal4 driver system and/or non-uniform accumulation of the oncogenic product could also contribute to variability in these contexts.

We considered the possibility that inappropriate growth might indirectly activate p53 by provoking DNA damage. In order to test this, we stained *bam*$^{\Delta 86}$ ovaries for pH2Av [56]. We observed very few pH2Av foci in *bam* tumors and, notably, these foci did not co-localize with p53 biosensor activity (Figure 2-12). Therefore, p53 activity in these tumors is not triggered by DSBs but instead, appears to be directly triggered by signals associated with hyperplastic growth.

As seen in Figure 2-11, diverse types of hyperplastic growth triggered constitutive p53 activity. To ask whether p53 functions in these tumors, we examined bam$^{-/-}$ ovaries that were either WT or null for p53. Tumor size was not significantly altered in the absence of p53, but we did observe dramatically altered cytology in tumors that lacked p53. As seen in Figure 2-13, bam$^{-/-}$ ovarian cysts are typically filled with stem-like cells that exhibit round or dumbbell-shaped fusomes when stained with α-HTS [57]. As documented in Figure 2-11C, defective fusomes were seen in all bam$^{-/-}$;p53$^{-/-}$ cysts and, in nearly half of these unusually large nuclei were observed. Though not quantified, micronuclei were also prevalent in these samples. Since defective fusome morphologies and irregular

nuclei are consistent with aberrant mitosis, our data suggests a role for p53 in promoting proper cell cycle progression in these stem-like tumors.

To further examine the functional role of p53 in this context, we examined gene expression profiles of $bam^{-/-}$ ovaries that were WT or null for p53 by microarray. In total, we found that 297 gene transcripts were altered by at least two-fold or greater in the absence of p53. Table 2-6 lists the top 20 genes that are affected (upregulated or downregulated) by p53 in these tumors. Using the Gene Expression Commons (GEXC) tool, we compared these gene sets to existing germline, embryonic and somatic expression profiles. We did not find a coherent pattern among the top 20 genes that are normally upregulated by p53. However, among the top 20 genes that are normally suppressed by p53 in these germline tumors, we observed a modest enrichment for transcripts that were absent in either the embryonic stages or other somatic tissues (Table 2-5). These data, together with our histological studies (Figure 2-13), establish that p53 exerts functional activities that impact cellular and molecular properties of *Drosophila* stem cell tumors.

An unbiased genetic screen to uncover upstream regulators of p53 in GSCs

p53 activity is confined to the GSCs and CBs after ionizing radiation (Figure 2-1), despite widespread p53 protein expression in the ovary [58]. We hypothesize that

the germline stem cells contain specific upstream regulators that promote selective p53 activity. Alternately, the organ may have inhibitory components that prevent p53 activity outside of the stem cell compartment. As shown in Figure 2-1E, Chk2 was required for p53 activation in stem cells. Chk2 could contribute to the selective activation in stem cells seen here, but Chk2 is also broadly expressed and functionally associated with oocyte development throughout the ovary [59]. Therefore, we have yet to uncover the precise genetic components that promote selective p53 activity in GSCs.

To identify unknown p53 regulators in stem cells, we designed an unbiased RNAi screen in the *Drosophila* germline using the Gal4-UAS expression system (Figure 2-14A). Close to 1000 distinct RNAi strains were examined for effects upon p53 activity in this stem cell compartment after ionizing radiation. Three classes of reporter activation were of interest to us (Figure 2-14 B-D). First, after IR challenge, when GSCs and meiotic cells failed to activate the p53 biosensor, we termed this class 'Failure to activate generally' (Figure 2-14B). Second, when meiotic cells remained responsive to p53 activity but GSCs failed to activate, we called this class 'Failure to activate in GSCs only' (Figure 2-14C). These two 'failure to activate' classes were rare (Table 2-6). We screened over 1000 RNAi lines and 4 lines fell into these classes, including our proof of principle, RNAi-Chk2 (Figure 2-14B) (Table 2-7). The third class of reporter activation we observed, was widespread p53 biosensor activation outside of the stem cell

compartment upon ionizing radiation and we termed this 'IR dependent modifier' (Figure 2-14D). This third class was more common (Table 2-7) and was usually accompanied with oogenesis defects. As shown in Figure 2-15 we inadvertently found genes that were involved in stem cell maintenance and differentiation. We are currently validating these screen hits by generating null alleles.

To test whether a chemical screen would be possible, we tested whether GSCs could remain alive and activate the p53 biosensor *ex vivo*. As shown in Figure 2-16 and Figure 2-17, we took two approaches. First, we irradiated adult flies and immediately after IR, the ovaries were dissected and placed in media. After 5 hours in media, the ovaries were fixed for immunostaining. As shown in Figure 2-16B, upon ionizing radiation, the *ex vivo* ovaries robustly activated the p53 biosensor in GSCs at comparable levels to *in vivo* irradiated ovaries. Importantly, unirradiated *ex vivo* ovaries did not lead to elevated p53 activity indicating that the dissection and media are not a source of stress. Our second *ex vivo* approach involved dissecting the ovaries and soaking them in wnt inhibitor or DMSO control for 2 hours. We then applied IR to the ovaries and continued soaking them for an additional 4 hours before performing IHC (Figure 2-17A). As shown in Figure 2-17B, the p53 biosensor activity was dampened when ovaries were irradiated *ex vivo*. However, we observed a modest effect of the wnt inhibitor on biosensor activation (Figure 2-17B). We are currently repeating these

studies to determine whether the wnt signaling pathway is involved in p53 stem cell activation.

DISCUSSION

We found that adult *Drosophila* exposed to genotoxic stress or genome destabilizers selectively activated p53 in GSCs and their immediate progeny. This striking specificity was observed despite widespread Dp53 expression [18,19] and widespread tissue damage (Figure 2-7). We note that stem cell specificity was not an artifact intrinsic to the biosensors, since independent reporters behaved similarly in both the female and male germline and required the wild type Dp53 locus in both cases. Furthermore, in certain mutant backgrounds stress-induced activity restricted to GSCs was lost and non-selective p53 activation was widespread throughout the ovary (Figure 2-2). Therefore, despite the fact that it is present and activatable throughout the gonad, functional p53 is restricted to stem cells and their immediate progeny by specific genetic determinants.

Collectively, our work supports previous indications that there is an intimate and ancient link between p53 and stem cell biology [40]. Our findings also offer rare and novel opportunities to operationally mark the stem cells in the fly germline, as visualized by p53R-GFP. This marker is distinct from conventional stem cell labels [60] since it is not constitutively expressed but, instead, represents a

functional output that is conditional upon a perturbation. We further note that like all reporter systems, our p53 biosensors may not reflect the full scope of effector output regulated by this network, and activities visualized here could transmit only subsets of p53 mediated responses. Nevertheless, despite this possible limitation, our results are consistent with suggestions that stem cells may be acutely sensitive to sources of genomic instability with a higher propensity for engaging adaptive responses relative to other cells [61,62]. We propose that in reproductive tissues, the p53 regulatory network is either exclusively licensed in stem cells or selectively blocked outside of this compartment.

What upstream regulators might specify p53 activation in GSCs/CBs? Given that stem cells have unique properties, p53 activation in these cells might lie downstream of a novel pathway. Consistent with that one upstream candidate, ATR, was not rate limiting for p53 activation in the germline (Figure 2-2, Table 2-1). Furthermore, unlike meiotic induction, p53 induction in GSCs/CBs was independent of the topoisomerase, Spo11 (Table 2-1) [23]. Chk2 could contribute to the selective activation in stem cells seen here, but since Chk2 is also broadly expressed and functionally associated with oocyte development throughout the ovary [59] any potential role in GSCs must extend beyond a simple presence or absence of this kinase.

Our findings also imply stimulus-dependent effectors of p53 in stem cells that are not yet appreciated. For example, within detection limits, we observed no obvious connection between p53 status and apoptosis, DNA double-strand break repair, or cell cycle arrest. However, irradiated *p53*$^{-/-}$ GSCs were significantly delayed in the re-entry phase for cell cycle. Future studies will explore this defect and also examine progeny derived from stressed GSCs for transgenerational phenotypes that might be adaptive.

Our discovery that p53 action is coupled to hyperplasia in a non-vertebrate species was unexpected for two reasons. First, the role of this gene family as a tumor suppressor is thought to be a derived feature that evolved only in vertebrate lineages. Second, the canonical ARF/MDM2 pathway that links aberrant growth to p53 is absent outside of higher vertebrates [14]. Surprisingly, our combined results suggest that ancient pathways linking p53 to aberrant stem cell proliferation may predate the divergence between vertebrates and invertebrates.

PERSPECTIVES AND FUTURE DIRECTIONS

Two obvious questions from this work remain to be answered. First, what is the precise function of p53 in GSCs? In light of our findings in Chapter 3, p53 may be suppressing retrotransposons in stem cells after ionizing radiation. This possibility will be discussed in more detail in the next chapter. We also have yet to determine what effectors allow for the selective nature of p53 activity. This is an important future direction that we are continuing to pursue.

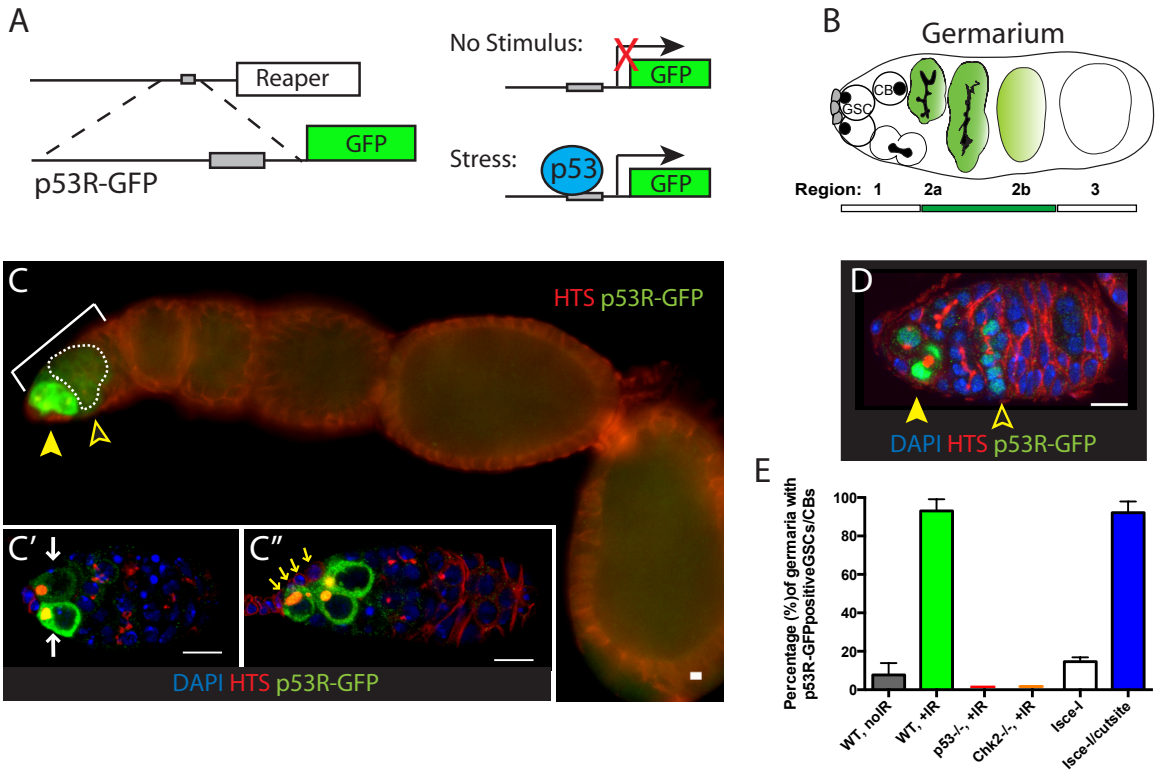

Figure 2-1. Genotoxic stress selectively triggers p53 activity in ovarian stem cells

(A) Construction of p53 biosensors. A well-characterized p53 enhancer (black line) that contains a p53 consensus binding site (grey box) conserved from flies to humans resides upstream of the *reaper* locus (white box) [17]. A 150bp fragment containing this enhancer was placed upstream of GFP (p53R-GFP). Transgenic fly strains are made with two reporter constructs, one contains a nuclear localization signal for GFP (p53R-GFPnls) and the other one does not (p53R-GFPcyt). Stimuli that trigger p53 activation induce GFP expression. These biosensors require wild type p53 and are effective readouts for p53 function.

(B) Germline Stem Cells (GSCs) are in contact with cap cells (in grey) at the apical tip of the germarium and undergo self-renewing division to produce a GSC and cystoblast (CBs) [63]. In unperturbed ovaries, programmed activation of the p53R-GFP biosensor is triggered by meiotic recombination in region 2 of the germarium, marked by open arrowhead in (C) and (D) [23].

(C) After radiation challenge (IR) the p53R-GFPcyt biosensor (green) is selectively induced in ovarian GSCs and CBs noted by a solid arrowhead. Bracket denotes the germarium. The open arrowhead and dotted line indicates p53 activation in region 2 prompted by meiosis. Insets **(C'** and **C")** are confocal images from different irradiated germaria counterstained with DAPI (blue). p53R-

GFPcyt induction (green) initiates in GSCs that exhibit rounded fusomes **(C'** white arrows**)** labeled by α-HTS
(Hu li tai shao, red) and are in contact with cap cells **(C"** yellow arrows**)**. Cells that activate p53 in **(C'** and **C")** were confirmed to be germ cells by α-Vasa staining (shown in Figure 1-figure supplement 2C-D").
(D) An engineered DNA double-stranded break (DSB) mediated by I-SceI (see texts and methods) induces the p53R-GFPnls biosensor (green) in GSCs/CBs, noted by a solid arrow. Open arrow indicates meiotic p53. The germarium is counterstained α-HTS (red) and DAPI (blue).
(E) Quantifies the percentage of germaria activated for the p53 biosensors in GSCs and their immediate progeny. Note that the perturbation-dependent responses reported here are all highly penetrant. Selective activation is IR (green) and I-SceI (blue) dependent at the 0.001 significance level. Note that biosensor activation did not occur in *p53*$^{-/-}$ (red) or *chk2*$^{-/-}$ (orange) mutants (see Figure 1-figure supplement 2A' and A"). Sample sizes are combined from at least two independent trials (available in Figure 1-table supplement 1). All scale bars represent 10μm. In panels C-C" the p53R-GFPcyt reporter was used. In panel D, the p53R-GFPnls biosensor was used.
All discoveries presented in Figure 2-1 were initially made by Wan-Jin Lu and she took the images in Panels C and D. I extended these observations in panels C' and C" showing that p53R-GFP positive cells are germline stem cells since they exhibit rounded fusome morphology and are in contact with cap cells.

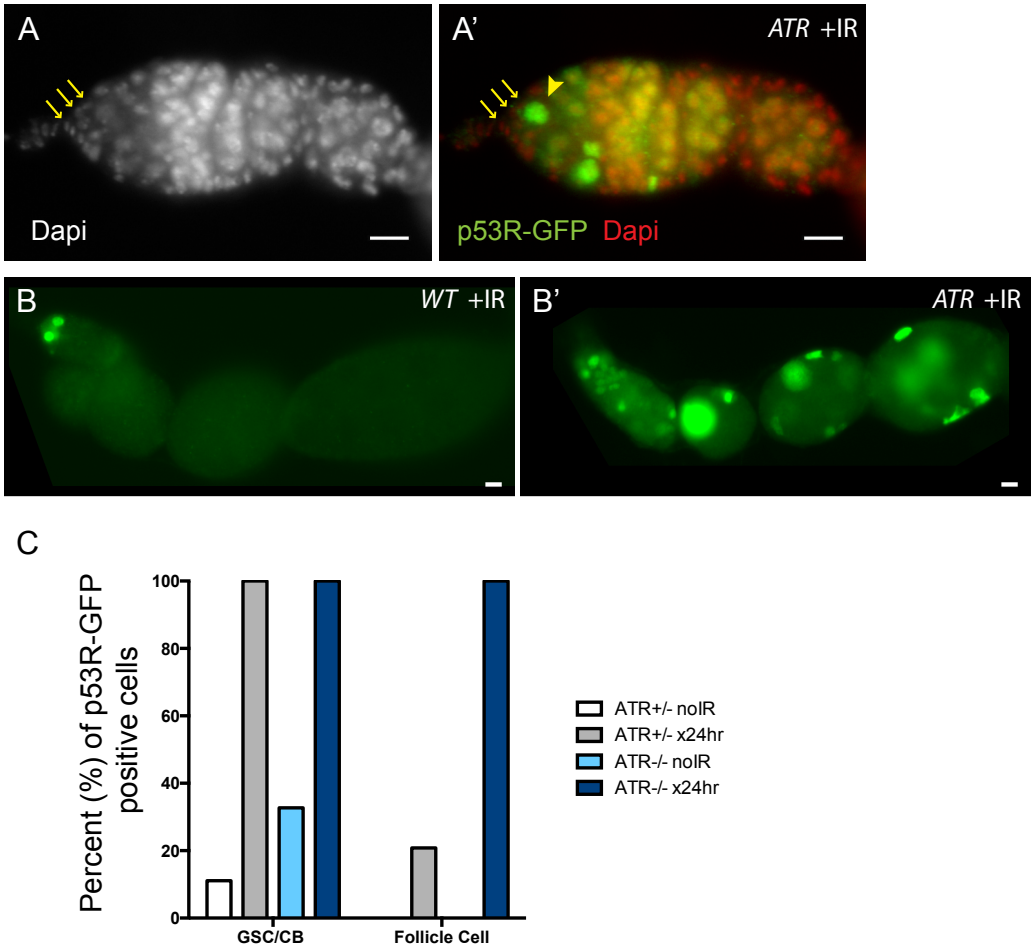

Figure 2-2. ATR is not rate limiting for p53 activation in the germline
p53R-GFPnls activation (green) was examined in ATR mutants **(A-B')** after irradiation. **(A-A')** GSCs (yellow arrowhead) that are in contact with cap cells (yellow arrows in A and A') identified by DAPI staining (white in A, red in A'). These observations show that ATR is not rate limiting for p53 activation in GSCs. Panels **(B-B')** show that induction of the p53R-GFPnls biosensor is not selective in ATR mutants **(B')** when compared to WT controls **(B)**. Genotype for (A-A') is *mei-41*$^{[D3]/[D3]}$ and for (B') is *mei-41*$^{[D3]/[RT]}$. The p53R-GFPnls biosensor was used for panels A-B'.
(C) Quantification of p53R-GFPnls reporter in GSCs/CBs and follicle cells in ATR heterozygous controls and ATR mutants with and without irradiation. Both the ATR$^{+/-}$ control and ATR$^{-/-}$ show a robust induction of p53R-GFPnls in GSCs after irradiation. ATR mutants also show a robust induction of reporter activation in follicle cells after irradiation. Scale bars, 10μm. Wan-Jin Lu performed all experiments presented in Figure 2-2.

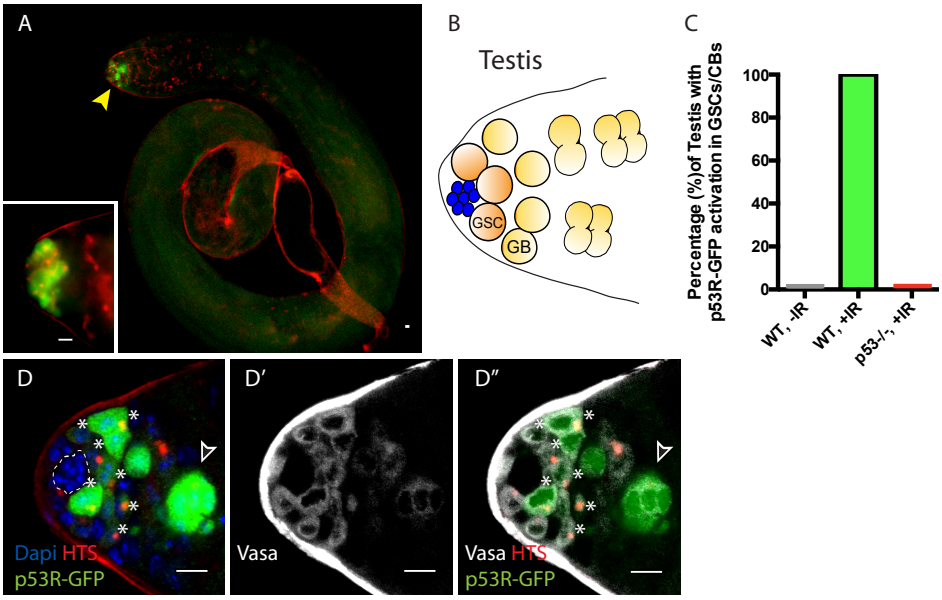

Figure 2-3. Selective p53 activity also occurs in male germline stem cells
(A) p53R-GFPcyt (green) is induced at the apical tip of an irradiated testis (arrowhead) where stem cells are located (see **B**). α-HTS co-staining (red) highlights early stages of germline development. The inset in panel **(A)** shows a higher magnification view from a different irradiated testis. **(B)** Male GSCs are in contact with cap cells (blue flower pattern) at the apical tip of the testis and divide to produce a gonioblast daugther (GB). **(C)** Quantifies the percentage of testis activated for the p53 biosensors in GSCs and their immediate progeny. Selective activation is IR (green) dependent and conditional upon p53 since p53R-GFP activation did not occur in *p53*$^{-/-}$ mutants (red bar).
(D-D") Confocal images from other irradiated testes confirmed that stem cells induced for p53R-GFPcyt (green, **D** and **D"**) are also positive for rounded HTS staining (red, **D** and **D"**) and the germline specific marker Vasa (white, **D'** and **D"**) as expected. The hub (dotted line, **D**) was routinely identified by the characteristic nuclei pattern as illustrated in (**B**, blue cells) and by negative Vasa staining (**D'** and **D"**). Asterisks mark p53R-GFP positive cells that are adjacent to the hub and Vasa positive or Vasa positive with rounded fusomes. Also note that the hub was identified by α-Armadillo staining (Figure 2-4C). Open arrowhead in (D and D") is likely a dying cyst as indicated by pyknotic and condensing nuclei and irregular HTS (Figure 2-4D-E'). In panels A, D-D" the p53R-GFPcyt reporter was used. All scale bars represent 10μm. Wan-Jin Lu made the initial observation in Figures 2-3 that p53R-GFP is activated in male GSCs after IR stress. I characterized and validated this observation extensively in Figures 2-3 and 2-4.

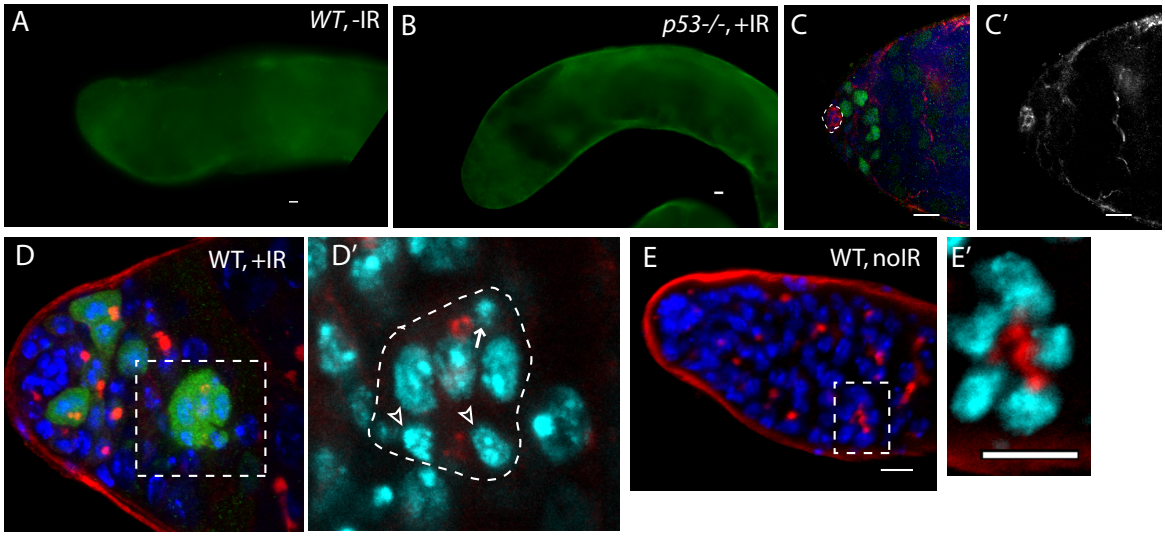

Figure 2-4. p53 activation in testis by Irradiation requires p53
Reporter activation in the male germline (seen in Figure 2-3A) is conditional upon irradiation **(A)** and is p53 dependent **(B)**. Compare A and B to Figure 2, panel A. **(C-C')** p53R-GFPnls (green) activation in testis after irradiation. The hub is identified here by α-Armadillo staining (red in H, white in H') which is noted by a dotted line in H. **(D-D')** Image in (D) is a different z projection from the same irradiated testis shown in Fig. 2D where HTS (red) and DAPI (blue) are used to identify cells. The p53R-GFP positive dying cyst (green) indicated by the open arrowhead in Fig. D-D"' exhibits pyknotic nuclei (D' arrow), condensing nuclei (D' open arrowheads) and irregular HTS. Image in (D') represents a magnified view of the dashed box in (D). Compare D and D' to the unirradiated WT testis control in **(E-E')** that shows a branched fusome detected by α-HTS (red in E and E') and nuclei of similar size by DAPI (blue in E and E'). In panels A, B, and E the p53R-GFPcyt reporter was used. In panels C the p53R-GFPnls reporter was used. All scale bars are 10μm.

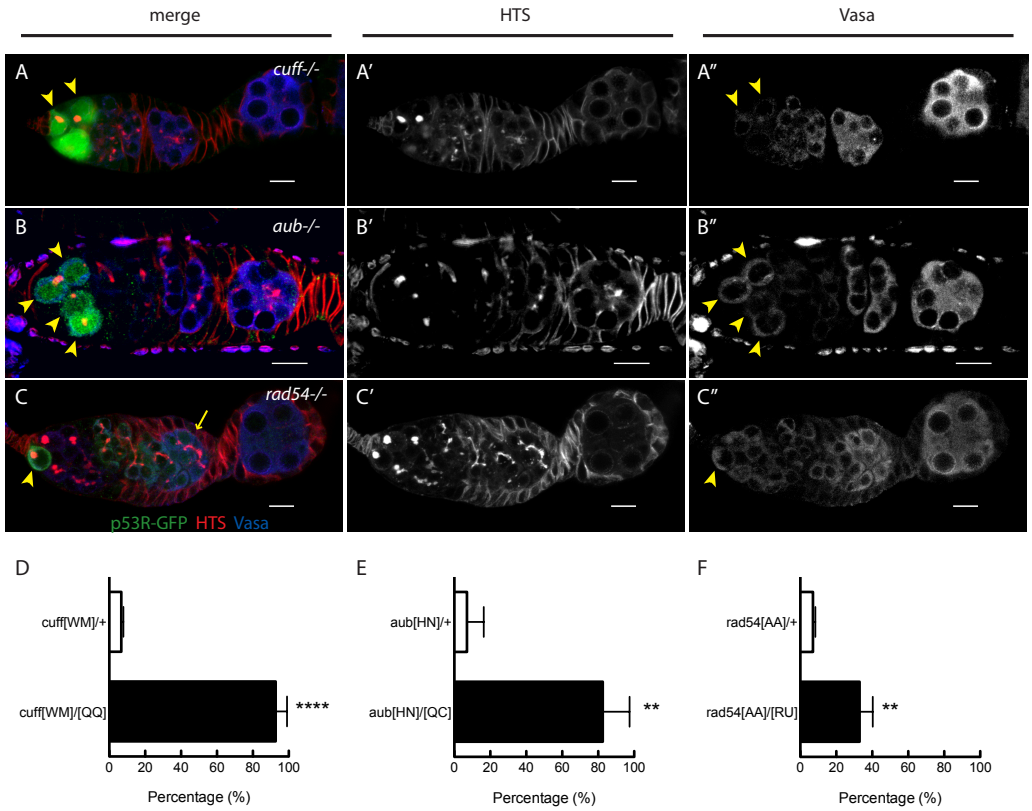

Figure 2-5. Stem cell associated p53 activity in defective DNA repair and retrotransposon silencing mutants

(A-B) Activation of the p53 biosensor (green) in the germarium of piRNA mutants, **(A)** *cutoff*$^{[QQ]/[WM]}$ and **(B)** *aubergine*$^{[HN]/[QC]}$. **(C)** Activation of the p53 biosensor in *rad54,* a meiotic DNA repair mutant. **(D-F)** Germaria were found to express p53R-GFPcyt in GSCs/CBs with a penetrance of 90% for *cutoff* mutants **(D**, p<0.0001**)**, 80% for *aubergine* mutants **(E**, p=0.0018**)**, and 33% for *rad54* mutants **(F**, p=0.0039**)**. Asterisks indicate significant differences between heterozygous controls and homozygous mutants. GSCs/CBs were identified by rounded fusomes detected with α-HTS (red in merge **A, B, C** and white in **A', B', C'**). Arrowheads indicate that p53R-GFP positive cells are also germ cells identified by Vasa staining (blue in **A, B, C** and white split channel in **A", B", C"**). Note that this particular anti-VASA antibody cross-reacts against the muscle sheath that surrounds each ovariole. If the sheath is not fully dissected and removed, then background staining is evident, as seen in Fig. 2-5B". Control genotypes were *cuff*$^{[WM]}$*/CyO*, *aub*$^{[HN]}$*/CyO*, *rad54*$^{[AA]}$*/CyO*. Note that *aub* and *rad54* mutants occasionally showed p53 activation beyond region 2 of the germarium (arrow in C), quantified in Table 2-2. All scale bars represent 10μm. In panels A, B, and C, the p53R-GFPcyt reporter was used. Wan-Jin Lu made this initial discovery. I validated that p53R-GFP positive cells are Vasa positive and exhibit rounded fusome morphology (Panels A-C").

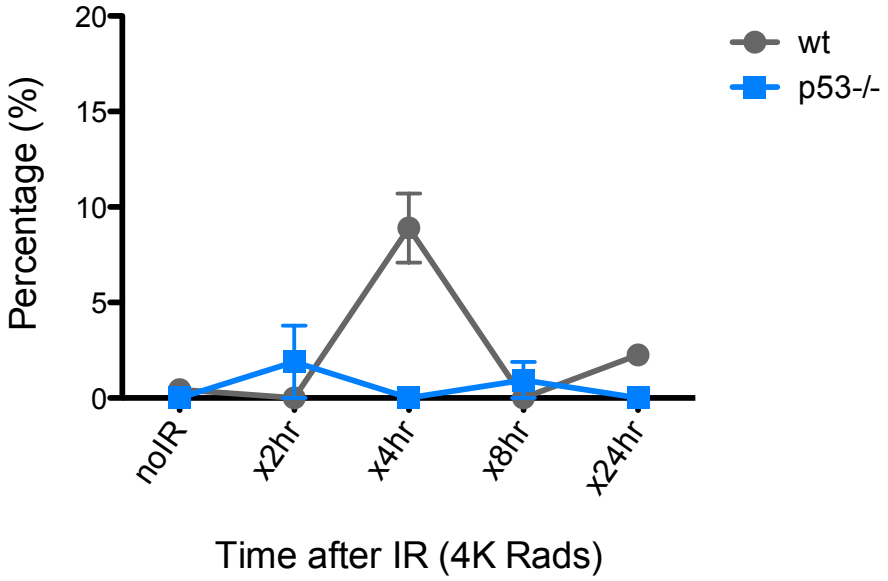

Figure 2-6. Reporter activation after Irradiation does not lead to purging of GSCs through apoptosis.
Time course analysis of stainings for cleaved-caspase3 (CC3) in GSCs/CBs after 4.0 krad of irradiation. The percent of germaria with CC3 positive GSCs/CBs are plotted on the Y axis. The highest incidence of CC3 was only 8% at 4 hours post irradiation in wild type flies. This is considerably different from the incidence of p53R-GFP positive stem cells after irradiation (~90%, see Figure 2-1E). Error bars represent standard deviations from two trials for no irradiation, 2hr, 8hr, 24hr and three trials for 4hr for both genotypes. Percentages and number of germaria assayed are provided in Table 2-3.

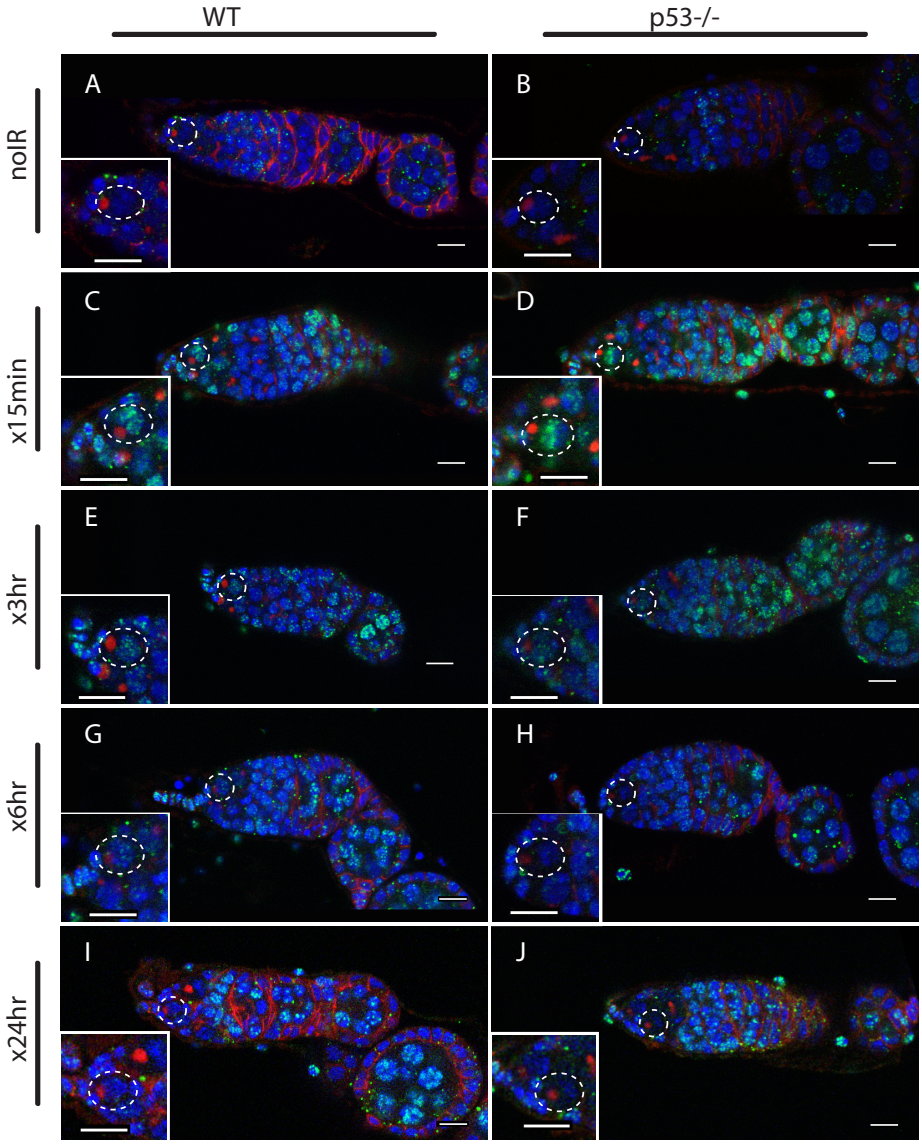

Figure 2-7. Radiation-induced DNA double-stranded breaks appear and disappear with similar kinetics in WT and p53$^{-/-}$ GSCs.
Time course of α-pH2Av (green) clearance after irradiation of wild type (**A, C, E, G, I)** and p53 mutants **(B, D, F, H, J)** at a dose of 4 krad. Little or no pH2Av staining is observed in unirradiated WT **(A)** or p53$^{-/-}$ stem cells **(B)**. Similar pH2Av staining is observed in WT and p53$^{-/-}$ stem cells 15 minutes after irradiation **(C, D)**. In both cases damage was generally cleared from GSCs within 24hrs **(I, J)**. Note that many cells are damaged after irradiation (compare A to G) yet p53 biosensor activation is restricted to GSCs/CBs (Figure 1). White circles indicate stem cells. Insets are magnified views of tip of the germarium from the same image for better GSC visualization. HTS (red) and DAPI (blue) are used to highlight cells in the germarium. Scale bars, 10μm.

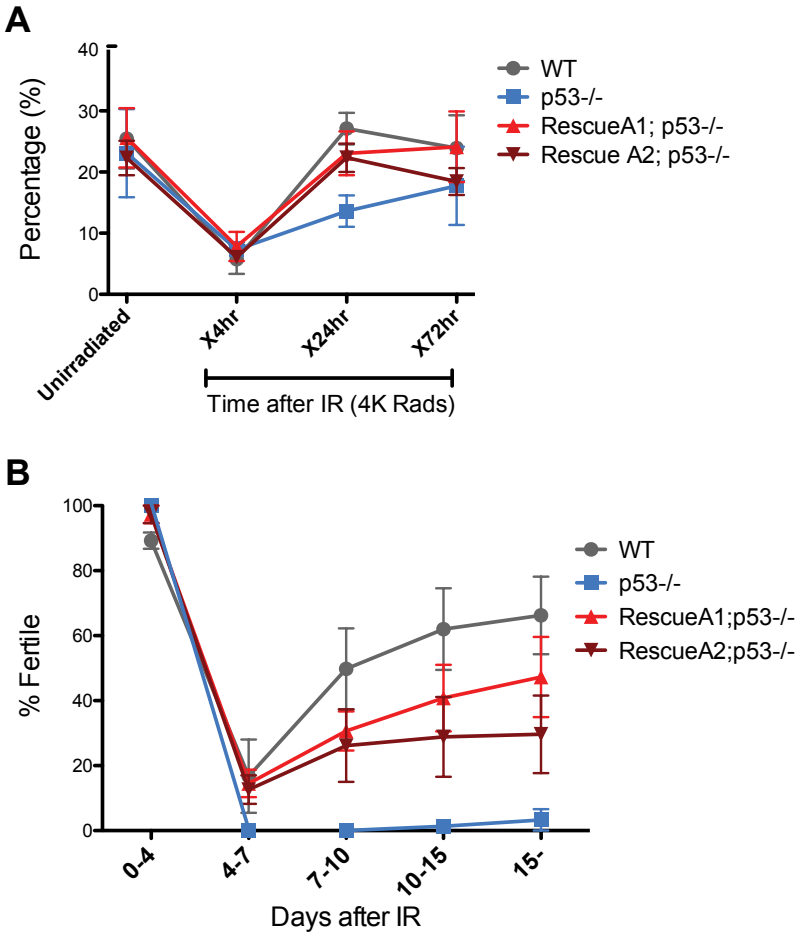

Figure 2-8. p53 mutants exhibit impaired fertility and delayed re-entry into the cell cycle after irradiation

(A) BrdU incorporation in GSCs after 4 krad of IR. The percentage of germaria containing BrdU positive GSCs/CBs was plotted on the Y axis. WT and $p53^{-/-}$ GSCs arrest with similar kinetics but $p53^{-/-}$ GSCs were significantly delayed for re-entry into the cell cycle. Error bars represent standard deviation from tests of three independent cohorts. WT and two rescue strains are significantly different from $p53^{-/-}$ at the 0.05 level at the x24hr time point. Percentages and number of germaria assayed are included in 2-3. In panels A and B, $p53^{-/-}$ represents animal transheterozygous for two p53 null alleles, $p53^{ns}$ and $p53^{K1}$.

(B) Fertility in wild type (WT) and $p53^{-/-}$ females was measured after exposure to 11.5 krad of IR (see methods) which induces persisting sterility in p53 mutants. WT fertility is significantly different from $p53^{-/-}$ during time points 7-10, 10-15, and 15- at the 0.05 level (see methods). Two rescue strains showed partial restoration of fertility. Rescue 1A strain showed restored fertility is significantly different from $p53^{-/-}$ at the 0.05 level at days 10-15 and 15-. Error bars represent standard deviation from 5 independent trials.

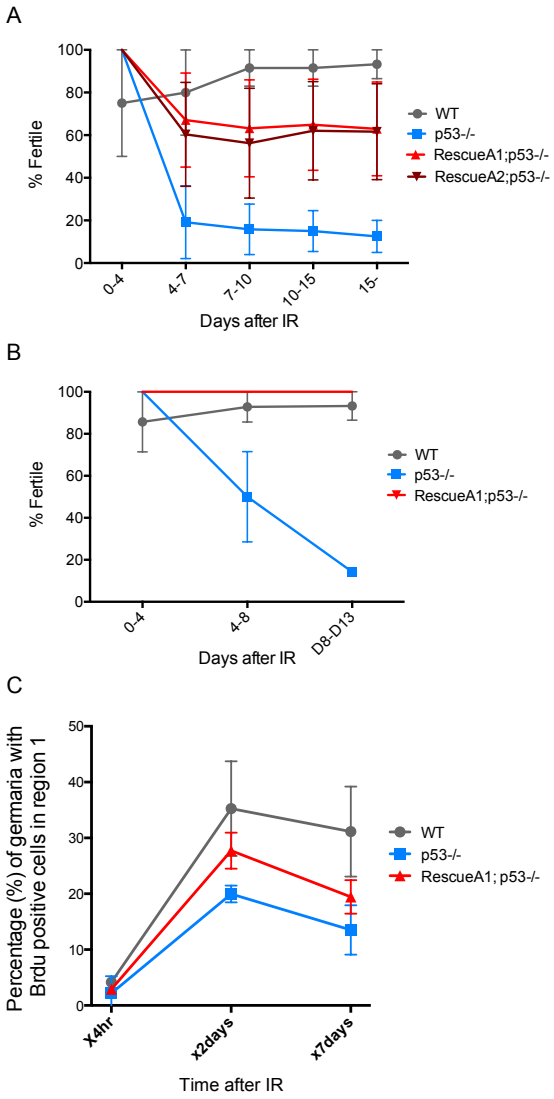

Figure 2-9. Fertility recovery correlates with proliferation by GSCs and their progeny.

(A) Fertility recovery after 9.0 krad of IR. A similar pattern is observed as seen at higher doses (Figure 2-8B, 11.5 krad). WT fertility is significantly different from $p53^{-/-}$ at all time points ($p < 0.05$). The A1 Rescue and $p53^{-/-}$ are significantly different at 10-15 and 15- days after IR ($p<0.05$). Error bars represent standard deviation from 4 independent trials. To link the fertility defect to cell cycle kinetic differences we observe at lower doses (Figure 4A, 4.0 krad), we performed 2 trials where we assayed fertility **(B)** and BrdU incorporation in region 1 of the germarium **(C)** after 9.0 krad of irradiation. Panel **(C)** shows that GSCs and CBs in $p53^{-/-}$ flies have a reduced proliferation potential at 2 and 7 days post irradiation (Figure 4-table supplement 1C). Fertility recovery suggests a radiation sensitivity phenotype since $p53^{-/-}$ flies recover fertility in a dose dependent manner (compare to Figure 2-8).

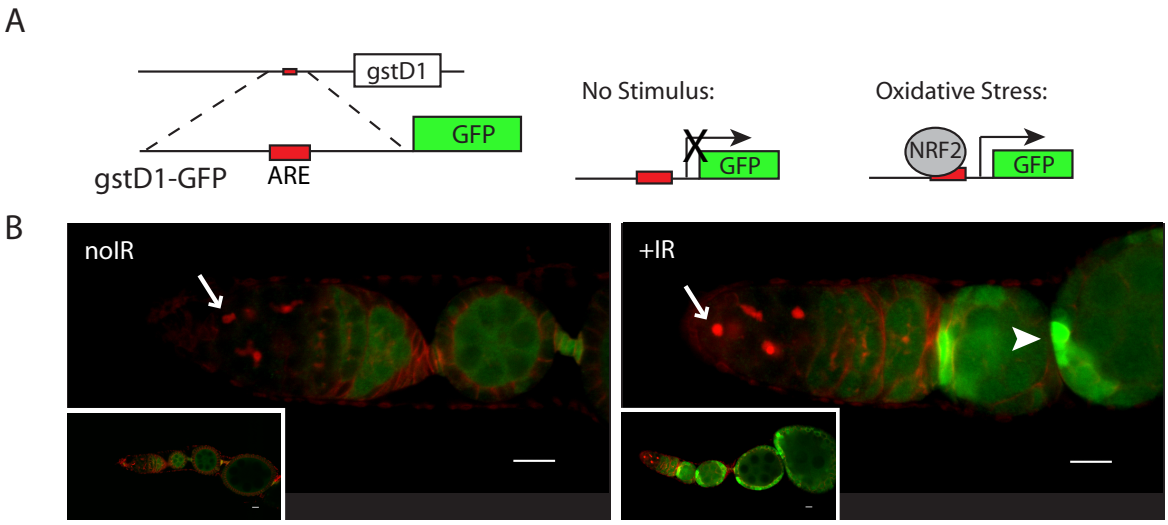

Figure 2-10 Oxidative Stress Signaling in the *Drosophila* Ovary
(A) Illustration of the Reactive Oxygen Species (ROS) reporter. An oxidative stress response gene, gstD1 (white box) contains an antioxidant response element (ARE) (red box) in its promoter region. The gstD1 promoter region containing the ARE was placed upstream of GFP. Upon oxidative stress, the NRF2 transcription factor (grey circle) binds the ARE and promotes GFP expression. Dirk Bohmann provided the transgenic gstD1-GFP reporter in **(A)** [44].
(B) gstD1-GFP reporter activity (green, anti-GFP) in unirradiated germaria, counterstained with HTS (in red). GSCs and CBs are negative for reporter activity (arrow, round HTS fusome). Inset is a lower magnification image of **(B).**
(C) gstD1-GFP reporter activity in irradiated germaria. GSCs and CBs (arrow, round fusome) remain GFP negative after IR stress. Somatic cells are highly responsive (arrowhead) for ROS signaling pathway after IR. Inset is a lower magnification image of **(C).**

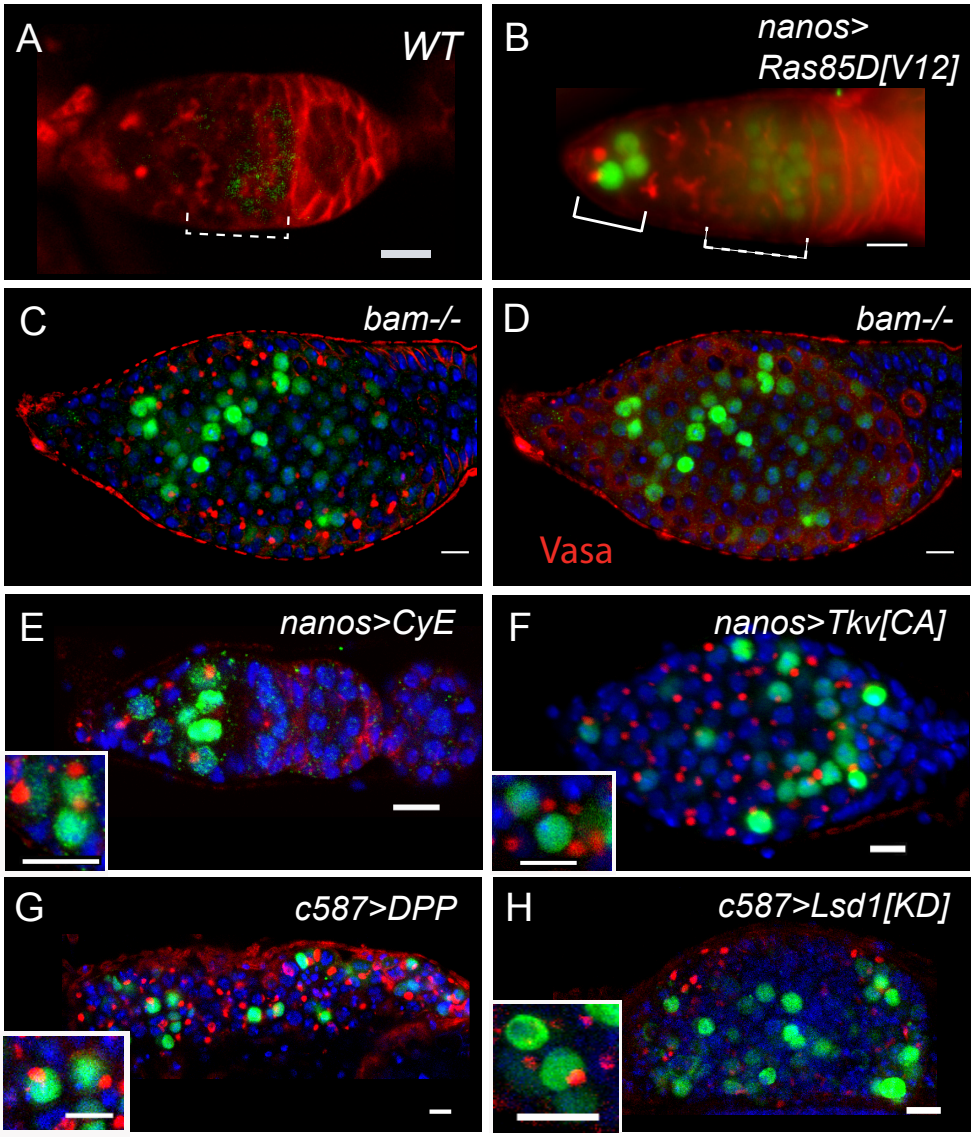

Figure 2-11. Deregulation of growth in the stem cell compartment provokes p53 action

(A) In an unperturbed wild type (WT) germarium, the p53R-GFPnls biosensor is absent from GSCs/CBs, marked here by rounded fusomes stained with α-HTS (red). The modest signal in region 2 reflects meiotic p53 activity (dotted bracket) [23]. When perturbed by Ras^{V12} **(B)** the p53 biosensor (green) is induced in GSCs/CBs (solid bracket in B, see Figure 5-table supplement 1). Perturbation from failed differentiation programs caused by the *bam* mutation **(C-D)** or Cyclin E over-expression **(E)** provokes similar p53 biosensor activity. Likewise, increased DPP signaling caused by a constitutively active Tkv receptor **(F)** or ectopic DPP ligand expression **(G)** also prompts induction of the p53 reporter.

Induction of the p53 reporter is also seen when the stem cell niche is expanded by silencing of *Lsd1* **(H)** [41]. Insets in panels E-H are magnified views of tumor cysts showing that p53R-GFP positive cells exhibit stem-like properties with rounded fusomes detected by α-HTS co-staining (red). Note in panels B, E and F, the indicated UAS transgenes were expressed using the germline specific driver, nanos-Gal4VP16 [47]. For panels G and H, expression was achieved by the driver c587-GAL4 in somatic cells of the ovariole tip [48]. All images shown are immunostainings for the p53R-GFPnls biosensor (green), HTS (red) and/or DAPI (blue) except for panel D which was co-stained with α-Vasa (red) to show that p53 activated cells retain the germline marker in *bam* mutants. All other panels (A-C, E-H) were stained with α-HTS (red). Note that panel D stained with α-Vasa is the same *bam* ovariole shown in C with α-HTS. Relevant quantification including the nanosGal4 driver alone are shown in Figure 5-table supplement 1. Scale bars=10μm.

Wan-Jin Lu made the observations presented in Figure 2-11. Wan-Jin Lu took the images for panels A, G and H. Dr. Michael Buszczak provided guidance in experimental design and provided the following fly strains: nanos>TKV, c587>DPP, and c587>LSD1[KD]

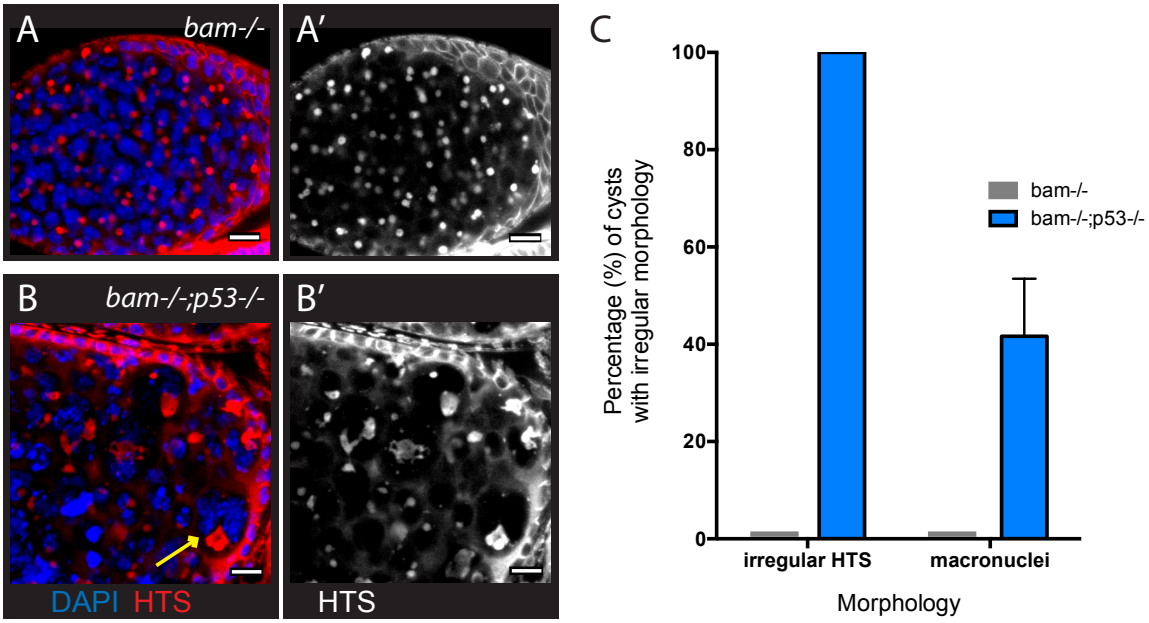

Figure 2-12. Abnormal fusomes and irregular nuclei are seen in bam$^{-/-}$p53$^{-/-}$ tumors.
(A-A') Cells in bam$^{-/-}$ tumors have rounded fusomes normally associated with the undifferentiated GSC fate. These are detected by α-HTS staining (red in B, white in B'). The nuclei of these cells have diameters less than 10μm (blue in B).
(B-B') bam$^{-/-}$;p53$^{-/-}$ tumors frequently exhibit disorganized fusomes detected here by α-HTS staining (red in C, white in C', yellow arrowhead). These tumors also have many fragmented and enlarged nuclei with a diameter significantly greater than 10μm (blue in C, yellow arrow).
(C) Quantification of altered fusome structure and irregular nuclei in bam$^{-/-}$ and bam$^{-/-}$;p53$^{-/-}$ tumors. Note that in panel C, counts for irregular nuclei do not include micronuclei. A total of 14 cysts were assayed in bam$^{-/-}$;p53$^{-/-}$ and 8 cysts were assayed for bam$^{-/-}$. All scale bars, 10μm.

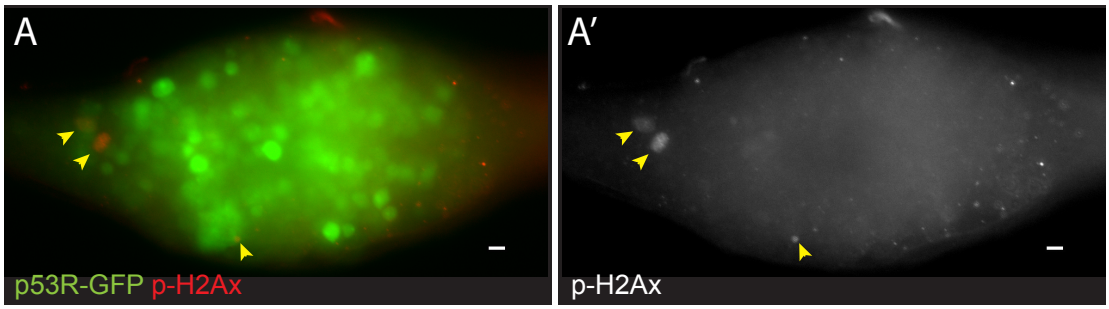

Figure 2-13. Reporter induction during forced proliferation signals is independent of DNA damage.
(A) immunostaining for α-pH2Av (red) and p53R-GFPnls (green) in *bam*$^{\Delta 86}$ ovaries. **(A')** shows α-pH2Av channel from (A). Note the incidence of pH2Av (arrows) is rare and infrequently colocalizes with GFP.
Wan-Jin Lu performed the experiments presented in Figure 2-13.

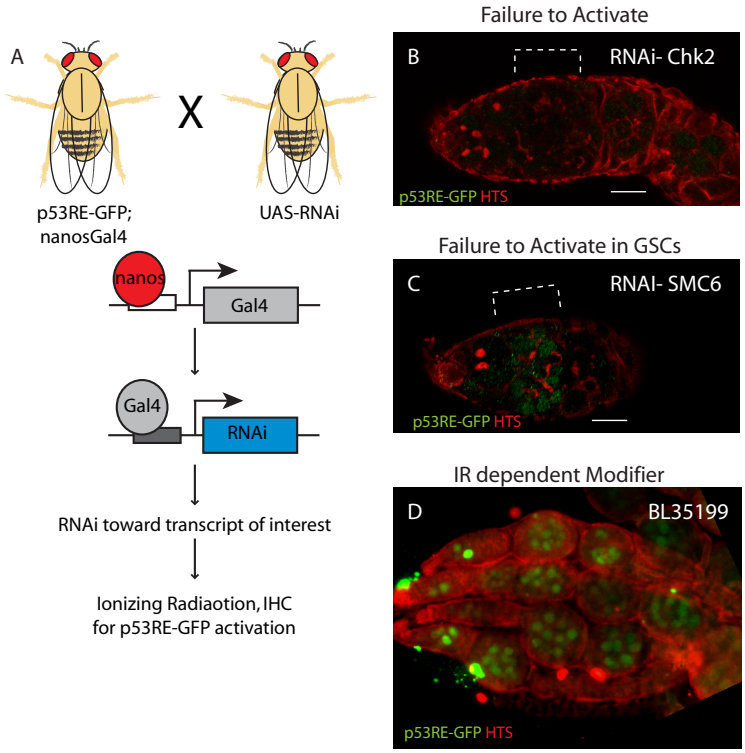

Figure 2-14.An unbiased *in vivo* RNAi screen to find upstream regulators of p53 in GSCs

(A) Diagram of an *in vivo* RNAi screen to identify genetic components in involved in selective p53 activity. Female fly strains carrying the p53R-GFP reporter and a nanosGal4 driver are crossed to fly strains carrying an RNAi transgene under the control of the UAS promoter. Nanos is a germline specific transcription factor and promotes the production of Gal4 in the *Drosophila* germline. The Gal4 transcription factor binds to the Gal4 Upstream Activating Sequence (UAS, dark grey box) and promotes expression of RNAi transcripts that target the gene of interest for destruction. Flies containing all three transgenes (p53R-GFP, nanosGal4, UAS-RNAi) are irradiated and ovaries are assessed for p53R-GFP activity. **(B)** Example of a screen hit where the p53RE-GFP reporter (green) fails to activate in the GSCs (round fusome, HTS in red) and meiotic cells (brackets). This is classified as a 'Failure to activate generally." **(C)** Example of a screen hit where the p53RE-GFP reporter (green) fails to activate in the GSCs (round fusome, HTS in red) but meiotic progenitors (bracket) are still responsive (brackets). This is classified as a 'Failure to activate in GSCs only." **(D)** Example of a screen hit where widespread p53RE-GFP reporter activation (green) is observed outside of the stem cell compartment upon ionizing radiation. This is classified as an 'IR dependent modifier.'

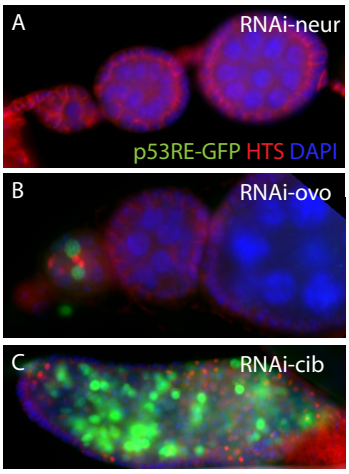

Figure 2-15. 'Stem Cell Phenotypes' observed in the RNAi screen.
Abnormal ovary development and 'stem cell phenotypes' were observed in a significant proportion of RNAi targets. **(A)** Example of a screen hit where stem cells are lost as noted by a lack of rounded fusomes with HTS staining (red). This class produced a false 'Failure to activate' since the stem cells were not present to activate the p53RE-GFP reporter (green) **(B)** Example of a screen hit where stem cells are retained (round fusome, HTS in red) and activate the p53RE-GFP reporter (green) but egg chambers are progressively lost. **(C)** Example of a screen hit where block in differentiation leads to a tumorous cyst of stem-like cells. Similar to $bam^{-/-}$ ovaries, widespread p53RE-GFP reporter activation (green) is observed.

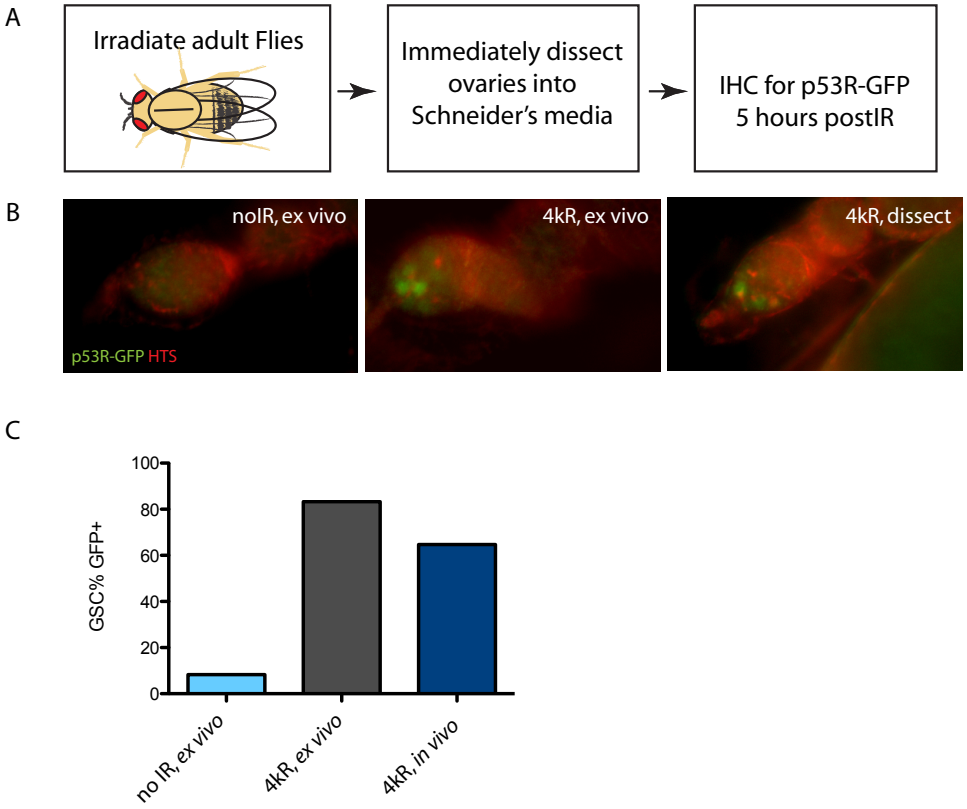

Figure 2-16. *Ex vivo* biosensor activation in the *Drosophila* ovary
(A) Diagram for assessing *ex vivo* p53R-GFP biosensor activation. Transgenic flies carrying the p53R-GFP were irradiated. Immediately after IR, the ovaries ere dissected and placed on Schneider's media supplemented with Fetal Bovine Serum (FBS). The ovaries were kept in media for 5hrs then fixed for immunostaining. Representative images of germaria stained for GFP (green) and HTS (red) are shown in **(B)**. The left panel is a representative image of an unirradiated ovary that was dissected and kept on media for 5 hrs. Note that unirradiated GSCs in *ex vivo* conditions do not robustly activate the p53R-GFP as quantified in **(C).** For the middle panel in **(B)**, ovaries were dissected and placed on media immediately after IR. Stem cell activation is observed at comparable levels to irradiated *in vivo* ovaries that were dissected 5 hours after IR (right panel), as quantified in **(C).**

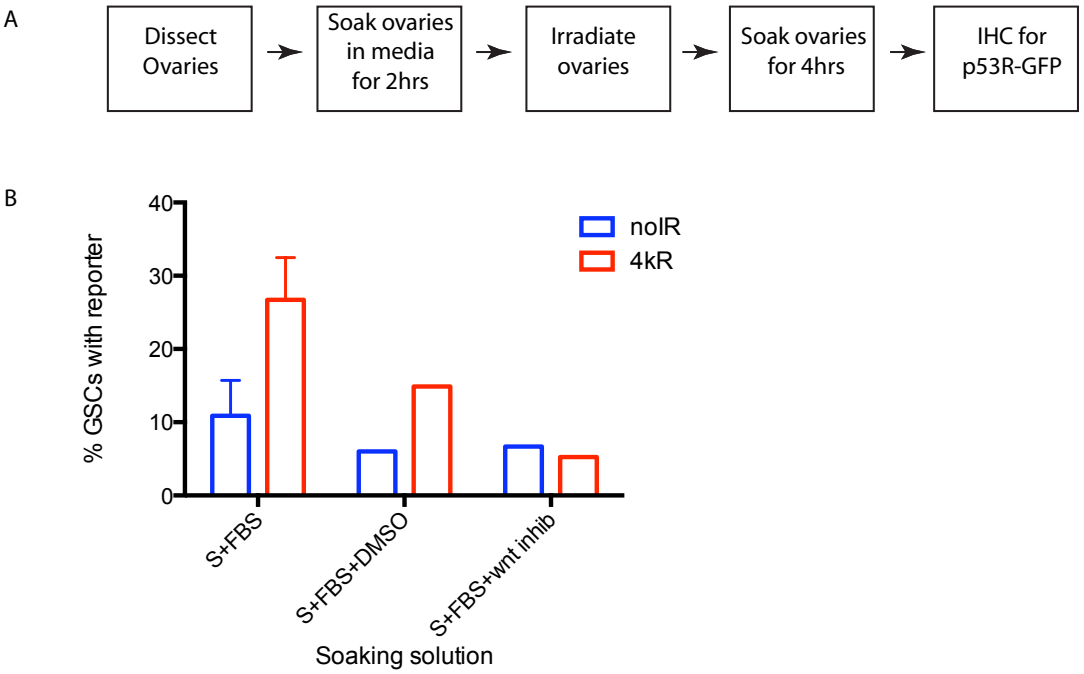

Figure 2-17 An *ex vivo* chemical screen in the *Drosophila* ovary
(A) Diagram of the *ex vivo* chemical screen to identify components involved in selective p53R-GFP biosensor activity. Ovaries from transgenic flies carrying the p53R-GFP dissected into Schneider's media, after soaking in media for 2 hours, ovaries were irradiated in a watch-well, placed in fresh media for 4hours, and fixed for immunostaining.
(B) Quantification of biosensor activation in ovaries soaked in Schneider's + FBS, Schneider's + FBS+DMSO, or Schneider's + FBS+ wnt inhibitor cocktail.
Elevated reporter activation is observed after ionizing radiation in ovaries soaked in Schneider's + FBS, Schneider's + FBS+DMSO (compare blue bars to red bars). Reporter induction was reduced in ovaries soaked in the wnt inhibitor cocktail.

(A)

		Unirradiated		Irradiated	
Genotype and organ	**Reporter**	**% GFP+**	**Total (n=)**	**% GFP+**	**Total (n=)**
WT ovary	*p53R-GFPcyt*	4.3	196	90.6	206
WT Testes	*p53R-GFPcyt*	0	10	100	27
WT ovary	*p53R-GFPnls*	11.9	315	-	-
$p53^{-/-}$ ovary	*p53R-GFPnls*	0	445	0	57
$p53^{-/-}$ Testes	*p53R-GFPcyt*	-	-	0	10
$chk2^{-/-}$ ovary	*p53R-GFPcyt*	0	163	0	100
$spo11^{-/-}$ ovary	*p53R-GFPcyt*	12.2	348	90.3	134

(B)

Genotype	Reporter	% GFP+ GSC/CB	Total germaria (n=)
I-SceI only	*p53R-GFPnls*	15.05	186
I-SceI/cut site	*p53R-GFPnls*	92.8	259

(C)

		Unirradiated		Irradiated	
Genotype and cell type	**Reporter**	**% GFP+**	**Total (n=)**	**% GFP+**	**Total (n=)**
$ATR^{+/-}$ GSCs	*p53R-GFPnls*	11.11	36	100	24
*$ATR^{-/-}$*GSCs	*p53R-GFPnls*	32.7	110	100	17
$ATR^{+/-}$ Follicle cell	*p53R-GFPnls*	0	36	20.83	24
$ATR^{-/-}$ Follicle cell	*p53R-GFPnls*	0	110	100	17

Table 2-1. Validation of the p53R-GFP biosensors
In A and B reporter activation is quantified as indicated.
(A) Reporter activation in female GSCs/CBs is p53 dependent and Chk2 dependent but independent of the topoisomerase, Spo11. Reporter activation in testis is also stimulus dependent and p53 dependent. p53, Chk2 or Spo11 status are noted in column 1. The reporter used (nuclear or cytoplasmic) is indicated in column 2. Column 3 shows unirradiated controls in which the percent reporter activation in GSCs/CBs is provided as well as the total number of germaria or testis that were assayed. Column 4 shows reporter activation in irradiated tissue at 24hrs post-irradiation with percentage of germaria or testis with GFP positive GSCs/CBs and the number of samples assayed. Quantification of reporter activation is from 3 independent trials in the ovary and 2 independent trials in the testis.

(B) Quantification of p53-GFPnls in region 1 of flies containing I-SceI endonuclease by itself or with the I-SceI cutsite. Reporter activation in I-SceI expressing animals that also have the I-SceI cutsite is comparable to wild type irradiated flies (A). Quantification of reporter activation is from 2 independent trials.

(C) Quantification of p53-GFPnls in GSCs and follicle cells of flies heterozygous ($ATR^{+/-}$) or mutant for ATR ($ATR^{-/-}$). After irradiation challenge, p53 activation is highly penetrant in both $ATR^{+/-}$ and $ATR^{-/-}$ genotypes. ATR mutants show a robust induction of reporter activation in follicle cells after irradiation.

Wan-Jin Lu performed the quantification presented in Table2-1.

(A) Meiotic repair							
Genotype	**Reporter**	**GSC/CB**		**Region3**		**Stage 2-8 egg chamber**	
		%GFP+	(n=)	% GFP+	(n=)	%GFP+	(n=)
rad54$^{+/-}$	*p53R-GFPcyt*	7.03	468	21.36	468	3.17	1528
rad54$^{AA/RU}$	*p53R-GFPcyt*	32.9	1754	68.2	459	48.23	1754
rad50$^{ep1/d5.1}$	*p53R-GFPcyt*	97.0	211	-	-	-	-
(B) Retrotransposon silencing							
Genotype	**Reporter**	**GSC/CB**		**Region3**		**Stage 2-8 egg chamber**	
		% GFP+	**(n=)**	**% GFP+**	**(n=)**	**% GFP+**	**(n=)**
aub$^{+/-}$	*p53R-GFPcyt*	7.0	127	26.4	127	4.3	127
aub$^{QC/HN}$	*p53R-GFPcyt*	82.5	184	58.6	184	81.2	35
cuff$^{+/-}$	*p53R-GFPcyt*	6.73	231	8.6	231	1.3	231
cuff$^{QQ/WM}$	*p53R-GFPcyt*	92.7	332	4.7	332	3.4	281

Table 2-2. Quantification of p53 activation in defective DNA repair and retrotransposon silencing mutants

Mutants defective for **(A)** meiotic repair (*rad54* and *rad50*) and **(B)** retrotransposon silencing (*aubergine* and *cutoff*) have increased spontaneous reporter activation compared to heterozygous controls. The percentage of ovarioles positive for p53R-GFP in the regions indicated (GSC/CB, region 3, stage 2-8 egg chamber) were calculated and the number of ovarioles assayed per region are indicated. Quantification of reporter activation is from 3 independent trials.

Wan-Jin Lu performed the quantification presented in Table2-2.

(A) Cleaved caspase-3 after Irradiation (4.0 krad)										
Genotype	**Non-irradiated**		**x2hr**		**x4hr**		**x8hr**		**x24hr**	
	% CC3	**Total (n=)**	**% CC3**	**Total (n=)**	**% CC3**	**Total (n=)**	**% CC3**	**Total (n=)**	**% CC3**	**Total (n=)**
WT	0.7	141	0	119	8.1	210	0	59	2.2	90
p53$^{-/-}$	0	92	1.8	57	0	155	1.2	81	0	82

(B) BrdU incorporation after Irradiation (4.0 krad)								
Genotype	**Non-irradiated**		**x4hr**		**x24hr**		**x72hr**	
	% BrdU	**Total (n=)**	**% BrdU**	**Total (n=)**	**% BrdU**	**Total (n=)**	**% BrdU**	**Total (n=)**
WT	24.9	381	6.2	291	26.9	286	23.6	288
p53$^{-/-}$	22.7	309	7.4	272	13.9	381	19.2	198
Rescue A1; p53$^{-/-}$	24.6	284	7.8	320	23.7	279	22.1	131
Rescue A2; p53$^{-/-}$	21.9	324	6.3	255	21.8	317	18.6	301

(C) BrdU incorporation after Irradiation (9.0 krad)						
Genotype	**x4hr**		**x2Day**		**x7Day**	
	% BrdU	**Total (n=)**	**% BrdU**	**Total (n=)**	**% BrdU**	**Total (n=)**
WT	4.16	141	35.25	121	31.13	97
p53$^{-/-}$	2.1	61	20	94	13.53	90
A1;p53-/-	2.9	70	27.72	95	19.43	103

Table 2-3. Quantification of proliferative potential and apoptosis of germaria challenged with irradiation.

(A) Quantification of germaria that have cleaved-caspase3 (CC3) positive GSCs/CBs. Columns indicate the time points after irradiation. Rows indicate the genotype. The percentage of germaria that have CC3 positive GSCs/CBs and the number of germaria are quantified from 3 independent trials for the x4hr time point and from 2 independent trials for the non-irradiated, x2hr, x8hr, and x24hr time points. **(B, C)** Quantification of germaria that have BrdU positive cells in region 1. The percentage of germaria that have BrdU positive cells in region 1 and the number of germaria assayed are quantified from 3 independent trials in (B) and 2 trials in (C) per time point.

(A)			
		% GFP+ germaria region 1	**Total (n=)**
nanos>	*p53R-GFPnls*	22.3	76
nanos> Rasv12	*p53R-GFPnls*	47.9	76
nanos>cyclinE	*p53R-GFPnls*	68.6	105

Table 2-4. Quantification of biosensor activity in germline tumors
This table quantifies the number of p53R-GFPnls positive stem-like cells associated with a rounded fusome (α-HTS). Ovaries containing the nanosGAL4 driver alone (control) or the UAS oncogene indicated (Rasv12 or cyclinE) and the same Gal4 driver were scored. Note that the numbers of stem cells activated for p53 is much greater when either rasv12 or cyclinE are present when compared to the control alone.

Pattern description	Percentage among the top 20	Percentage among the whole genome	Fold enrichment
Absent in embryos	95% (19/20)	40.9% (5478/13389)	2.3
Absent in adult somatic tissues	95% (19/20)	30.1% (4029/13389)	3.2
Not localized on X chromosome	13 genes mapped on the second chromosome 7 genes mapped on the third chromosome 0 genes mapped on the X chromosome		

Table 2-5. Expression features of the top 20 genes suppressed by p53
The top 20 genes that were suppressed by p53 in *bam*$^{-/-}$;*p53*$^{-/-}$ tumors (see Table 1) were examined using GEXC [49] to identify enriched pathways. Using this collection we observed a mild enrichment for genes that were absent in embryos or absent in adult somatic tissues relative to all genes in the fly genome.

	Downregulated by p53	
	Gene Symbol	Fold Change
1	CG31681	8.7
2	CG5156	8.0
3	LysX	7.9
4	CG31901	7.6
5	CG16762	7.5
6	CG32277	7.3
7	CG17239	7.2
8	CG17012	7.1
9	CG9897	7.1
10	Ser12	6.8
11	CG2191	6.8
12	CG33258	6.6
13	CG18125	6.5
14	CG12780	6.4
15	CG4783	6.3
16	Cyp6a18	6.3
17	CG17234	6.2
18	CG18063	6.2
19	CG9568	6.1
20	CG32834	6.0

Upregulated by 53	
Gene Symbol	Fold Change
CG31809	-7.2
CG31810	-5.6
CG2177	-5.2
CG7106	-5.1
CG1504	-4.5
CG15614	-4.3
unpg	-4.2
CG7329	-4.2
CG15236	-4.1
CG9294	-4.1
esg	-3.9
Ugt36Ba	-3.7
CG14297	-3.6
CG17129	-3.6
Cyp6a14	-3.6
CG5568	-3.4
CG1077	-3.3
CG11226	-3.3
CG33105	-3.1
CG3328	-3.1

Table 2-6. p53 status impacts expression profiles in *bam*$^{-/-}$ tumors
We performed microarray analysis on bam$^{-/-}$ and bam$^{-/-}$;p53$^{-/-}$ tumors. The genes that are altered by p53 status in bam$^{-/-}$ tumors are recorded. Listed on the left are the top 20 genes whose abundance is directly or indirectly suppressed by p53. Listed on the right are the top 20 genes whose abundance is directly or indirectly induced by p53. The gene symbol is listed on the left and the fold change in gene expression between bam$^{-/-}$ and bam$^{-/-}$;p53$^{-/-}$ tumors is listed on the right. Note that the expression of many genes listed here are dramatically affected when p53 is absent.
Wan-Jin Lu performed the microarray analysis presented in Table 2-6.

Failure to Activate Generally		
	RNAi Line Symbol	Gene
1	35721	Lola
2	33627	SMC6
3	35152	Chk2
Failure to Activate in GSCs		
4	36081	SMC6
IR independent GSC Activity		
5	32901	Twin
6	35454	Shutdown
7	35171	Rhino
8	35643	PI4KIIIalpha
9	35182	cuff
IR dependent Modifiers		
10	32911	Tctp
11	35199	Cdk7
12	35218	PyK
13	35393	smi35A
14	35642	BEAF-32
15	35415	stwl
16	35458	dpa
17	35242	dalao
18	35394	aret
19	35267	cdc2c
20	36067	
IR independent Modifiers		
21	35029	VhaAC39-1
22	36583	Dhc64C
23	35157	Pitslre
24	35428	TfIIFalpha
25	35724	pita
26	35425	yemalpha
27	33339	wde
28	33654	CycE
29	35392	sti
30	35406	cup,CG34310
31	35484	nop5
32	35388	ash2
33	35204	Ars2
34	32478	Caf1-180
35	35421	hts
36	35592	Tfb5,CG31917
37	35407	G-ialpha65A
38	33631	bam

Table 2-7High priority hits for RNAi Screen to identify upstream regulators of p53 in GSCs.

The RNAi screen identifier is on the left and the gene symbol that is targeted is listed on the right. Note when we observed constituteively active p53R-GFP activity in stem cells without IR (5-9), these genes have previously been implicated in transposon regulation. This is similar to the results found in Figure 2-4 where aubergine and cutoff mutants were had p53 activity in GSCs.

Chapter 3:

p53 genes act to restrain mobile elements

In my third year of graduate school, I discovered that p53 genes act to restrain mobile elements. Wan-Jin Lu, a previous graduate student in the Abrams lab, made two initial observations that laid the ground work for this project: 1) lesions in the *Drosophila* piRNA pathway consistently triggered p53 activity and 2) p53 genetically interacted with the piRNA pathway. Alex D'Brot, a postdoc in the Abrams Lab, generated the 'humanized' flies used in this chapter. I performed all other experiments described here in collaboration with several faculty members: James F. Amatruda, John V. Moran, Dinesh Rakheja, Sarah Comerford, Robert Hammer, and Christine Garcia. A manuscript describing these findings is under invited resubmission at *Genes and Develompent*.

SUMMARY

p53 genes occupy central positions in stress response networks throughout the animal kingdom and the human member of this gene family is mutated in most cancers. p53 proteins specify adaptive transcriptional responses, but precisely how downstream targets mediate tumor suppression is not well understood. Using *Drosophila*, zebrafish, and mouse models, we show that p53 functions to restrict the activity of retrotransposons. Furthermore, *Drosophila* p53 genetically interacted with components of the piRNA pathway and, in complementation

studies, normal human p53 alleles restrained mobile elements, but mutant p53 alleles from cancer patients could not. Consistent with these results, we also found patterns of unrestrained retrotransposons in p53-driven human cancers. Together, these observations indicate that ancestral functions of p53 operate through conserved mechanisms to suppress retrotransposons. Furthermore, since human p53 mutants are disabled for this activity, our findings raise the possibility that p53 mitigates oncogenic disease, in part, by restricting retrotransposon mobility.

INTRODUCTION

The broadly conserved p53 family of transcription factors regulates target genes to specify distinct adaptive responses [1-3]. Although p53 mutations occur in most human cancers, the precise mechanisms by which p53 acts to restrict oncogenesis are not well understood. In mice, for example, p53 retained tumor suppression activity despite the combined absence of three downstream canonical effector proteins (p21, Puma, and Noxa) that arrest proliferation and engage apoptosis [7]. Moreover, evolutionary analyses strongly suggest that the p53 gene clearly predates the adaptive need for tumor suppression. Thus, tumor suppression by p53 was likely co-opted from unknown ancestral functions conferred by this gene family [14]. These and related observations suggest the existence of crucial, unidentified p53 effectors and highlight conspicuous gaps in our understanding of p53 function.

It is well appreciated that genotoxic stress leads to p53 activation. As described in Chapter 2 of this dissertation, using validated p53 biosensors as *in vivo* proxies, we examined the *Drosophila* germ line after radiation challenge. Despite widespread genotoxic damage to all cells, functional p53 activity occurred only in the stem cell compartment of both the ovary and the testes (6). While exploring the role of p53 in this context, we made a series of observations that justify a comprehensive examination of the relationship between p53 and transposon biology. We found that lesions in the Drosophila piRNA pathway consistently triggered p53 activity[64] (Figure 2-5A,B) raising the possibility that p53 might function to restrain retrotransposons that are targets for piRNA suppression. This underlying observation led to the findings described in this Chapter.

Transposons are mobile elements that are present in prokaryotes and eukaryotes. Generally, there are two types of transposons: DNA transposons mobilize through a 'cut and paste' mechanism and retrotransposons move through a 'copy and paste' mechanism [65]. As outlined in Figure 3-1, retrotransposons encode essential proteins for mobilization and propagate through an RNA intermediate, are reverse transcribed, and integrate into the genome [65]. Retrotransposons have dramatically influenced the size of eukaryote genomes and are thought to comprise over 40% of the human and mouse genomes [65]. The majority of these are fossilized remnants of past integrations events but the human genome contains ~100 copies of LINE-1 retrotranpsosons

that are transposition capable [66,67]. These can be a source for genomic instability since the propagation event can be mutagenic and has been shown to cause human disease [68]. However, there are systems in place that restrain mobile elements, most prominently the highly conserved piRNA pathway acts in the germline in *Drosophila*, mice and humans to repress mobile elements. The piRNA pathway consists of small, 24-32 nucleotide long, small RNAs called PIWI-interacting RNAs (piRNAs) that associate with PIWI subfamily members of the Argonaute family of proteins [69]. These piRNAs are complementary in sequence to their retrotransposon target sequence and the piRNA- PIWI protein complexes inhibit retroelements by cleaving the RNA transcripts, inhibiting translation, or promoting gene silencing through chromatin modifications [69]. Thus, mutations in the piRNA pathway lead to massive transposon activity and fertility defects in the germline of *Drosophila* and mammals [70,71].

MATERIALS AND METHODS

Fly Stocks and Genetics

All fly stocks were maintained at 22-25°C on standard food media. We obtained *aubergine* and *cutoff* mutants: *aub*HN, *aub*QC, *cuff*WM, and *cuff*QQ from T. Schupbach (Princeton University, Princeton, NJ, USA). All other stocks were obtained from Bloomington Stock Center (Indiana University, Bloomington, IN, USA). Unless otherwise noted, two p53 null alleles, 238H (ns) and 5A-1-4 (k1), were used in trans-combination to reduce genetic background influences. Two

wild type strains, yw and w1118, were used in trans-combination for comparison. The Spo11 mei-W68[1] allele was obtained from the Bloomington Stock center and was crossed into the $p53^{-/-}$ 238H (ns) and 5A-1-4 (k1) strains. To test genetic interactions between Spo11 and p53, we generated flies that had the p53 alleles in trans : $Spo11^{-/-}$;$p53^{-/-}$[ns]/[k1]. As previously described in [64] the Dp53 rescue strain was engineered by φC31 integration of a 20kb genomic fragment BAC containing the Dp53 locus into an attP site on the X chromosome of the PBac{y+-attP-9A}VK00006 line (Bloomington #9726). The parent BAC CH322-15D03 was obtained from the P[acman] resource library [45] and Rainbow Transgenic Flies performed the injection and screening for recombinants. The Dp53 rescue strain was crossed into two p53 null alleles, 238H (ns) and 5A-1-4 (k1), and used in trans-combination to reduce genetic background influences, unless otherwise noted. Similarly, as described in [58], the humanized p53 lines were generated by replacing the Dp53 ORF of BAC CH322-15D03 with either wild type or mutant human p53 cDNA via recombineering and then integrating into the attP site on the X chromosome of the PBac{y+-attP-9A}VK00006 line (Bloomington #9726). The five p53 hot-spot mutants, which represent the five most mutated hot-spot codons, were generated by site-directed mutagenesis of the p53 cDNA before recombineering into the BAC. The p53[EGFP] allele was generated in the Hugo Bellen Lab using the mimic system [72] and Paula Kurtz, a graduate student in the lab, characterized this additional p53 allele as a severe hypomorph. For Figure 3-18 and Figure 3-19, the $p53^{-}$, Dp53Rescue, and all

humanized lines were in homozygous for fly p53 5A-1-4 (k1) null allele and were compared to yw WT strain.

RT-PCR

Mobilization of retrotransposons was assayed using elevated transcript levels as a surrogate for transposition. WT, $p53^{-}$, and p53Rescue fly ovaries were dissected in PBS and total RNA was isolated using TRIzol® reagent (Life Technologies, Grand Island, NY, USA). RNA was isolated from single ovary pairs for Figure 3-2B. Five ovary pairs per RNA preparation were used for all other RT-PCR data. cDNA was generated using iScript cDNA synthesis kit (Bio-Rad, Hercules, CA, USA). Semi-quantitative RT-PCR was performed using GoTaq Green Master Mix (Promega, Madison, WI, USA). Samples were run on a 1.2% Ethidium Bromide gel and visualized on the Typhoon Trio Imager. Quantitative RT-PCR was performed using the iQ SYBR Green Supermix (Bio-Rad) on the CFX96 real time PCR machine (Bio-Rad). Primer efficiency was taken into account for all reactions. rp49 was used for normalization. Controls for DNA contamination include reactions with and without reverse transcriptase. Primers are listed in Table 3-6. Droplet digital RT-PCR reactions were previously described [73]. Primers and fluorescent probes specific for the TAHRE transcript are listed in Table 3-6. rp49 was used for normalization.

Fluorescent *in situ* hybridization (FISH)

Custom Stellaris® FISH Probes were designed against TAHRE transcripts by utilizing the Stellaris® RNA FISH Probe Designer (Biosearch Technologies, Inc., Petaluma, CA,USA) available online at www.biosearchtech.com/stellarisdesigner (version 4.1). The wt, $p53^{-}$, and p53Rescue ovaries were hybridized with the TAHRE Stellaris RNA FISH Probe set labeled with Quasar 570 (Biosearch Technologies, Inc.), following the manufacturer's instructions available online at www.biosearchtech.com/stellarisprotocols. Briefly, ovaries were dissected into PBS and fixed at room temperature for 45 minutes with 4% formaldehyde solution in PBS. After fixation, ovaries were placed in 70% EtOH overnight at 4ºC. The following day, the EtOH was aspirated and wash buffer (2x SSC, 10% deionized formamide in nuclease free water) was added for 5 minutes. The probe was diluted at a concentration of 50nM in hybridization buffer (2x SSC, 10% Dextran Sulfate (D8906, Sigma, St. Louis, MO, USA), 1mg/mL tRNA (R8759, Sigma), 2mM Vanadyl robonucleoside complex (New England Biolabs, Ipswich, MA, USA), 10% deionized formamide in nuclease free water). The wash buffer was aspirated and the hybridization+probe solution was added to each sample and placed at 37ºC for 24hrs. The samples were then washed with wash buffer for 2 times at 37ºC for 30 minutes each. VECTASHIELD (Vector Laboratories, Burlingame, CA, USA) with DAPI was added before mounting and imaging. Probes are listed in Table 3-6.

Embryo Collections

Embryos from WT (yw), *p53*$^{-}$ [K1], and p53Rescue;p53^{-} [k1] strains were collected on standard juice agar plates for 3hours and aged 1hour for early stage embryos or aged 21 hours for late stage embryos. Embryos were collected and dechorionated in 50% bleach, washed, and transferred to trizol for RNA extraction. For maternal loading assays, WT virgin females were crossed to p53^{-} males and p53^{-} virgin females were crossed to WT. Embryos from these parental genotypes were collected for 3hours, aged 1hour, and processed for RNA extraction.

***Drosophila* Fertility Studies**

In fertility assays, the p53 null allele, 238H (ns), was compared to the p53 rescue transgene in the p53ns background (p53Rescue). To reduce genetic background influences the p53ns allele and the p53 rescue transgene were backcrossed into the yw wild type background for 17 and 10 generations respectively. Female virgins were collected for 5 days. To assess fertility at the single animal level, one female virgin and three yw wild type males were placed in a vial. Females were allowed to lay eggs for four days and fertility was scored by presence of larvae ten days after the parents were removed.

Egg Phenotypes

As previously described [23] eggs were collected on standard juice agar plates and manually orientated horizontally on the plate with a paint brush for imaging. Images were taken on the Zeiss SteREO Discovery V.12 and processed with Image J using the following script: “Enhance Contrast (saturated=0.5), RGB Color, Set Scale (distance=0 known=1 pixel=1 unit=pixel)”. Sample sizes, n= 419 (*aubHN/QC; p53ns/k1*), 298 (*aubHN/+; p53ns/k1*), 312 (*aubHN/+*), 469 (*aubHN/QC*), 248 (*cuffQQ/WM; p53ns/k1*), 891 (*cuffQQ/+; p53ns/k1*), 153 (*cuffQQ/+*), 564 (*cuffQQ/WM*). Prism 6 software (GraphPad, San Diego, CA, USA) was used to perform statistics.

Immunostaining of Fly Tissue

3-5 days old well-fed females were dissected in PBS and fixed in 4% EM-grade formaldehyde (Polysciences, Warrington, PA, USA) diluted in PBS-0.1% triton x100 (PBST), with three times the volume of heptane. After washing, tissues were blocked in 1.5% BSA, and then incubated with primary antibodies at 4ºC overnight. Antibodies used: α-aubergine and α-armitage were gifts from Mikiko Siomi [74,75], α-rhino was gift from William Theurkoff [76], and α-vasa (DSHB, Iowa City, IA, USA). For fluorescence visualization, Alexa-488 (Invitrogen, Grand Island, NY, USA) secondary antibody was used and 0.1µg/mL of DAPI (Invitrogen) for DNA staining was added in the first wash step. After three

washes, ovaries were further hand dissected and mounted in VECTASHIELD (Vector Laboratories) for microscopy imaging.

Ionizing Radiation Studies

Well-fed WT and p53- flies were exposed to ionizing radiation using a Cs-137 Mark 1-68A irradiator (J.L. Shepherd & Associates, San Ferando, CA, USA) at a dose of 11.5 krad. All vials were exposed to IR at the same time on a rotating turntable inside the irradiator. Ovaries were dissected in PBS at 15 minutes, 1 hour, 4 hour, and 24 hours post irradiation along side an unirradiated control. 5 ovary pairs per RNA prep were placed in Trizol on ice and were processed as outlined in the RT-PCR part of the methods.

DNA FISH on *Drosophila* Salivary Glands

TAHRE and HeT-A regions of interest were PCR amplified with the iProof High Fidelity polymerase on WT genomic DNA. See Table.. for primer sequences. The PCR products were labeled with Invitrogen's FISH Tag DNA Multicolor kit and purified as suggested. Whole mount salivary glands from WT and $p53^{-/-}$ larvae were fixed in 4% formaldehyde in PBS and hybridized as described in *Drosophila* protocols (Sullivan et al. 2000).

Zebrafish Maintenance, Strains, and Injections

Zebrafish were maintained according to standard procedures [77]. All work with zebrafish was carried out under protocols approved by the Institutional Animal Care and Use Committees at University of Texas Southwestern Medical Center (Dallas, TX), an Association for Assessment and Accreditation of Laboratory Animal Care (AAALAC)-accredited institution. The pLRE3-*mEGFPI* and pLRE3H230A-*mEGFPI* constructs have been previously described [78-80]. These constructs were injected into 1 to 2 cell zebrafish embryos from the parental AB (wt) or *p53*$^{-}$ strains (*tp53*$^{M214K/M214K}$). 2-4 nL of each construct was injected injected at a concentration of 125ng/uL and the injection mixture included phenol red and 0.3x Danieau's Solution (1740 mM NaCl, 21mM KCl, 12 mM MgSO4•7H2O, 18 mM Ca(NO3)2, 150 mM HEPES buffer). Uninjected controls were carried alongside for both genotypes.

Immunostaining of Zebrafish Tissue

Forty-eight-hour-old embryos were dechorionated, euthanized with tricaine, and fixed in 4% EM-grade formaldehyde (Polysciences) diluted in PBS-0.1% triton x100 for 24 hours at 4ºC. 11-hour-old embryos were fixed in 4% EM-grade formaldehyde (Polysciences) diluted in PBS-0.1% triton x100 for 24 hours at 4ºC or 4 hours at room temperature and then hand-dechorionated. After washing, tissues were blocked in 1.5% BSA, then incubated with anti-GFP (1:1000, Thermo Fisher Scientific, Waltham, MA, USA) or anti-human ORF1 (1:500)

primary antibody at 4°C overnight. The anti-human ORF1 monoclonal antibody was a gift from Kathleen Burns, Johns Hopkins University) [81]. For fluorescence visualization, Alexa-488 (Invitrogen) or Alexa-568 (Invitrogen) secondary antibody was used. After three washes, zebrafish were placed in PBS or mounted in 1% Agar in PBS for microscopy imaging.

Zebrafish Fertility Studies

To assess fertility in zebrafish, WT and $p53^{-/-}$ matings were set up. Embryos were collected within 2 hours of laying. For each genotype, we documented the total number of eggs and the number of unfertilized eggs layed within the first 6 hours after laying to obtain the percentage of unfertilized embryos (Table 3-5). This was performed over 3 individual trials, each trial containing 20 or more adult zebrafish per genotype. WT and $p53^{-/-}$ adult zebrafish were age matched.

Preparation of Ovary Extracts and Western Blot Analysis

For each humanized fly strain and $p53^{-}$ control, 20 ovaries were dissected into PBS, then homogenized with a glass pestle in RIPA lysis buffer and protease inhibitor cocktail (Roche). Extract concentration was measured by standard Bradford protein assay. 20µg of tissue extracts were subjected to 10% SDS-PAGE (NuPAGE, Invitrogen), after which the proteins were transferred to PVDF membrane. The immunoblots were performed at 4°C overnight using the following primary antibodies: mouse anti-hp53 DO-1 (Santa Cruz Biotechnology)

was used at 1:1000 and 1:5000 anti-tubulin (E7, Developmental Studies Hybridoma Bank, University of Iowa). Bound antibodies were visualized by chemiluminescence ECL Plus kit (Amersham Biosciences/GE Healthcare) using a 1:5000 dilution of anti-mouse IgG (Jackson ImmunoResearch Laboratories, Inc.).

Mouse Strains and Immunostaining

17kT and T-antigen mice were generated using bi-genic transgenes as described in [82]. .Briefly, Bi-genic ApoE-rtTA:TRE2-Tag or ApoE-rtTA:TRE2-1kT transgenic mice expressing the 2.7□kb SV40 early region in the liver in a doxycycline (dox)-dependent manner were generated as described in([82]). For the Myc liver tumor mouse model, Albumen-driven Myc transgene was highly expressed in the liver to induce hepatocellular carcinoma. These mice were placed in either the WT or $p53^{-/-}$ backround. Rabbit anti-mouse IAPgag (Bryan Cullen) and rabbit anti-mouse LINE-1 ORF1p (Alex Bortvin) expression was assessed in mouse tissue sections. Briefly, slides were deparaffinized and rehydrated in 10 minute washes of Xylene (2x), 100% Ethanol (2x), 95% Ethanol, 70% Ethanol, 50% Ethanol, and DI water (2x). Endogenous peroxidases were blocked with 3%Hydrogen Peroxide and microwave antigen retrieval was performed with sodium cintrate bfr for 10 minutes. Slides were blocked in 10% Normal Goat Serum for 1 hour and incubated in primary antibody overnight (1:500 for IAPgag, and 1:500 for LINE-1 ORF1p). The next day, slides were washed in PBS two times, for 5 minutes and

incubated in goat anti-rabbit IgG Biotin (Jackson #111-065-045) at a 1:500 concentration for 2 hours. Slides were then washed with PBS and incubated in Streptavadin-HRP (1:750) for 2hours. The retroelement signal was exposed with AEC substrate and slides were counterstained with Hematoxylin.

Wilms Tumor Immunostaining

Wilms tumor samples were collected as previously described [83]. Deparaffinization and immunostaining of $p53^{+}$ and $p53^{-}$ Wilms tumors were performed in parallel. Antigen retrieval was performed with Sodium Citrate Buffer (10mM Sodium Citrate, 0.05% Tween 20, pH 6.0) in a pressure cooker. Tissue sections were then permeabilized at room temperature with PBS + 1%TritonX-100 (PBST) for 1 hour and then blocked with blocking solution (5% Normal Donkey Serum, 1% Bovine Serum Albumin in PBST) for 2-4 hours. The mouse anti-Human ORF-1 primary antibody [81] was diluted at a concentration of 1:500 in blocking solution and samples were incubated at 4ºC overnight. For fluorescence visualization, Alexa-488 (Invitrogen) secondary antibody was used. After three washes, VECTASHIELD with DAPI (Vector Laboratories) and a coverslip was placed on the slide for microscopy imaging.

Microscopy and Image Processing

Fluorescent *in situ* hybridization confocal images (Fig. 1C) were taken with a Leica TCS SP5 confocal microscope using a 40X objective lens with 3X digital

zoom with Leica software. *Drosophila* ovary (SFig. 3D-G') and Wilms tumor confocal images (Fig. 5A and SFig. 5 and SFig. 6) were taken with a Multiphoton Zeiss LSM780 inverted confocal microscope using a 40X objective lens with 3X digital zoom with Zeiss Zen software. Zebrafish 11 hour post fertilization embryo confocal images for ORF1p quantification were taken with a Multiphoton Zeiss LSM780 upright confocal microscope using a 10X objective lens with Zeiss Zen software. Fluorescent images of whole-mount zebrafish were taken on the Zeiss SteREO Discovery V.12 microscope using the 1.50x lens with AxioVision software. 48 hour post fertilization embryos were imaged with 18x zoom and 11 hours post fertilization embryos were imaged with 65x zoom. Antibody staining or FISH signal image comparisons between wt and $p53^{-}$ samples were done with the same laser image intensities and master gain settings. Z-stacks were taken at 0.5um sections. Z-stacks of images were projected using Image J software (NIH, Bethesda, MD, USA). Figures were prepared using Adobe Photoshop and Illustrator CS2 (Adobe Systems, San Jose, CA, USA).

Zebrafish 11hour post fertilization ORF1p Image Processing

Eleven hour post fertilization (hpf) embryos were mounted in 1% agarose in PBS. Embryos were imaged on the Multiphoton Zeiss LSM780 upright confocal microscope. To obtain the ORF1p volume using Imaris8 software (Bitplane, Zurich, Switzerland), the surface of the ORF1p was built using a baseline subtraction of 10,000. To obtain the embryo volume using Imaris8 software

(Bitplane), the surface of the embryo autofluorescence was built using a baseline subtraction of 2000. The ORF1p volume was divided by the embryo volume and multiplied by 100 to obtain the $ORF1^+$ Volume/embryo in percent (%) (Fig. 3B'). Embryos were imaged for one trial but similar ORF1p expression patterns between wt and $p53^-$ embryos were repeated over multiple trials.

Wilms Tumor Image Processing

10 fields of view were taken on the Multiphoton Zeiss LSM780 inverted confocal microscope for each tumor and matched normal kidney. Images were deconvoluted with AutoQuant (AutoQuant, Albany, NY, USA) software using 10 iterations of 3D deconvolution. The average fluorescence of intensity of the ORF1 signal for each field of view was obtained using Image J software. The Z-stacks were projected using the sum slices projection type and the mean grey value was recorded. The average fluorescence intensity of the ORF1 signal was normalized to the nuclei density. To obtain the nuclei volume using Imaris8 software (Bitplane), the surface of the blue channel was built using a baseline subtraction of 15,000. The ORF1 mean grey value was divided by the nuclei volume per field of view. To obtain the normalized fluorescence intensity, all images were then normalized to the average value of all 10 fields of view for the CMC87 sample.

Statistics

For all statistical analysis, data were placed into GraphPad Prism software. For statistics on the ddPCR of TAHRE transcripts on single fly ovaries (Fig. 1B), a one-way ANOVA test was performed on all genotypes and $p53^{-/-}$ was significantly different from wt (p value = 0.0172) and p53Rescue (p value = 0.0347) at the 95% confidence interval. Quantification of TAHRE FISH (Fig. 1C'), was analyzed using a two-tailed unpaired t-test. At the 99% confidence level, wt was significantly different from $p53^{-/-}$ (p value = 0.001). Note that THARE FISH on the p53Rescue was performed once and statistics could not be calculated.

For statistics on the qRT-PCR of retroelement transcripts on bulk ovaries (Fig. 1D, D'), a one-way ANOVA test was performed on all genotypes at the 95% confidence interval. For Idefix, $p53^{-/-}$ was significantly different from wt (p value = 0.0278). For TAHRE, $p53^{-/-}$ was significantly different from wt (p value = 0.0094) and p53Rescue (p value = 0.0234). For Burdock, $p53^{-/-}$ was significantly different from wt (p value = 0.0028) and p53Rescue (p value = 0.0031). For HeT-A, $p53^{-/-}$ was significantly different from wt (p value = 0.0004). For Gypsy, $p53^{-/-}$ was significantly different from wt (p value = 0.0002) and p53Rescue (p value = 0.0016).

For statistics on the qRT-PCR of retroelement transcripts on WT, $Spo11^{+/-};p53^{-/-}$, and $Spo11^{-/-};p53^{-/-}$ ovaries (Fig. 2), a one-way ANOVA test was performed on all

genotypes at the 95% confidence interval. For TAHRE, Spo11$^{+/-}$;p53$^{-/-}$ was significantly different from wt (p value = 0.0004) and Spo11$^{-/-}$;p53$^{-/-}$ (p value = 0.0035). For HeT-A, Spo11$^{+/-}$;p53$^{-/-}$ was significantly different from wt (p value = 0.0218) at the 95% confidence interval and Spo11$^{-/-}$;p53$^{-/-}$ (p value = 0.0803) at the 90% confidence interval. For Idefix, Spo11$^{+/-}$;p53$^{-/-}$ was significantly different from wt (p value = 0.0315) and Spo11$^{-/-}$;p53$^{-/-}$ (p value = 0.0164). For Gypsy, Spo11$^{+/-}$;p53$^{-/-}$ was significantly different from wt (p value = 0.0051) and Spo11$^{-/-}$;p53$^{-/-}$ (p value = 0.0068). For Burdock, Spo11$^{+/-}$;p53$^{-/-}$ was significantly different from wt (p value = 0.0516) at the 90% confidence interval and Spo11$^{-/-}$;p53$^{-/-}$ (p value = 0.006) at the 95% confidence interval.

Quantification of ORF1p expression in wt and p53$^{-/-}$ zebrafish injected with the pLRE3-mEGFP reporter (Fig. 3B') was analyzed using a two-tailed unpaired t-test. At the 99% confidence level, wt was significantly different from p53$^{-/-}$ (p value = 0.0025). Quantification of EGFP+ cells in wt and p53$^{-/-}$ zebrafish injected with the pLRE3-*mEGFP* reporte*r* (Fig. 3C') was analyzed using a two-tailed unpaired t-test. At the 99% confidence level, wt was significantly different from p53$^{-/-}$ (p value < 0.0001).

For statistics on the ddPCR on TAHRE transcripts in the humanized flies (Fig. 4), a one-way ANOVA test was performed on all genotypes at the 95% confidence interval. R175H was significantly different from Hp53 Rescue 1 (p value = 0.

0.0030) and Hp53 Rescue 2 (p value = 0.0059). G245S was significantly different from Hp53 Rescue 1 (p value = 0.0116) and Hp53 Rescue 2 (p value = 0.0333). R248Q was significantly different from Hp53 Rescue 1 (p value = 0.0102) and Hp53 Rescue 2 (p value = 0.0318). R273C was significantly different from Hp53 Rescue 1 (p value = 0.0077) and Hp53 Rescue 2 (p value = 0.0139). R273H was significantly different from Hp53 Rescue 1 (p value = 0.0076) and Hp53 Rescue 2 (p value = 0.0212).

For statistical analysis on normalized fluorescence intensity of Wilms tumors (Fig. 5A'), an ordinary one-way ANOVA was performed on all samples at the 99.9% confidence interval. The wt p53 samples (85, 87, 89) were not significantly different from each other (85 vs 87, p value =0.9789; 85 vs 89, p value > 0.9999; 87 vs 89, p value = 0.9659). All wt p53 tumors (85, 87, 89) were significantly different from the p53 mutant tumors (11, 23, 59) as listed below. 85 was significantly different from 11 (p value = 0.0002), 23 (p value < 0.0001), and 59 (p value < 0.0001). 87 was significantly different from 11 (p value < 0.0001), 23 (p value < 0.0001), and 59 (p value < 0.0001). 89 was significantly different from 11 (p value = 0.0003), 23 (p value < 0.0001), and 59 (p value< 0.0001). For statistical analysis on normalized fluorescence intensity of matched normal tissue (Fig. 4A'), an ordinary one-way ANOVA was performed on all samples at the 99.9% confidence interval. All samples were not significantly different from each

other except 89 was significantly different from 11 (p value = 0.0002) and from 23 (p value < 0.0001).

For statistical analysis on normalized fluorescence intensity of the additional Wilms tumors (Fig. 5B), an ordinary one-way ANOVA was performed on all samples at the 99.9% confidence interval. The wt p53 samples (3, 5, 7, 25, 29, 83, 91) were not significantly different from each other. All wt p53 tumors (3, 5, 7, 25, 29, 83, 91) were significantly different from the p53 mutant tumor (23) (p value < 0.0001).

We performed a multinomial distribution for statistical analysis on the WIlms tumor data (Figure 5). Four possible outcomes were possible based on ORF1p expression and p53 status, each with a probability of 0.25. The stratification of elevated ORF1p expression and $p53^{-}$ mutations was highly significant (p value= 0.00000426).

Fertility between $p53^{-}$ and p53Rescue flies (STable 2) was analyzed using a unpaired t-test with equal SD. $p53^{-/-}$ flies were significantly different from p53Resuce (p value = 0.0381) at the 95% confidence level.

For statistical analysis on egg length (SFig. 3A,B), a one-way ANOVA test was performed on all genotypes at the 99.9% confidence interval. aub[HN]/[QC]; p53[NS]/[K1] was significantly different from aub[HN]/+ (p value < 0.0001),

aub[HN]/[QC] (p value < 0.0001), and aub[HN]/+; p53[NS]/[K1] (p value < 0.0001). aub[HN]/+; p53[NS]/[K1] was not significantly different from aub[HN]/+ (p value > 0.9999) but was significantly different from aub[HN]/[QC] (p value < 0.0001). aub[HN]/+ was significantly different from aub [HN]/[QC] (p value < 0.0001). cuff[QQ]/[WM]; p53[NS]/[K1] was significantly different from cuff[QQ]/+ (p value < 0.0001), aub[QQ]/[WM] (p value < 0.0001), and aub[QQ]/+; p53[NS]/[K1] (p value < 0.0001). cuff[QQ]/+; p53[NS]/[K1] was not significantly different from cuff[QQ]/+ (p value = 0.1602) or [QQ]/[WM] (p value = 0.2810). cuff[QQ]/+ was not significantly different from cuff[QQ]/[WM] (p value = 0.0085).

Flamenco transcript between wt and p53- bulk fly ovaries (SFig. 3C) was analyzed using an ordinary one-way ANOVA at the 99% confidence interval. For primer pair 1, $p53^{-/-}$ flies were significantly different from wt (p value = 0.0042). For primer pair 2, $p53^{-/-}$ flies were significantly different from wt (p value = 0.0037).

Fertility between p53- and WT zebrafish (STable 4) was analyzed using a unpaired t-test with equal SD. $p53^{-/-}$ zebrafish were significantly different from WT zebrafish (p value = 0.0012) at the 99% confidence level.

RESULTS

p53 restrains retrotransposons in the Drosophila ovary

Previously, we showed that lesions in the *Drosophila* piwi-interacting RNA (piRNA) pathway consistently triggered p53 activity [64], (Figure 2-5) raising the possibility that p53 might function to restrain retrotransposons that are targets for piRNA suppression. To address this possibility, we examined the expression of TAHRE elements in $p53^{-}$ flies, since these retrotransposons are well documented piRNA targets [84]. In ovaries of $p53^{-}$ females, TAHRE retrotransposons were highly expressed relative to wild type counterparts, as shown by RT-PCR on bulk samples (Figure 3-2). These experiments were performed using two p53 alleles (p53[NS] and p53[K1]) in trans to decrease background influences (see methods). To extend these findings and enable measurements of individual animals, we developed a droplet digital PCR (ddPCR) assay (see methods). As seen in Figure 3-2B, similar p53-dependent effects on TAHRE expression were observed using this assay. Furthermore, while TAHRE dysregulation was consistently seen in $p53^{-}$ individuals, the extent of derepression was variable from animal to animal. Importantly, dysregulated TAHRE expression was not observed in p53Rescue strains, which transgenically restore the fly p53 gene to strains mutated at the native dp53 locus [64]. We further validated these findings by *in situ* detection using fluorescent *in situ* hybridization (FISH) probes. As seen in Figure 3-2C, C', TAHRE transcripts visibly accumulated in $p53^{-}$ animals but were undetectable in wild type or p53Rescue counterparts. Derepressed TAHRE

transcripts were first detectable in the early egg chambers of p53^{-} ovaries (Table 3-1) and, like several piRNA pathway proteins, RNAs from these dysregulated retroelements distinctly accumulated in the germ plasm (Figure 3-2 C, C') of stage 9 and 10 egg chambers (Figure 3-11 A, D). The oocyte germ plasm induces primordial germ cells in the developing embryo [85] and, to examine whether TAHRE transcripts are maternally loaded into the embryo, we tested for TAHRE dysregulation in staged samples resulting from reciprocal crosses. Figure 3-3A shows that p53^{-} females crossed to wild type males produced embryos exhibiting TAHRE transposon dysregulation but, wild type females mated to p53^{-} males did not. These results establish that TAHRE dysregulation in the early embryo is a maternal effect phenotype and indicates that retrotransposon transcripts are maternally loaded. Consistent with this, we observed elevated TAHRE transcripts in early 1-4hr stage p53^{-} embryos but not late 21-24hr stage p53^{-} embryos (Figure 3-3B). Together, these data establish that p53 normally functions to restrict TAHRE elements in the female germline. Furthermore, observations in Figure 3-2C, C' and Figure 3-3A raise the intriguing possibility that TAHRE transcripts, and possibly other retroelement RNAs, engage mechanisms [86] that promote germline propagation by accumulating in the oocyte germ plasm.

To further validate these findings we tested TAHRE transcript levels in a third p53 mutant fly strain, p53[EGFP] (see methods) [72]. TAHRE transcripts were ~60

fold elevated in the p53[EGFP] ovaries at similar levels to the $p53^{-/-}$[K1] flies (Figure 3-4). Strikingly, when these alleles were tested *in trans*, 300-700 fold TAHRE derepression was observed (Figure 3-4). This suggests that background modifiers were acquired over time to suppress retrotransposons since the *Drosophila* p53 mutant strains are carried as homozygous stocks. Therefore, our data in Figure 3-4 indicate that placing two p53 alleles in *trans* releases background modifiers and results in massive transposon eruptions.

To determine whether p53 generally suppresses retroelements, we tested whether other retrotransposons were active in $p53^{-}$ ovaries. Figure 3-5 shows qRT-PCR indicating that multiple retrotransposon classes are derepressed in $p53^{-}$ ovaries. Notably, the expression of telomeric non-Long Terminal Repeat (non-LTR) retrotransposons (TAHRE and HeT-A) as well as non-telomeric LTR-retrotransposons (Idefix, Burdock, and Gypsy) were elevated in $p53^{-}$ ovaries and, in all cases, this effect was reversed in p53Rescue strains. Thus, in *Drosophila*, p53 loss is associated with widespread dysregulation of retroelements. Since sterility is commonly observed in mutants defective for retroelement suppression, we also assessed fertility in $p53^{-}$ and p53Rescue adults. Consistent with previous reports [87], we observed partial infertility phenotypes in $p53^{-}$ female flies that were rescued in p53Rescue strains (Table 3-2, see methods).

CHK2 mutants do not phenocopy p53$^{-/-}$ mutants for transposon dysregulation

To test whether upstream regulators of p53 phenocopy the p53 null state, we examined retrotransposon transcripts in chk2 mutant ovaries. Chk2 is a highly conserved upstream kinase that phosphorylates p53 upon DNA damage [88]. As shown in Figure 3-5 B, transposon transcripts were not dysregulated in chk2$^{-/-}$ when compared to chk2$^{+/-}$ heterozygous ovaries. This suggests that transposon repression by p53 is a basal function of p53 and is not mediated through the chk2 phosphorylated state normally associated with stimulus-dependent activation [88]. Furthermore, this indicates specificity to p53 since not all mutants in the DNA damage pathway phenocopy the p53 null state.

Spo11 mediated meiotic double strand breaks are the inciting event for transposon eruption in the p53$^{-/-}$ state

Retrotransposition could be stimulated in meiotic progenitors, since DNA breaks needed for recombination may facilitate integration of retrotransposons [89]. Intriguingly, we previously showed that p53 is transiently activated in these same cells during the process of meiotic recombination [23]. In light of our new observations (Figure 3-2), p53 could plausibly act in this context to contain retrotransposon activity during meiosis. To test this possibility we generated animals deficient for both p53 and Spo11 [90], a universally conserved enzyme that forms double-stranded DNA breaks to initiate meiotic recombination. Using these double mutants we found that spo11 is epistatic to p53 when transposon

derepression was assessed (Figure 3-6). Specifically, transposon derepression was completely reversed for Idefix, Gypsy, and Burdock elements (which were present at or below WT levels) and partially reversed for the TAHRE and HeT-A retroelements (Figure 3-6) in the ovaries of spo11^{-};p53^{-} animals. Hence, programmed DNA breaks during meiotic recombination are required for transposon eruptions that accompany the p53^{-} state. Furthermore, since the action of Spo11 is cell autonomous, and evidently confined to meiotic cells, these data strongly suggest that p53 normally restrains mobile elements within meiotic cells of the germline. The fact that TAHRE and HeT-A retroelements were only partially affected by loss of spo11 is consistent with this interpretation, since these elements are also involved in telomere elongation [91].

Ionizing radiation does not lead to massive transposon eruption in the Drosophila ovary

DNA damage is thought to lead to transposon movement [92] and we observed severe sterility issues in the p53$^{-/-}$ females after ionizing radiation (IR) (Figure 2-8B). To test whether IR leads to significant transposon derepression, we extracted total RNA from ovaries of WT and p53$^{-/-}$ irradiated flies. We observed consistent TAHRE dysregulation in p53$^{-/-}$ ovaries at 15 minutes, 1 hour, 4 hour and 24hours post-irradiation when compared to WT ovaries (Figure 3-7). However, ionizing radiation did not lead to global transposon eruptions in this organ since similar TAHRE dysregulation was observed in unirradiated and

irradiated $p53^{-/-}$ ovaries (Figure 3-7). DNA damage could lead to transposon movement in somatic cells since the piRNA pathway is highly expressed in the ovary but not in somatic tissue [69]. It will be interesting to test whether ionizing radiation and other stressors lead to transposon activity in the soma.

We previously showed that ionizing radiation and lesions in the piRNA pathway consistently triggered p53 activity in the germline stem cells (GSCs) (Figure 2-1 and Figure 2-5) [64]. If transposition occurs in GSCs, subsequent generations will inherit these mobilization events. Thus, stem cells may be acutely sensitive to sources of genomic instability and p53 activity may be triggered here to restrain transposons after stress. Consistent with this, when we performed a microarray on $bam^{-/-}$ and $bam^{-/-};p53^{-/-}$ stem-like ovary tumors (Figure 2-13), retrotransposons transcripts were dysregulated in the absence of p53 (Table 3-3). Therefore, although we do not observe global transposon derepression in the ovary after ionizing radiation (Figure 3-7), we hypothesize that mobile elements may be targeting GSCs for integration. This is consistent with our observation whereby TAHRE transcripts target primordial germ cells by accumulating in the oocyte germ plasm (Figure 3-2 C, C').

Dp53 restrains retroelements in the soma

As indicated in Figure 3-2, Figure 3-3, Figure 3-4, and Figure 3-5A, p53 restrains retroelements in the *Drosophila* germline. To test whether this function might also occur in somatic cells, we quantified transposon transcript levels in *Drosophila* heads by qRT-PCR. Figure 3-8 shows that TAHRE, Idefix, HeT-A and Gypsy transposon transcripts are consistently elevated in the $p53^{-/-}$ soma and this is reversed in p53Rescue strains. Interestingly, somatic tissue may be more permissive for transposon movement since HeT-A and gypsy retroelements were more highly dysregulated in the $p53^{-/-}$ head than in the ovary (Compare Fig 3-5 and Figure 3-8). These data indicate that p53 effectively represses retrotransposon in both somatic and germline tissue.

Exploring p53 interaction with the piRNA pathway

In metazoans, the highly conserved piRNA network acts through protein components, P-element induced wimpy testis (PIWIs), in concert with small RNAs (piRNAs) to silence the expression of retrotransposons at the transcriptional and post-transcriptional levels [69,93-95]. To examine whether p53 might collaborate with the piRNA system to suppress retrotransposons, we tested for possible genetic interactions between p53 and core elements of the piRNA pathway, *aubergine* (*aub*) and *cutoff* (*cuff*). For these assays, we scored stunted egg morphology as a maternal-effect readout and, despite normal localization of piRNA pathway proteins in $p53^{-}$ ovaries (Figure 3-10), we found that aub^{-};$p53^{-}$ and $cuff^{-}$;$p53^{-}$ double mutants produced significantly stunted eggs

(Figure 3-9 A,B). Consistent with these data, we also found that piRNA biogenesis was altered in p53 mutants. Mature piRNAs are processed from large precursor RNAs that map to transposon 'graveyards', representing fossilized templates of previous exposures [69,93-95]. In *Drosophila*, precursor RNAs encoded by the *flamenco* locus generate piRNAs that silence retroelements [69,93-95] and, like other mutants defective for piRNA biogenesis [95], the flamenco piRNA precursor abnormally accumulated in $p53^{-}$ animals (Figure 3-9C). Together, these observations suggest that p53 collaborates with the piRNA pathway to repress retrotransposons.

To test whether p53 could suppress retrotransposons by regulating the localization of piRNA pathway components, we stained WT and $p53^{-/-}$ ovaries for piRNA proteins that are essential for retrotransposon repression (Figure 3-10). We found that vasa, armitage, aubergine and rhino proteins localize similarly in WT and $p53^{-/-}$ animals. Interestingly vasa and aub proteins localize to the oocyte germ plasm and are necessary for pole plasm formation (Figure 3-10 A, D) [96]. In light of our observations, in Figure 3-2C, we wonder whether retroelements engage the piRNA pathway to target primordial germ cells for integration.

In the *Drosophila* germline, the p53 protein forms distinct foci that are lamin associated [58]. Since we observed genetic interactions between p53 and piRNA pathway components (Figure 3-9), we wondered whether p53 might interact with

piRNA pathway components to repress retroelements. To test this, we performed co-localization studies between p53 and aubergine proteins in the ovary. As shown in Figure 3-11, we found that p53 foci colocalize with aubergine protein approximately 40% of the time in the germarium and stage 3 egg chambers. This could suggest that p53 directly interacts with aubergine to suppress retrotranspososns. However, since aubergine is widely expressed, additional experiments are needed to exclude possible co-localization due to random chance.

Dysregulated retroelement activity predicts elevated integration events in p53$^{-/-}$ animals

Elevated retrotransposon transcripts levels are commonly used as a surrogate for elevated transposition, since these elements mobilize through an RNA intermediate (Figure 3-1). To test whether p53$^{-/-}$ flies have increased retrotransposon copy number, we hybridized HeT-A and TAHRE DNA FISH probes in WT and p53$^{-/-}$ salivary glands since this organ is polyploid and has previously been documented for analyzing retrotransposon copy number [97]. We observed a modest increase in TAHRE copy number in the p53$^{-/-}$ animal but HeT-A copy number did not differ between the two genotypes (Figure 3-12). However, the annotated copies of HeT-A and TAHRE in the WT genome is greater than what we observed in our assay suggesting that our probes are not

sensitive enough to detect single insertion events. Therefore, this is not the proper assay to assess transposon copy number.

To directly visualize *de novo* integration events in vertebrate animals, we developed assays to measure *de novo* retrotransposition in zebrafish, using a well characterized retrotransposition indicator that takes advantage of an engineered reporter construct, designated pLRE3 [89]. As illustrated in Fig. 3-13, this construct is a retrotransposition competent human LINE-1 (L1) element containing a reporter cassette in its 3'UTR (Figure 3-13) that encodes a backward copy of a CMV-driven enhanced green fluorescence protein (EGFP) gene. A key feature of this integration reporter is that EGFP is interrupted by an artificial intron oriented in the same transcriptional direction as L1 expression [98]. This arrangement ensures that EGFP-positive cells will only arise when pLRE3-transcripts undergo successful retrotransposition [78,98]. Specifically, LRE3 RNAs must be expressed, properly spliced, reverse transcribed and ultimately integrated in order to produce a CMV-driven GFP signal [98]. To assay LINE-1 expression levels, we injected the pLRE3 reporter into wt and $p53^{-}$ zebrafish embryos and performed immunohistochemistry to detect the human LINE-1 open reading frame 1 protein (ORF1p) at 11 hours post fertilization (see methods). As shown in Figure 3-13 B and B', we observed abundant ORF1p expression in $p53^{-}$ embryos, but this signal was undetectable in the wt embryos. Thus, like the *Drosophila* p53 counterpart, zebrafish p53 similarly acts to restrain retroelement

expression. To determine whether derepressed LINE-1 activity in $p53^-$ gametes predicts extensive *de novo* integration events, we injected the pLRE3 reporter into wt and $p53^-$ zebrafish embryos and performed immunohistochemistry for EGFP at 48 hours post fertilization (see methods). EGFP positive ($EFGP^+$) cells were detected in both wt and $p53^-$ zebrafish (Figure 3-13 C, C' and Table 3-4). but the frequency of retrotransposition within individual animals was dramatically elevated in $p53^-$ mutants (Fig. 3-13 C, C'). Consistent with our previous data (Fig. 3-2B), the number of $EGFP^+$ cells seen in $p53^-$ individuals varied from animal to animal (Fig. 3-13C'). To confirm that $EGFP^+$ cells reflect authentic LINE-1 retrotransposition events, we injected a control LINE-1 reporter (pLRE3H230A-*mEGFPI*) which is unable to integrate by virtue of a mutation in the ORF2 enonuclease but is, otherwise, identical to LRE3 [79]. As expected the mutant pLRE3H230A-*mEGFPI* reporter failed to produce $EGFP^+$ cells in both wt and $p53^-$ zebrafish (Table 3-4), despite elevated LINE-1 expression in the $p53^-$ embryo (Figure 3-14). These data indicate that p53 repression of retroelements lies upstream of the integration event. Moreover, as in human cells, L1 retrotransposition depended on ORF2 endonuclease function [99] and exhibited a preference for *cis* transcripts [100]. Hence, using assays for expression (Fig. 1 and Fig. 3B, B') or movement (Fig. 3C, C'), we conclude that zebrafish p53 and *Drosophila* p53 similarly restrict retrotransposon activity. Furthermore, since little or no cell deaths occur during the stages examined in these assays [101],

dysregulated LINE-1 activity is very likely separate from apoptotic functions associated with p53.

Zebrafish p53 restrains mobile elements.

Figure 3-13 shows that zebrafish p53 can suppress an engineered human LINE-1 element (Figure 3-13). To test whether endogenous retroelements are similarly restrained by zebrafish p53, we performed qRT-PCR on WT and $p53^{-/-}$ zebrafish ovaries and observed a modest elevation of gypsy transcripts in the $p53^{-/-}$ animal (Figure 3-15A). Since sterility is commonly observed in mutants defective for retroelement suppression, we also assessed fertility in WT and $p53^{-}$ zebrafish. Consistent with previous reports [87] and our findings in *Drosophila* (Table 3-2), we observed a three fold increase in the number of unfertilized $p53^{-}$ zebrafish embryos when compared to WT (Figure 3-15B and Table 3-5, see methods). Together, our data in Figure 3-13 and 3-15, establish that zebrafish p53 restrains retroelements.

Human p53 represses mobile elements, but p53 'hotspot' cancer alleles cannot

To test whether suppression of transposons might be a conserved property also encoded by human p53 genes, we engineered a collection of fly strains that are, in effect, 'humanized' for p53 function (Figure 3-16). In these lines, the *Drosophila* p53 gene is replaced by wild type or cancer-associated p53 variants,

regulated by flanking sequences of the native fly locus (see methods) [58]. The majority of TP53 mutations in human cancers are missense and cause single amino-acid changes that correspond to the DNA binding domain [2]. We generated cancer-associated alleles that comprise five of the most prevalent hp53 mutations in cancer. These 5 hot spot mutations all reside in the DNA binding domain and these amino acid residues are normally involved in making contacts with the DNA (R248 and R273) or support the structure of the DNA binding surface (R175 and G245) [2]. As seen in Figure 3-17, the normal human p53 gene complemented the fly counterpart and effectively restrained retroelements in the ovary. However, despite comparable expression [58] (Figure 3-17 inset), all five cancer-associated p53 alleles failed to rescue this defect. Together, these observations establish that retrotransposon suppression by p53 genes is a broadly conserved property shared by the human counterpart. Moreover, since p53 mutant alleles commonly seen in cancer patients were disabled for this function, our results raise the possibility that suppression of retrotransposon activity may, in part, contribute to p53-mediated tumor suppression.

An entry point into understanding gain of function mystery of the p53 cancer alleles

If containment of transposons is a true tumor suppressing mechanism, WT human p53 must also be able to restrain retroelements in somatic tissue. As seen in Figure 3-18 the normal human p53 gene complemented the fly

counterpart and effectively restrained retroelements in *Drosophila* heads. However, in stark contrast, the R248Q and G245S cancer-associated p53 alleles failed to rescue this defect. Interestingly, TAHRE transcripts were more highly dysregulated in the p53 cancer alleles than the $p53^{-/-}$ flies alone. As described in Chapter 1, p53 missense mutations not only exhibit loss of function but acquire gain of function activitites. The data in Figure 3-18 suggest that the p53 cancer alleles not only fail to repress retrotransposons but promote transposon movement in somatic tissue. These observations suggest that the evident "gain of function phenotypes" reported for these alleles may instead reflect the inability of p53 cancer alleles to repress retrotransposons. We are currently extending this finding to all p53 cancer alleles and validating these findings with more biological replicates.

p53 represses retroelements in mice

To determine whether p53-mediated repression of transposons is evolutionarily conserved in mice we examined two classes of retrotransposons, the Intracisternal A particles (IAPs) and LINE-1 elements. We obtained antibodies for the LINE-1 ORF1p and the IAP-Gag, from Alec Bortvin and Bryan Cullen respectively, to study the expression of these retroelements using two cancer mouse models as outlined below. These studies were performed in collaborations with Sarah Comerford and Bob Hammer.

First, we examined retroelement activity from identically engineered mouse liver tumors that are Myc-driven but either wild type or mutant for p53 (see methods). We observed highly dysregulated IAPgag expression in the Myc- driven $p53^{-/-}$ tumors but not the myc driven p53 WT tumors (Figure 3-19A). To test whether other retroelements were dysregulated, we tested for LINE-1 ORF1p dysregulation in these same tumors. Similar to the IAP retroelement, we observed elevated LINE-1 ORF1p expression only in the Myc-driven $p53^{-/-}$ liver tumor (Figure 3-19B). These data indicate loss of p53 leads to widespread transposon expression and suggests that p53 activity to restrain retroelements is evolutionarily conserved in the mouse.

To validate these findings, we tested another cancer mouse model for transposon dysregulation. SV40 is an oncogenic DNA virus that encodes several early viral proteins including the large T antigen (LT) and the 17K T antigen (17kT) (Figure 3-20A). The LT protein is necessary and often sufficient for transforming cells and binds to numerous proteins, most notably the Retinoblastoma (Rb) and p53 tumor suppressors [82]. The 17kT protein is only weakly transforming and binds Rb but not p53. Consistent with this, in engineered mice that express either the LT or the 17kT in the liver (see methods), LT protein expression leads to liver dysplasia and hepatocellularcarninoma (HCC) but the 17kT protein is insufficient to produce HCC [82]. Since LT can bind and inactivate p53 but the 17kT cannot, we examined

IAP expression in these livers using an antibody for the IAPgag protein. As shown in Figure 3-20B, we observed robust IAPgag expression in the LT liver tumors. In stark contrast, the majority of the 17KT liver was negative for IAPgag. We next wondered if the heterogenous expression of IAPgag in the LT livers was due to variability in p53 expression since previous analysis of this model showed that LT and p53 form stabilized complexes and each are seen to co-localize in tumor nodules [82]. We found that stabilized p53 was consistent with strong IAP immunoreactivity (Figure 3-20B). Therefore, p53 stabilization and inactivity in this liver tumor model is consistent with elevated transposon dysregulation.

Is elevated transposon activity in human cancers coupled to p53 loss?

Recent studies have documented elevated retrotransposon activity in human cancer tissues [102-104] but this oncogenic trait has not been directly coupled to p53 status. To empirically assess whether elevated retrotransposon activity might be coupled to p53 loss, we profiled LINE-1 expression in wild type and p53 mutant Wilms tumors [83] using an α-ORF1p antibody [81].

First, we validated the α-ORF1p antibody [81] by IHC on human testis since expression of LINE-1 ORF1p has previously been reported in this organ [81]. As shown in Figure 3-21 we observed robust ORF1p expression in the primary spermatocytes of the seminiferous tubules. Next, we performed a blinded study on Wilms tumors that were either WT or mutant for p53. Figure 3-22 shows

ORF1p expression was unanimously detected in p53 mutant tumors and, in stark contrast, little or no ORF1p expression was detected in Wilms tumors that were normal for p53 (Figure 3-22A). Likewise, little or no ORF1p expression was seen in matched normal tissue controls (Figure 3-22A"). To extend this analysis, all remaining Wilms tumors that could be curated for p53 status in this same archive were similarly examined [83]. As seen in Figure 3-22B, these additional Wilms tumor samples (seven total) were all WT for p53 and also negative for ORF1p expression, in stark contrast to the p53 mutant stained in parallel as a positive control. Together, these results exposed a highly significant association between p53 mutations and dysregulated LINE-1 expression in Wilms tumors.

DISCUSSION

We show here that p53 genes from flies, zebrafish, mouse and humans act to restrain retrotransposons (Figures 3-2, 3-4, 3-5, 3-13, 3-15, 3-17, 3-18, 3-19, 3-20) and that at least one p53-driven human cancer type is strongly associated with elevated retrotransposon activity (Figure 3-22). Furthermore, we had previously shown that p53 is acutely responsive when these transposons are dysregulated [64]. Combined, these findings suggest that ancestral functions of the p53 gene family were linked to transposon control, raising the possibility that p53 restricts oncogenesis, in part, by suppressing the movement of mobile elements. Powerful support for this concept emerged from our complementation studies (Figure 3-17) where, human p53 corrected retroelement dysregulation seen in fly p53 mutants but all five cancer-associated p53 alleles were clearly disabled for this activity.

Retrotransposition in somatic tissues (PMID: 24286172 or PMID: 26104698) is relevant for human disease (PMID: 24286172 or PMID: 26104698) but retroelements also have the potential to impact subsequent generations and, as illustrated in Figure 3-2C-C", their RNAs can target the presumptive germ line during oogenesis. Long-standing questions have focused on stimuli that might instigate transposon movement and, in the germ line, DNA breaks formed by Spo11 during meiotic recombination are thought to provoke retrotransposition [105]. Consistent with this, we found that loss of p53 did not incite transposon

derepression if *spo11* was also defective (Figure 3-6). Hence, Spo-11 dependent p53 activity occurring in the meiotic precursors of flies and in mice [23] likely reflects functions that contain movement in the germ line and, viewed from this perspective, transposon eruptions in the germline are consistent with infertility phenotypes seen in in $p53^{-}$ flies (Table 3-2), $p53^{-}$ zebrafish (Table 3-5) and mice [87]. Combined, these observations suggest that p53-mediated tumor suppression was evolutionarily co-opted from ancestral meiotic functions that restricted mobile elements to insure germ line integrity. Consistent with this, we found that adult *Drosophila* exposed to genotoxic stress or genome destabilizers selectively activated p53 in GSCs and their immediate progeny, suggesting that p53 may act in this context to maintain genomic integrity specifically in GSCs. However, our data also indicate that p53-mediated repression of mobile elements is not confined to the germline (Figures 3-8) and, likewise, the dyregulated elements seen in somatic tissues do not reflect meiotic eruptions (Figure 3-3). We have yet to identify the inciting event for transposon eruptions in the soma. It is thought that the function of Spo11 is cell autonomous and confined to meiotic cells. However, Spo11 transcripts are expressed outside of the germline [90], which raises the possibility that Spo11 could promote retrotransposon mobility in somatic tissue.

What upstream regulators and downstream effectors are required for p53 action to repress retroelements? Transposon eruptions in the $p53^{-}$ germ line were

incited by Spo11 meiotic double strand breaks (Figure 3-6) but ionizing radiation did not lead to massive transposon eruptions (Figure 3-7). Chk2 is a highly conserved upstream kinase of p53 but Chk2 mutants did not exhibit elevated transposon transcripts in the *Drosophila* germline (Figure 3-5B), suggesting that transposon repression by p53 is a basal function of p53 and is not mediated through the chk2- phosphorylated state normally associated with stimulus-dependent activation [88]. Furthermore, this indicates specificity to p53 since not all mutants in the DNA damage pathway phenocopy the p53 null state. Since p53 restrains mobile elements in mice (Figures 3-19 and 3-20) and a multitude of knockout mice are available, this genetic model provides a powerful platform for genetically interrogating the upstream regulators and downstream effectors that may be involved in p53 mediated transposon repression.

How is p53 repressing retrotransposons? p53 could act directly on retroelements or indirectly through the piRNA pathway. Despite genetic interactions with critical piRNA pathway components (Figure 3-9A,B) and dysregulated piRNA precursor expression (Figure 3-9C), piRNA pathway proteins were normally expressed and localized in p53 mutants (Figure 3-10). p53 could act directly on the transposon DNA or RNA transcripts. Since p53 mutant alleles arising in cancers typically are compromised for DNA binding, repression could occur through direct action at putative p53 binding sites in mobile elements [106]. Indeed, our observations suggest that p53 contains these mobile elements by impacting the production

and/or stabilization of their corresponding transcripts (Figure 3-14). This is consistent with our data in *Drosophila* (Figure 3-5A) and mice (Figure 3-19) whereby p53 regulates both LTR and nonLTR elements, two classes of retrotransposons that differ in their mode of integration.

So far, we showed that p53 mutations stratify with dysregulated LINE-1 activity in Wilms tumors. To determine whether this association extends to other cancer types, we are using a bioinformatics approach. Amanda Jones, a postdoc in the Abrams lab has examined colon cancer RNAseq datasets from The Cancer Genome Atlas (TCGA) and found that loss of p53 was associated with a statistically significant elevation of transcripts corresponding to the Human specific LINE-1 ($L1_{Hs}$) sub-family. These represent the most recent LINE-1 lineage and contain the majority of retrotransposition competent elements [66,67]. Furthermore, as the evolutionary distance increased through the LINE-1 family, the p-value for this relationship also increased, suggesting that p53 preferentially impacts expression of elements within the $L1_{Hs}$ lineage. This effect was specific to retrotransposons, since no association emerged between $p53^-$ status and the expression of either simple repeats or pseudogenes in these same data sets. Therefore, p53 mutations are strongly associated with dysregulated transposon activity in at least two p53-driven cancers. It will be interesting to see whether this association is observed in other cancer types.

PERSPECTIVES AND FUTURE DIRECTIONS

Taken together, results presented in this chaper provide an attractive framework for understanding how p53 loss provokes destabilized genomes and could, more broadly, facilitate efforts to interrogate roles for p53 as a guardian against 'transposopathy' in human health and disease.

We are actively pursuing two questions that will determine the impact of this finding on human disease: First, is this a true tumor suppressing mechanism of p53? We find that p53 represses retrotransposons across the animal kingdom but have yet to provide evidence that transposon dysregulation is an oncogenic driver. Transposon eruptions in somatic tissue due to p53 loss could lead to elevated mutation rate and is an attractive explanation for the genome fluidity observed in human cancers. To test this possibility, we intend to inhibit retroelements in the $p53^{-/-}$ mouse. If our hypothesis is correct, repression of retroelements should mitigate or prevent tumor formation.

Second, how actionable is this knowledge in the clinic? We wonder whether retroelements can be detected in the plasma or urine of diseased patients and whether this could be used as biomarker of disease. We also wonder whether suppression of retroelements could be a therapeutic target for Wilms tumor patients that have p53 mutations. These p53 mutant tumors are much more difficult to treat and have poorer prognosis and suppression of retroelements

could provide a unique entry point for treatment. We aim to use mouse models to inhibit retrotransposons during tumor formation to determine whether repression of retroelements decreases tumor burden over time.

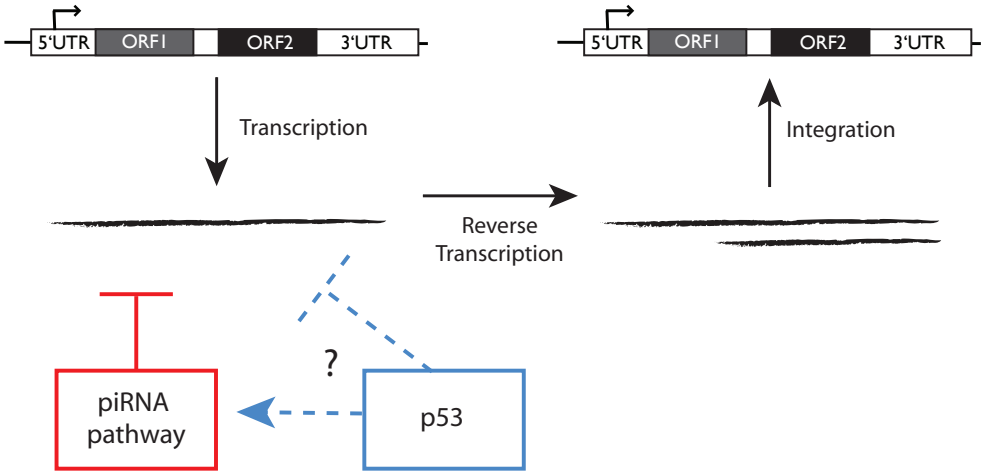

Figure 3-1. Retrotransposons mobilize through an RNA intermediate
Diagram of the human LINE-1 locus and the retrotransposition life cycle. Retrotransposons encode essential proteins for mobilization. ORF1(grey box) encodes a chaperone binding proteins and the ORF2 (black box) encodes a reverse transcriptase and endonuclease [65]. Retrotransposons mobilize through an RNA intermediate, are reverse transcribed by the encoded ORF2 protein and integrate into the genome. A highly conserved pathway, the piRNA pathway acts to repress retrotransposons in the germline. p53 may act directly on retroelements or indirectly through the piRNA pathway. Retrotransposon activity can be assessed by transcript levels, ORF1 protein expression, or visualizing the integration event.

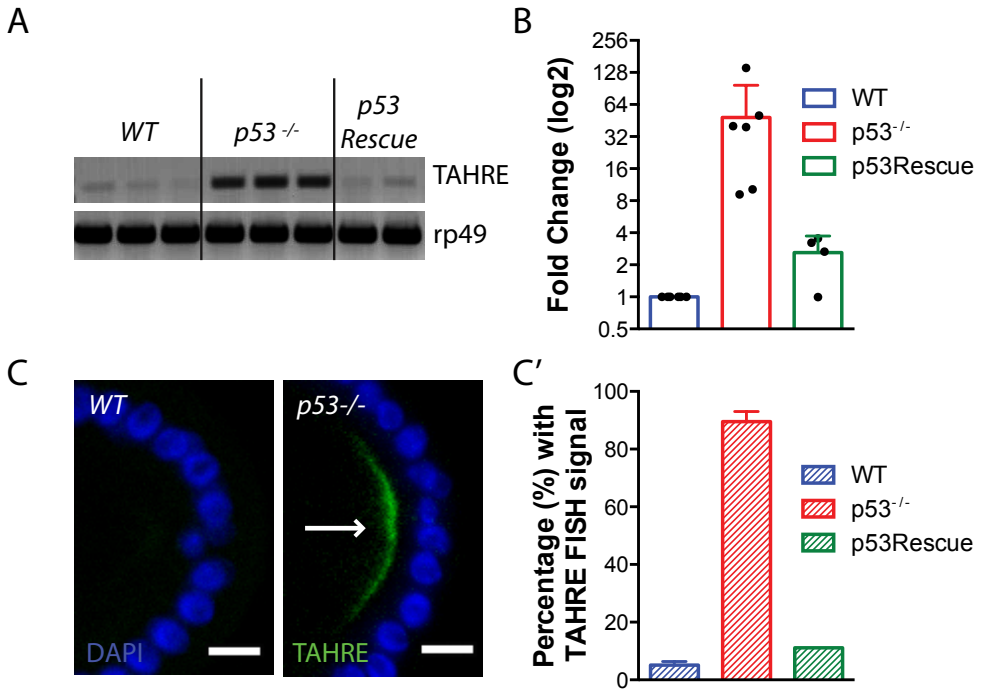

Figure 3-2. p53 restrains transposon activity in the *Drosophila* germline
(A) *TAHRE* retrotransposons, measured by RT-PCR, are highly expressed in dp53^{-} ovaries but minimally expressed in parental wild type (WT) or dp53^{-} flies carrying a p53 genomic rescue transgene (p53Rescue). The control reference gene, ribosomal protein L32 (rp49) is present at similar levels among all genotypes.
(B) Derepression of *TAHRE* transcripts in ovaries of single animals was quantified using droplet digital PCR (ddPCR) standardized to the housekeeping gene, rp49. Each dot represents measurements from an ovary pair from a single female. *TAHRE* retrotransposons were consistently dysregulated in dp53^{-} animals (red bar). Normal repression, comparable to wild type (blue bar) occurred when the p53Rescue transgene was present in these mutants (green bar).
(C-C') *TAHRE* expression was assayed by FISH. In **(C)** *TAHRE* RNAs (arrow) accumulate in the germ plasm of p53^{-} oocytes of stage 9 and 10 egg chambers but not in wt egg chambers. *TAHRE* signal is green and DAPI counterstain is blue. These data are quantified in **(C')**, illustrating *TAHRE* derepression in p53^{-} ovaries (red bar) Scale bars, 10μm.

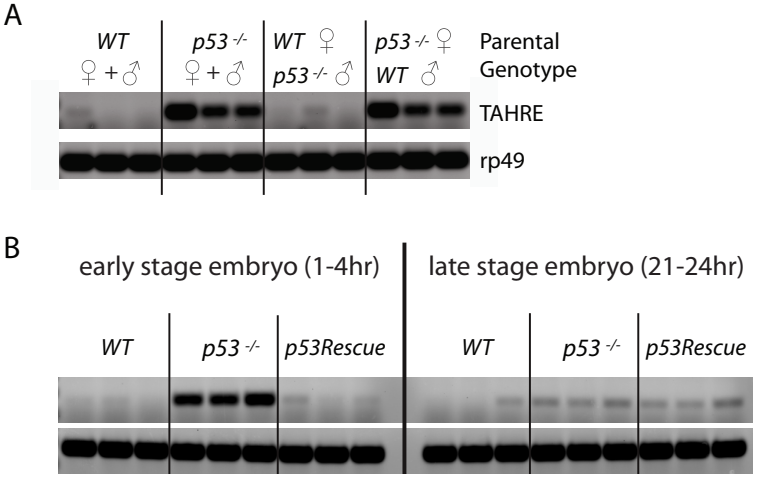

Figure 3-3. Retrotransposon transcripts are maternally loaded into the embryo

(A) TAHRE transcripts, measured by RT-PCR, are maternally loaded into the 1-4hr old embryo. TAHRE elements are derepressed in the $p53^{-/-}$ embryo (parental genotypes were $p53^{-/-}$) but undetectable in the WT embryo (parental genotypes were WT). Robust TAHRE expression was also observed in embryos from $p53^{-/-}$ mothers mated to WT fathers (parental genotypes are $p53^{-/-}$ ♀; WT ♂) but not in embryos from the reciprocal cross (WT ♀; $p53^{-/-}$ ♂). The control reference transcript, rp49, is present at similar levels among all genotypes. Three independent biological replicates are shown for all genotypes.

(B) TAHRE transcripts, measured by RT-PCR, are derepressed in the early 1-4hr old $p53^{-/-}$ embryo (left) when compared to WT and p53Rescue embryos. TAHRE dysregulation is not observed in late stage 21-24hr old embryos. The control reference transcript, rp49, is present at similar levels among all genotypes. Three independent biological replicates are shown for all genotypes.

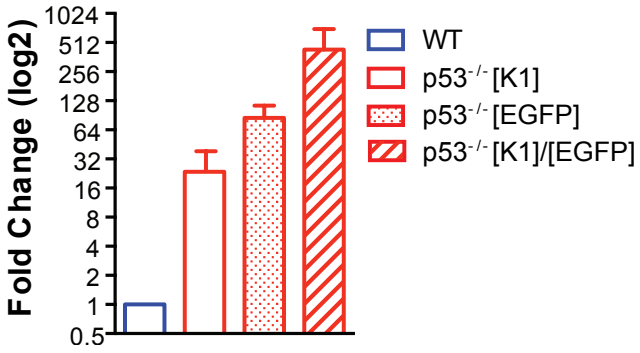

Figure 3-4. Massive transposon eruptions in the *Drosophila* germline when two p53 alleles are placed *in trans*

TAHRE transcripts, measured by ddPCR, are elevated in p53 mutant ovaries in two different dp53^{-} fly strains, p53[K1] (red bar) and p53[EGFP] (red dotted bar), when compared to WT ovaries (blue bar). Massive transposon eruptions are observed when these alleles are placed in trans (p53[K1]/p53[EGFP] (red lined bar). TAHRE transcripts were standardized to the housekeeping gene, rp49.

Paula Kurtz, a graduate student in the lab, functionally validated that the p53[EGFP] is a severe hypomorphic p53 allele (data not shown). Paula also discovered that the p53[EGFP] was dysregulated for TAHRE transcripts in independent RNA ovary preps not shown here.

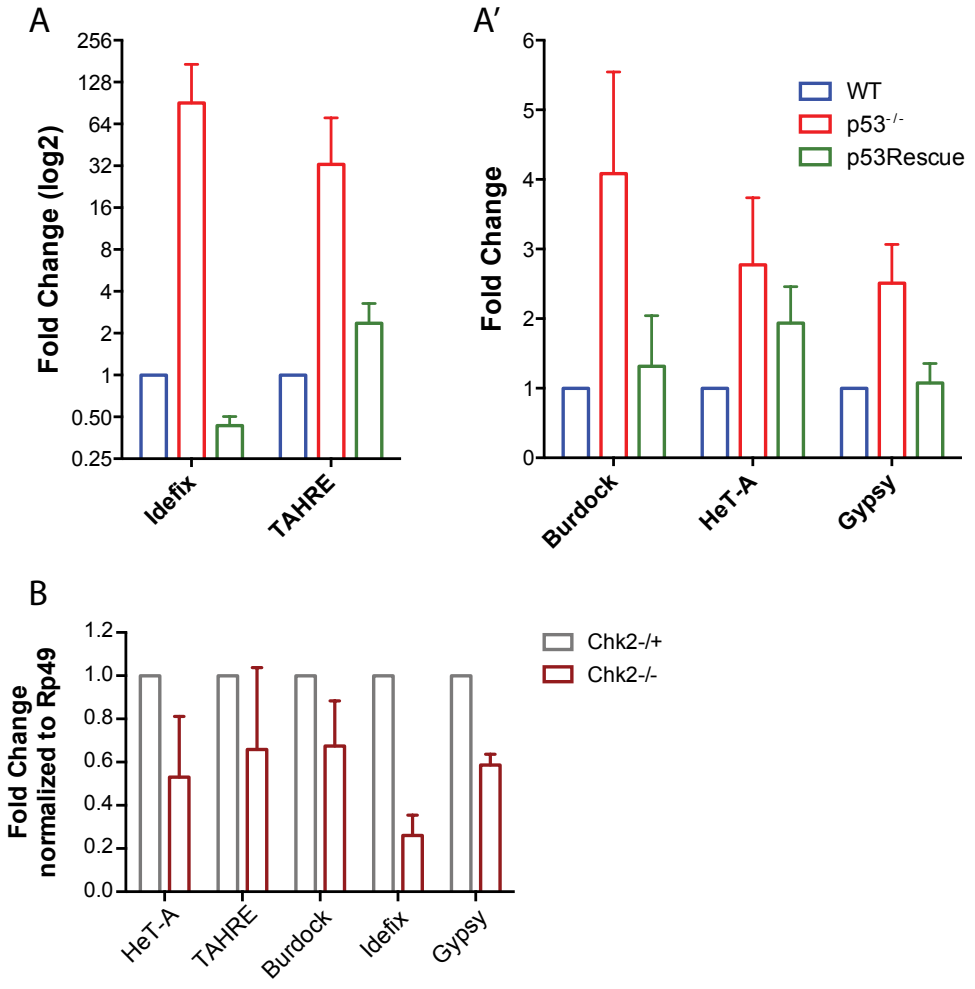

Figure 3-5. p53 generally restrains transposon activity in the *Drosophila* germline and Chk2 mutants do not exhibit transposon dysregulation.
Expression from the indicated retroelements was measured by quantitative RT-PCR. In **(A)** the Idefix and TAHRE elements were highly derepressed in dp53- ovaries (red bars) relative to WT (blue bars) or p53Rescue (green bars) samples. In **(A')** retroelements from the Burdock, Gypsy, and HeT-A families (red bars) were similarly, but more modestly, deprepressed in p53- ovaries. Note that in **(A)**, the fold change is plotted on a log2 scale to better appreciate differences in transcript levels between wt and p53Rescue flies. In **(A and A')** dp53- samples were statistically significant from wt samples and the error bars represent standard deviations.
(B) Retrolement transcript levels were measured by quantitative RT-PCR. Idefix, TAHRE, HeT-A, Gypsy, and Burdock are not dysregulated in Chk2 mutant ovaries when compared to $Chk2^{+/-}$ heterozygous flies. Error bars represent standard deviations.

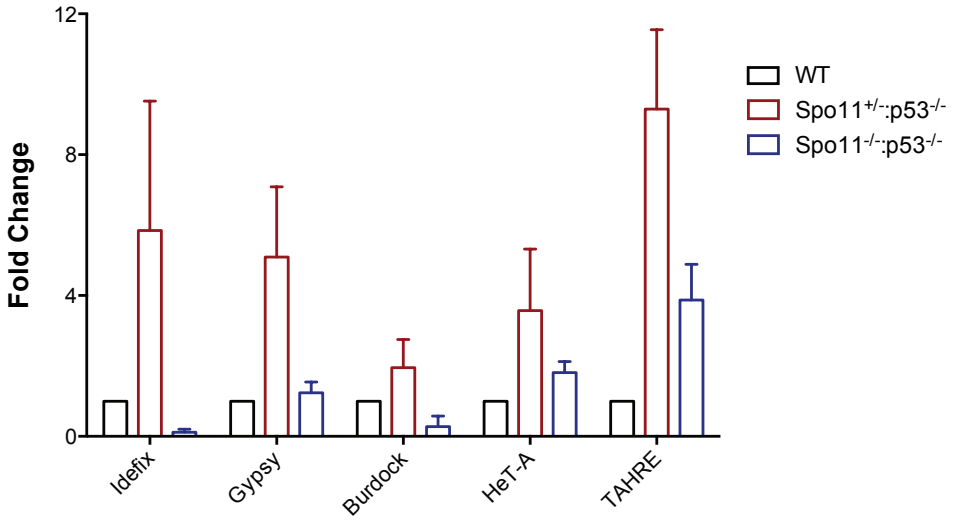

Figure 3-6. Retrotransposon derepression in the p53^{-} state requires meiotic double strand breaks mediated by Spo11

Expression from the indicated retroelements was measured in ovaries of the indicated genotypes by quantitative RT-PCR. *TAHRE, HeT-A, Idefix, Gypsy and Burdock* elements are derepressed in spo11$^{+/-}$; p53$^{-/-}$ ovaries (maroon bars) unlike WT (black bars) or spo11$^{-/-}$;p53$^{-/-}$ (dark blue bar) samples. Error bars represent standard deviations from three biological replicates. spo11$^{+/-}$;p53$^{-/-}$ samples were statistically significant from WT and spo11$^{-/-}$;p53$^{-/-}$ samples.

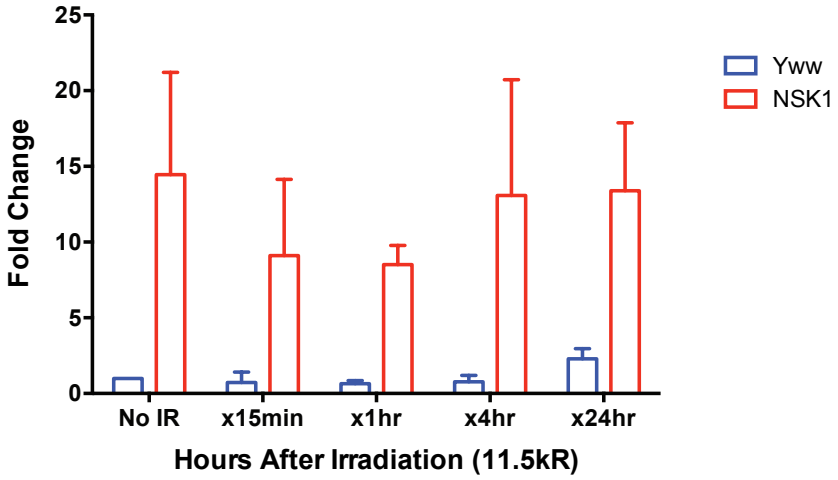

Figure 3-7. Ionizing radiation does not lead to massive transposon eruption in the *Drosophila* ovary

TAHRE transcript levels were measured by ddPCR in WT and $p53^{-/-}$ ovaries after 15 minutes, 1 hour, 4 hours and 24 hours after irradiation. TAHRE transcripts were consistently elevated in $p53^{-/-}$ ovaries when compared WT ovaries at all time-points. However, TAHRE transcripts are not significantly elevated after ionizing radiation stress when compared to the non-irradiated controls.

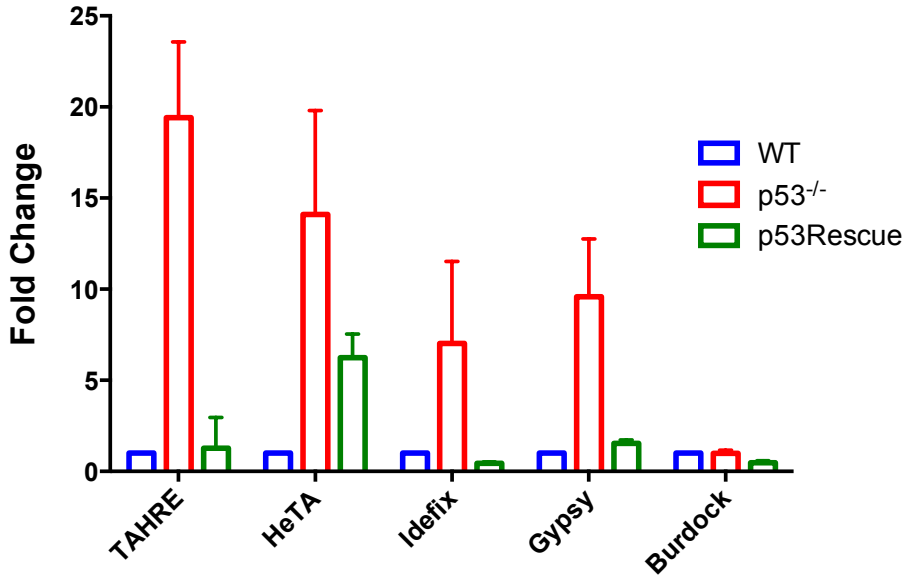

Figure 3-8. p53 restrains retroelements in the *Drosophila* soma
TAHRE, HeT-A, Idefix, and Gypsy elements are derepressed in $p53^{-/-}$ heads (red bars) when compared to WT (blue bars) or p53Rescue (green bar) samples, measured by quantitative RT-PCR. Error bars represent standard deviations from three biological replicates. $p53^{-/-}$ samples were statistically significant from WT and p53Rescue samples (see methods for p values). Daniel Hwan, a rotating medical student, made the initial discovery that TAHRE transcripts were dysregulated in the soma. Corey Timmermann, a summer SURF student, extended this finding to the Idefix retrotransposon.

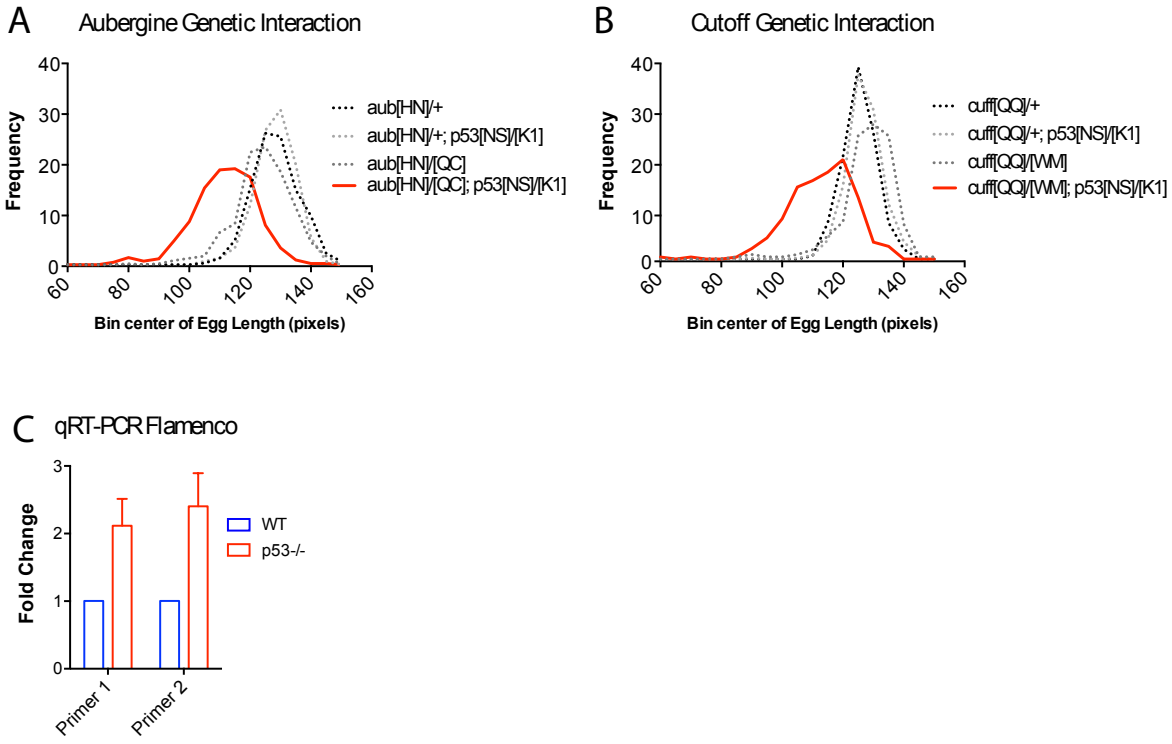

Figure 3-9. p53 interacts with the piRNA network

(A-B) illustrate genetic interactions between p53 and the piRNA effectors, *aubergine (aub)* **(A)** *and cutoff (cuff)* **(B)**, detected here using egg morphology as a maternal effect readout (see methods). Eggs are generally normal in single mutants (dotted grey lines), but in *aub*$^{-}$*;p53*$^{-}$ or *cuff*$^{-}$*;p53*$^{-}$ double mutants (red line) severely stunted eggs are produced. **(C)** The piRNA precursor transcript, *Flamenco*, is significantly elevated in p53^{-} ovaries (red) compared to wild type (wt) controls (black). A similar phenotype is has previously been documented for piRNA pathway mutants where piRNA biogenesis is affected [107,108]. Data represent quantitative RT-PCR assays, using non-overlapping primer pairs specific for this primary piRNA, as in [1].

Wan-Jin Lu uncovered the genetic interactions between p53 and piRNA pathway components presented in panels A and B.

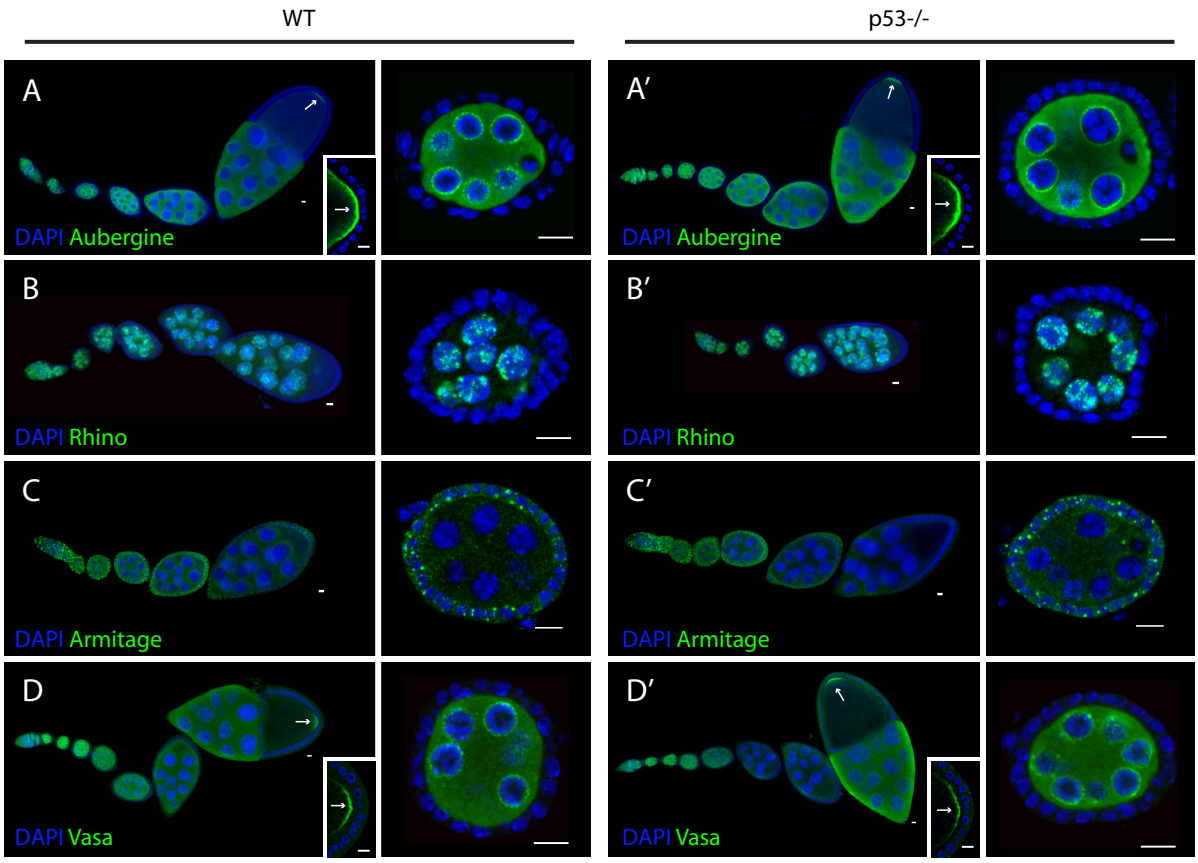

Figure 3-10. piRNA pathway components are expressed and localized normally in the p53^{-} ovary.
(A-D') We performed immunohistochemistry (IHC) for several piRNA pathway proteins in wt and p53^{-} ovaries. As seen here, *Aubergine* **(A, A')**, *Rhino* **(B, B')**, *Armitage* **(C, C')** and *Vasa* **(D, D')** were normally localized and expressed at comparable levels in wt **(A, B, C, D)** and p53^{-} **(A', B', C', D')** animals. Higher magnification images of an egg chamber are shown in panels to the right. Smaller insets in **(A, A', D and D')** are posterior regions of later egg chambers highlighting germ plasm localization of *Aubergine* and *Vasa* [109]. Scale bar 10μm**.** Antibodies used: α-aubergine and α-armitage were gifts from sMikiko Siomi [74,75], α-rhino was gift from William Theurkoff [76].

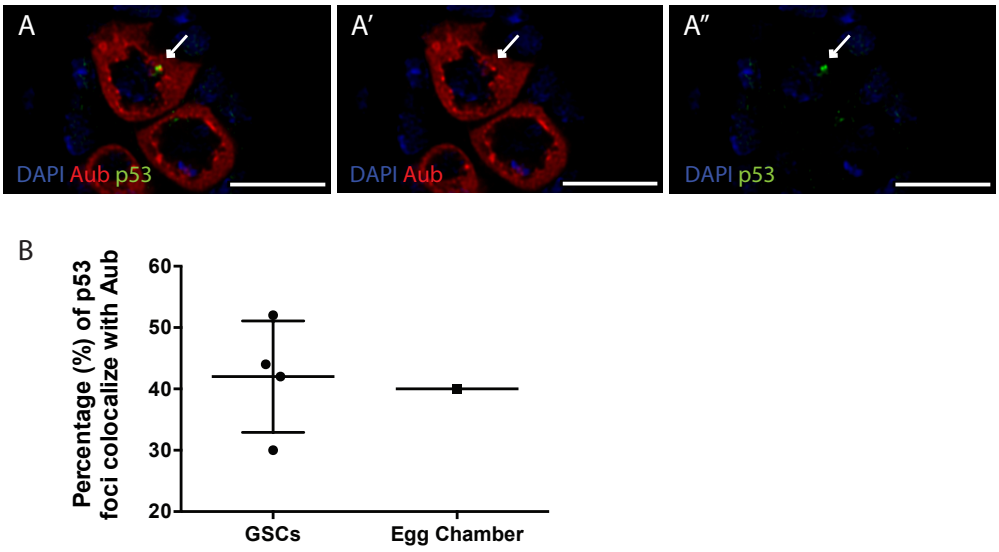

Figure 3-11. Co-localization studies between Aubergine and p53 in the *Drosophila* germline

(A) *Drosophila* ovaries were co-stained with anti-p53 (green) and anti-Aubergine (red) antibodies and counterstained with DAPI (blue). Colocalization studies were performed using IMARIS image analysis software. p53 foci and Aubergine colocalization in **(A)** are quantified in **(B)** indicating that a significant amount of p53 foci co-localize with Aubergine protein.

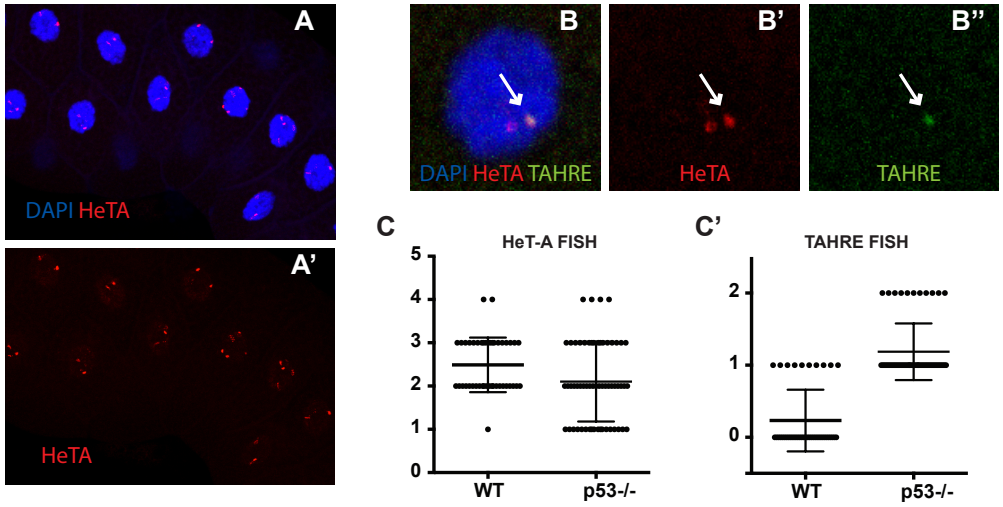

Figure 3-12. Detecting Transposon Copy number by DNA FISH in *Drosophila* salivary glands.

(A-A') Low magnification images of WT salivary glands hybridized with HeT-A DNA FISH probes (red in A and A') and counterstained with DAPI (blue in A). The HeT-A DNA probe forms distinct nuclear foci (A), which can be better appreciated without DAPI counterstain in (A').

(B-B'') High magnification image of WT salivary gland nucleus hybridized with DNA FISH probes for HeT-A (red) and TAHRE (green) retrotransposons and counterstained with DAPI (blue). HeT-A and TAHRE retrotransposon foci occassionaly co-localize (white arrow).

(C-C') Quantification of HeT-A foci (C) and TAHRE foci (C') in WT and $p53^{-/-}$ salivary glands. We observe a modest elevation of transposon foci in the $p53^{-/-}$ animal for TAHRE (C') but not HeT-A (C).

Paula Kurtz provided guidance in generating the DNA FISH probes.

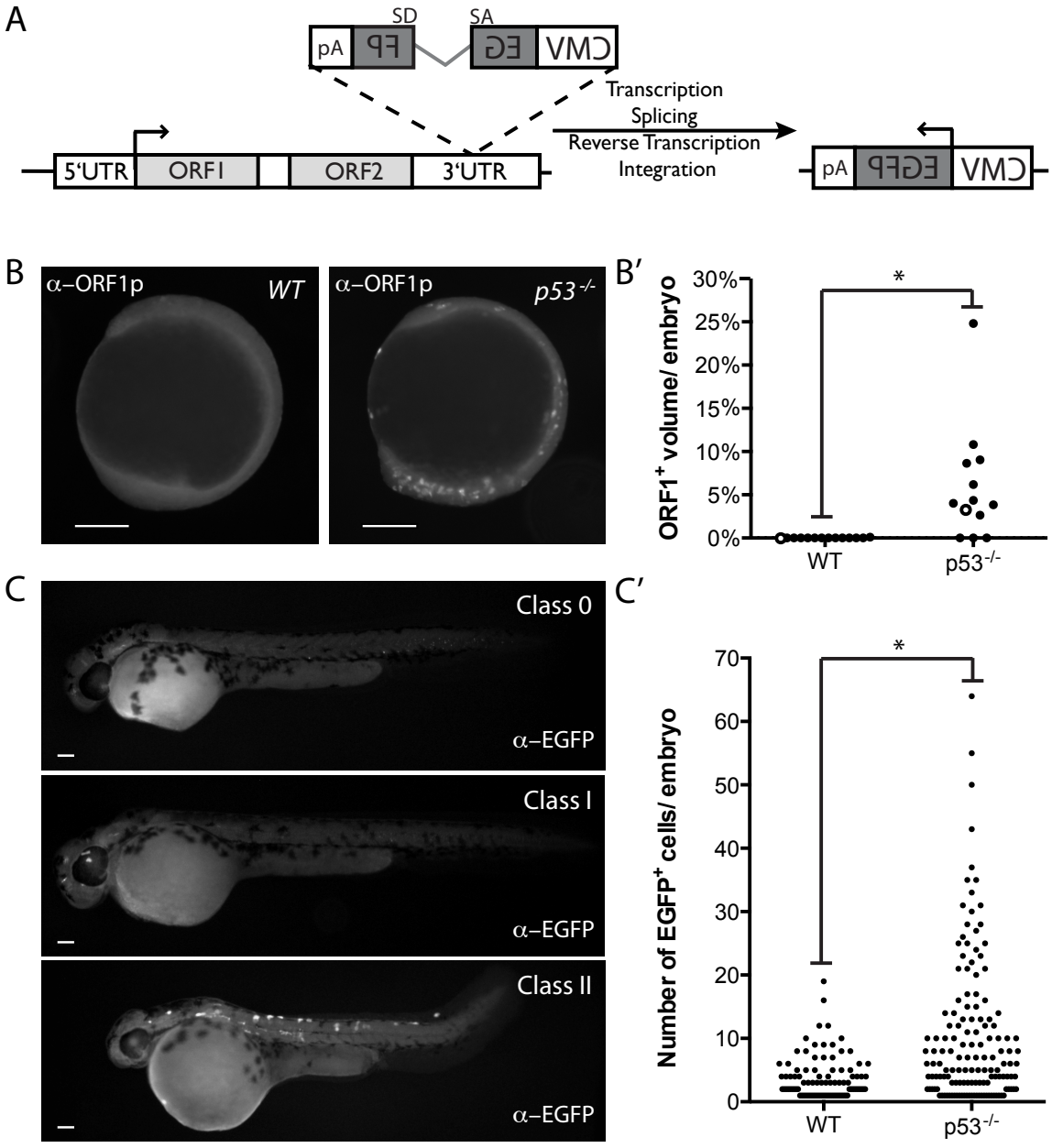

Figure 3-13. Unrestrained transposon activity and *de novo* integration in p53⁻ fish

(A) pLRE3-*mEGFPI* is a widely used integration reporter schematized here. It consists of a retrotransposition-competent human LINE-1 (LRE3) [89] containing an internal RNA polymerase II promoter in its 5' UTR (light grey box), two open reading frames (ORF1, light grey box and ORF2, light grey box), and the *mEGFPI* retrotransposition indicator cassette in its 3'UTR [78,98]. The *mEGFPI* retrotransposition indicator cassette encodes a backward copy of a CMV driven enhanced green fluorescence protein gene (EGFP, dark grey box) which is

interrupted by an intron (SD=splice donor; SA=splice acceptor) that is in the same transcriptional orientation as LRE3 [98]. The arrangement of the indicator cassette ensures that EGFP-positive cells will only arise if the LRE3 transcript undergoes a successful round of retrotransposition. LRE3 expression levels were assayed using a previously described antibody that detects the human ORF1-encoded protein (α-ORF1p) [81]. LRE3 retrotransposition events are visualized using an antibody against EGFP (α-EGFP).

(B-B') LRE3 ORF1p expression in 11 hour post-fertilization embryos injected with the pLRE3-*mEGFPI* expression construct. In **(B)** ORF1p immunoreactivity is undetectable in wt embryos (left panel), but is abundant in $p53^{-}$ embryos (right panel). In **(B')** quantification of ORF1p expression in wt and $p53^{-}$ embryos is plotted. The X axis indicates genotypes injected. The Y axis plots the volume of ORF1 expression normalized to total embryonic volume (see methods) for individual animals (black dots). The two embryos shown in **(B)** are each represented as an open circle on the graph in (B'). Note that prominent ORF1p expression is frequently observed in $p53^{-}$ embryos but is absent in wt animals (* p value <0.0025).

(C-C') Retrotransposition events derived from pLRE3-*mEGFPI* can be stratified into three classes in 48 hour post-fertilization embryos as indicated in **(C).** Class 0 consists of embryos with no EGFP-positive cells. Class I consists of embryos that have fewer than 13 EGFP-positive cells. Class II consists of embryos that have 13 or more EGFP-positive cells. Note that all animals in (C) are $p53^{-}$. In **(C')** the number of EGFP-positive cells in Class I and Class II embryos is plotted for the indicated genotypes (x axis). The Y axis indicates the number of EGFP-positive cells per embryo. Each dot represents an individual animal. Class II embryos were frequently observed in $p53^{-}$ embryos (27.3%), but only rarely were observed in wt animals (2.1%) (* p value <0.0001). The pLRE3H230A-*mEGFPI* expression plasmid contains a missense mutation in the endonuclease domain of the LRE3 ORF2-encoded protein (ORF2p) [79] and serves as a negative control (STable 3). The pLRE3H230A-*mEGFPI* control plasmid produced only class 0 embryos when injected into wt and $p53^{-}$ animals (WT n=149, $p53^{-/-}$ n=49, STable 3). Similarly, uninjected controls only produced class 0 animals (WT n=209, $p53^{-/-}$ n=178, Table 3-3). Scale bars, 200μm.

These studies were performed in collaboration with Jim Amatruda and John V. Moran. Dr. Amatruda provided guidance in experimental design and performed embryo injections for the first two trials in panels C and C'. Dr. Moran provided the pLRE-EGFP reporter construct and guidance in experimental design.

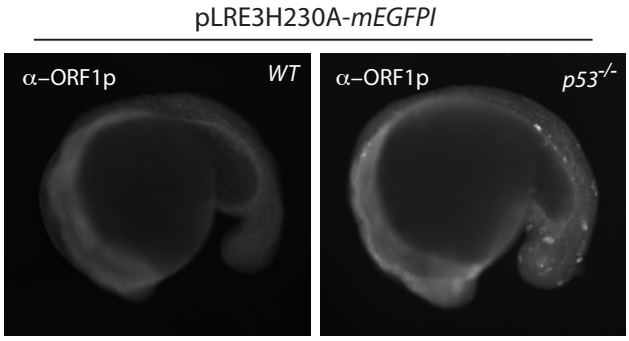

Figure 3-14. p53 acts upstream of the integration event
ORF1p expression in 18 hour post-fertilization embryos injected with the control pLRE3H230A-*mEGFPI* expression construct [79]. With this control, no integrations occur because the mutant pLRE3H230A-*mEGFPI* reporter lacks functional ORF2. Consistent with this, the reporter failed to produce EGFP^{+} cells in both wt and p53^{-} zebrafish (Supplemental Table 3). Furthermore, like its normal counterpart (Figure 2B) ORF1p, expressed from this control construct is abundant in p53^{-} embryos (right panel) but undetectable in parental wt embryos (left panel). Therefore, unlike integration events, derepression of ORF1p in p53 mutants is unaffected by mutations in ORF2. These data suggest that p53 restraint retroelements by impacting the production and/or stabilization of their corresponding transcripts.
These studies were performed in collaboration with Jim Amatruda and John V. Moran who provided guidance in experimental design. Dr. Moran also provided the pLRE-EGFP H230A reporter construct.

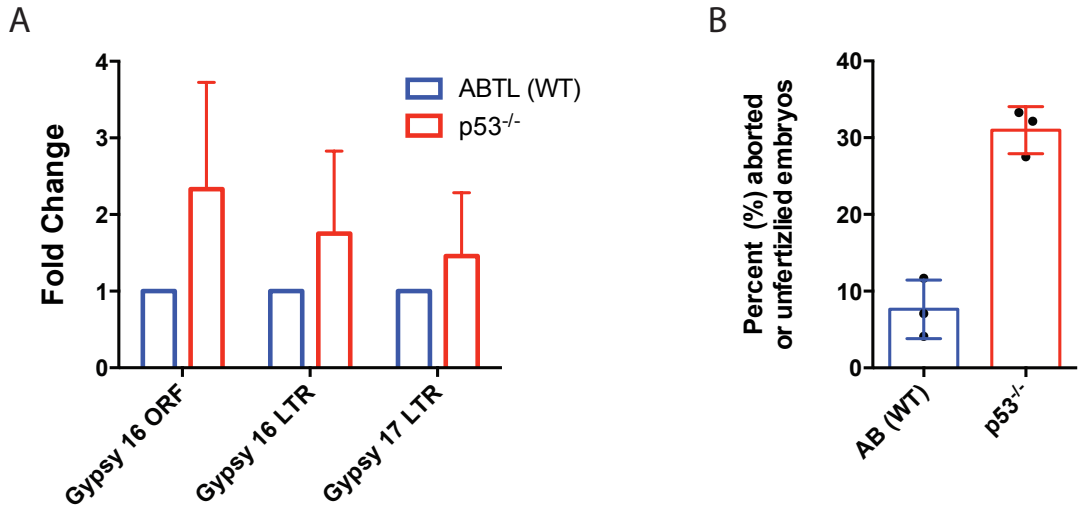

Figure 3-15. Zebrafish p53 restrains endogenous retroelements in the ovary and p53- animals exhibit elevated rates of infertility.

(A) Retrotransposon transcripts were measured in zebrafish ovaries by qRT-PCR. Gypsy retroelements were modestly elevated in $p53^{-/-}$ zebrafish ovaries (red bar) when compared to WT zebrafish ovaries (blue bar). Note that two primer pairs that detect different regions of Gypsy16 are plotted here.

(B) The fertility of $p53^{-/-}$ and WT zebrafish was assessed by scoring the number of unfertilized eggs after matings (see methods). We observed a consistent three fold increase in the number of unfertilized embryos in the $p53^{-/-}$ fish (red bar) when compared to the WT (blue bar). $p53^{-/-}$ infertility is significantly different from the WT (* p value =0.0012) when using an unpaired t-test at the 99% confidence level (see methods). The total number of zebrafish embryos assayed were n=1927 for WT and n=993 for $p53^{-/-}$. These data were from three independent trials from age-matched parental zebrafish.

These studies were performed in collaboration with Jim Amatruda who provided guidance in experimental design and zebrafish tissue.

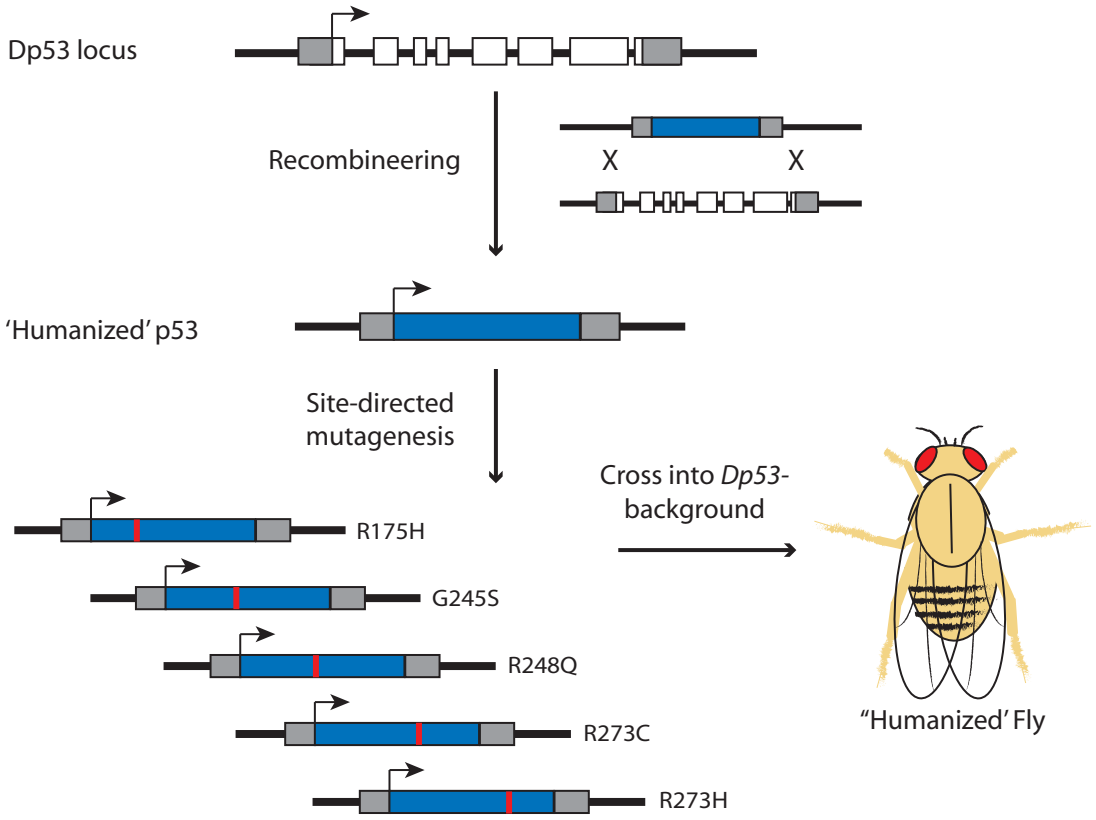

Figure 3-16. Generating 'Humanized' Flies
Schematic for how the "humanized' p53 flies were generated. Diagram of the *Drosophila* p53 locus contained in a BAC where Drosophila p53 exons are shown as white boxes and regulatory regions in grey boxes. The Dp53 coding sequence was replaced with the cDNA of the human p53 coding sequence (blue box) via recombineering. Thus, human p53 is under control of the *Drosophila* p53 regulatory regions. Site directed mutagenesis was performed to generate the hotspot p53 mutations, R175, G245S, R248Q, R273C, R273H (red line). These comprise the most prominent p53 alleles found in human cancers. Transgenic flies were made from 2 independent WT human p53 constructs and 5 cancer alleles and crossed into the Dp53- background. All 'humanized' constructs were inserted into the same genomic site, therefore allowing us to negate positional effects of these transgenes.
Alex D'Brot, a post-doc in the Abrams lab, generated these 'humanized' fly strains.

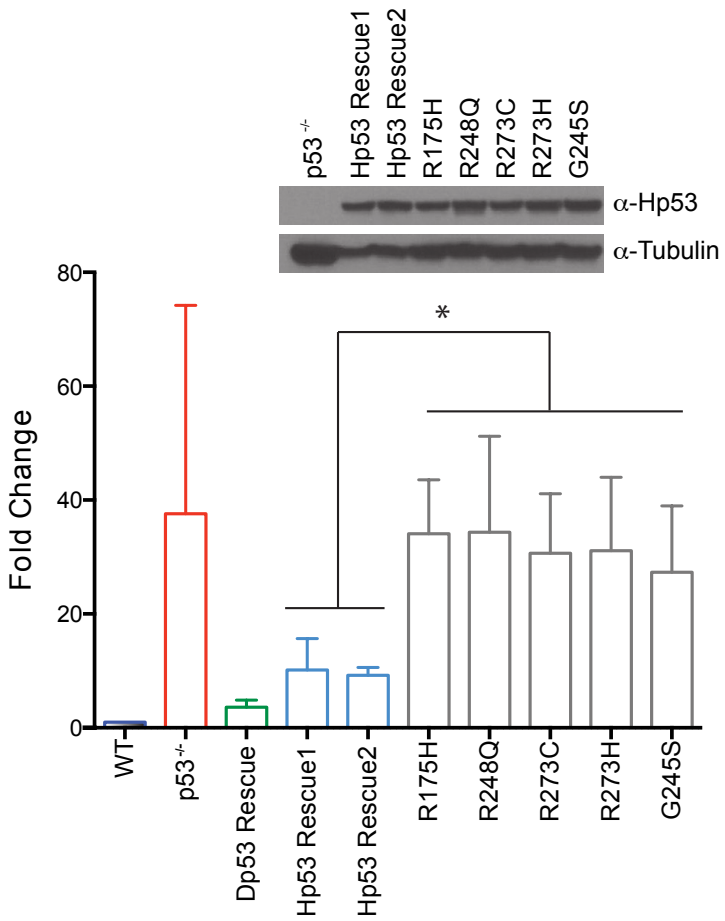

Figure 3-17. Human p53 corrects dysregulated transposon activity in p53^{-} flies but variants commonly seen in patients do not

TAHRE retrotransposon expression was quantified in ovaries from humanized p53 *Drosophila* strains (see text), using droplet digital PCR (standardized to the housekeeping gene, rp49). Note that dysregulation seen in p53^{-} flies (red bar) is effectively corrected in rescue lines encoding either the fly p53 gene (Dp53 Rescue, green bar) or the wild type (WT) human p53 gene (light blue bars). Lines humanized with distinct p53 mutant alleles commonly seen in cancers (grey bars) were not corrected for transposon dysregulation, despite comparable expression levels of human p53 protein from these alleles (shown in the inset using *Drosophila* Tubulin as a loading control). Note that each cancer-associated allele (grey bars) differs from wild type human p53 (light blue bars) by the single amino acid indicated and all human transgenes are positioned at the same 'landing site' in the fly genome (see methods). Hp53 Rescue1 and Hp53 Rescue2 are independently generated lines. All p53 cancer- associated alleles are significantly different from wild type human p53 strains, denoted by the asterisk (p value <0.05, see methods). Error bars represent standard deviations.

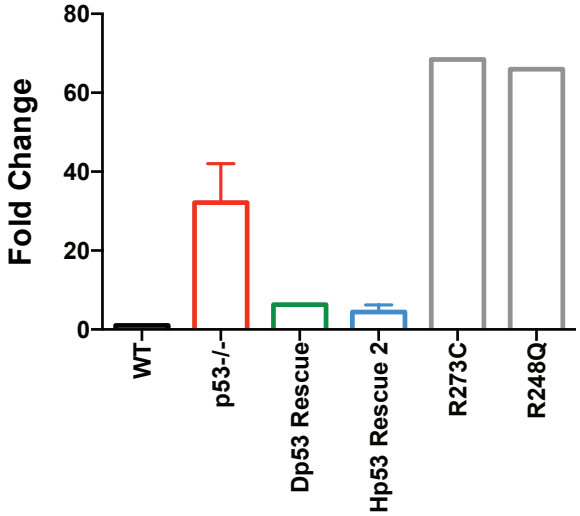

Figure 3-18. p53 cancer alleles fail to repress retroelements in the *Drosophila* soma

TAHRE retrotransposon expression was quantified in heads from humanized p53 *Drosophila* strains ddPCR (standardized to the housekeeping gene, rp49). Note that dysregulation seen in $p53^{-}$ flies (red bar) is effectively corrected in rescue lines encoding either the fly p53 gene (Dp53 Rescue, green bar) or the wild type (WT) human p53 gene (light blue bar). Lines humanized with distinct p53 mutant alleles commonly seen in cancers (grey bars) were not corrected for transposon dysregulation.

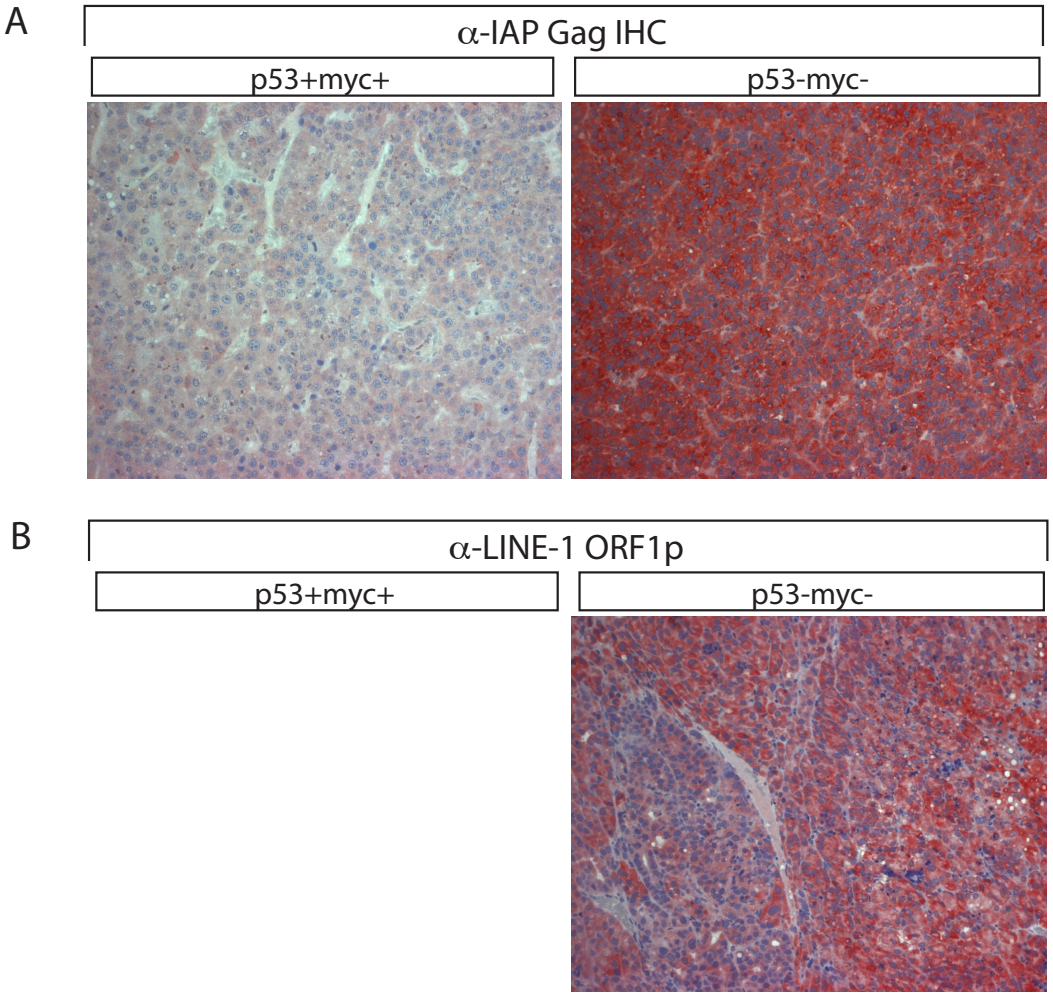

Figure 3-19. Retroelement dysregulation is observed in $p53^{-/-}$ myc driven mouse liver tumors

(A) IAP retroelement activity from identically engineered mouse liver tumors that are Myc-driven but either wild type or mutant for p53 (see methods). We observed highly dysregulated IAPgag expression in the Myc- driven $p53^{-/-}$ tumors but not the myc driven p53 WT tumors.

(B) High dysregulation of LINE-1 ORF1p expression is observed the Myc- driven $p53^{-/-}$. We are currently testing the myc driven p53 WT tumors for L1ORF1p dysregulation

These studies were performed in collaboration with Sarah Comerford and Bob Hammer who provided guidance in experimental design and antibody optimization.

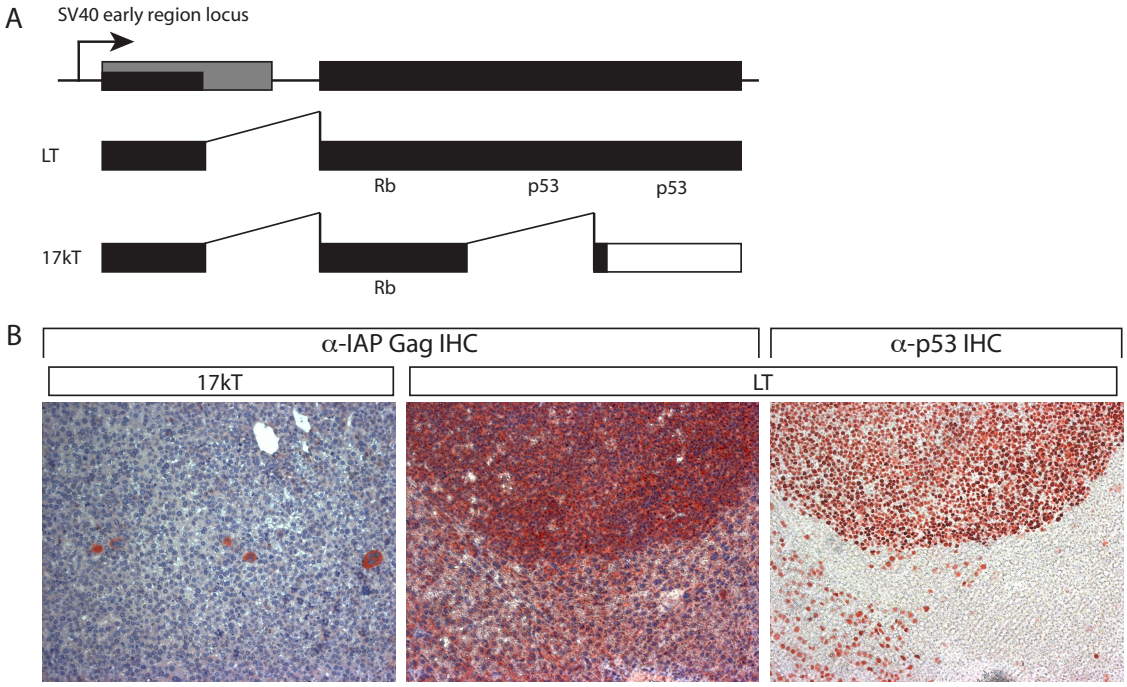

Figure 3-20. T-antigen mouse liver tumors are highly dysregulated for retroelement expression.
(A) Diagram of the SV40 early locus. SV40 encodes several early viral proteins including the large T antigen (LT) and an alternately spliced transcript that generates the 17K T antigen protein(17kT). The LT protein protein binds the Retinoblastoma (Rb) and p53 tumor suppressors while the 17kT protein binds Rb but not p53 [82].
(B) IAPgag (red) expression in 17kT (Left panel) and LT livers (middle panel) livers. We observed robust IAPgag expression in the LT liver tumors. In stark contrast, the majority of the 17KT liver was negative for IAPgag. Stabilized p53 in LT liver tumors (right panel) is consistent with strong IAP immunoreactivity.
These studies were performed in collaboration with Sarah Comerford and Bob Hammer who provided guidance in experimental design and antibody optimization.

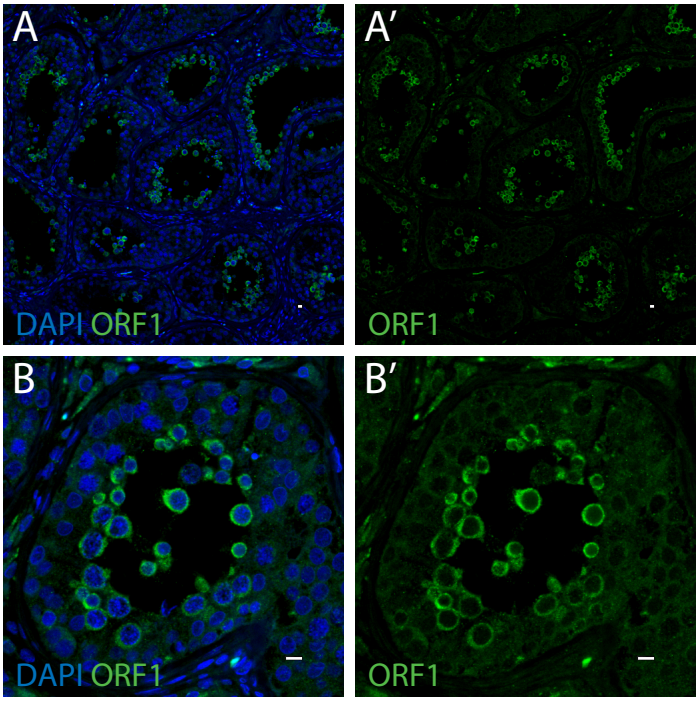

Figure 3-21. LINE-1 ORF1p expression in human testis
Validation of the LINE-1 ORF1p antibody by detecting ORF1p expression (green) in human testis. (A-A') are low magnification images of seminiferous tubules. (B-B') are high magnification images of a single seminiferous tubule. Robust ORF1p expression (green) is observed in the human male germline as previously reported [81]. (A' and B') are the same images as shown in (A and B, respectively) but without DAPI counterstain (blue) to better appreciate ORF1p expression. Human testis samples were provided by Dinesh Rakheja. These studies were performed in collaboration with Dinesh Rakheja, Jim Amatruda and Kenneth Chen.

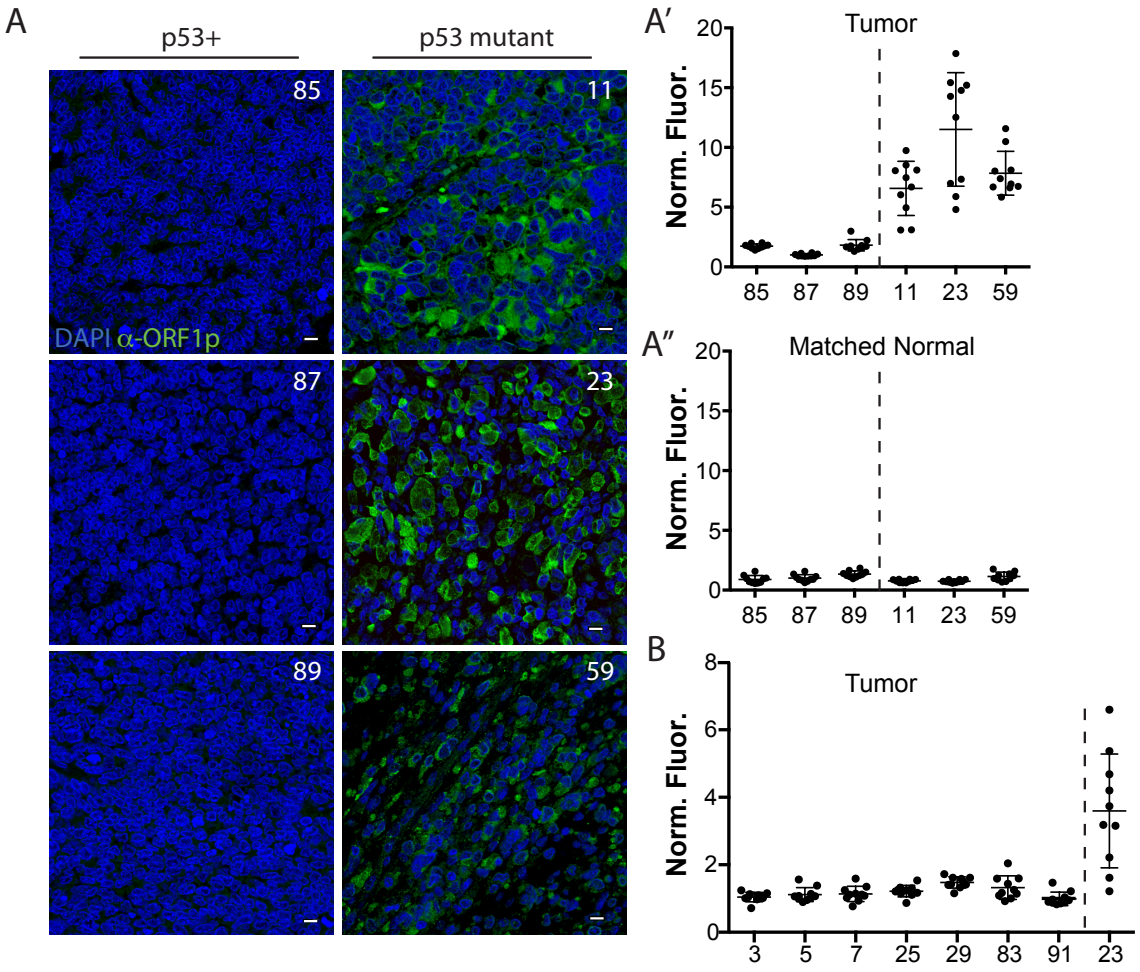

Figure 3-22. Deregulated retroelements stratify with p53 mutations in Wilms tumors

(A) Compared to Wilms tumors that are wild type for p53 (left panels: 85, 87, 89), Wilms tumors that are mutant for p53 (right panels: 11, 23, 59) show dramatically elevated LINE-1 ORF1p expression (α-ORF1p in green; counterstained with DAPI, blue). Scale bars, 10μm.

(A') Quantification of results in **(A)** was measured here using automated image analyses (see methods). On the X axis, tumors wild type for p53 (85, 87, 89) are separated by a dotted line from tumors mutant for p53 (11, 23, 59). The Y axis plots the normalized fluorescence intensity (Norm. Fluor.) where the fluorescence intensity of ORF1p expression is normalized to the DAPI volume (see methods) for individual fields of view, each represented as a dot **(A')**. 10 fields of view were taken per tumor (shown in SFig. 4). The normalized fluorescence intensity of tumors mutant for p53 (11, 23, 59) is significantly different from the tumors wild

type for p53 (85, 87, 59) (p value<0.0001, see methods). In **(A'')** note that fluorescence intensities were similar across all matched normal tissue.
(B) Seven additional Wilms tumors WT for p53 were quantified. On the X axis, tumors wild type for p53 (3, 5, 7, 25, 29, 83, 91) are separated by a dotted line from the tumor mutant for p53 (23, used as a positive control). The Y axis plots the normalized fluorescence intensity (Norm. Fluor.) where the fluorescence intensity of ORF1p expression is normalized to the DAPI volume (see methods) for individual fields of view, each represented as a dot **(B)**. 10 fields of view were taken per tumor. The normalized fluorescence intensity of the tumor mutant for p53 (23) is significantly different from the tumors wild type for p53 (3, 5, 7, 25, 29, 83, 91) (p value<0.0001, see methods). Archived Wilms tumor samples were provided by Dinesh Rakheja. These studies were performed in collaboration with Dinesh Rakheja, Jim Amatruda and Kenneth Chen.

Stage	WT			$p53^{-/-}$			p53Rescue		
	Number with TAHRE signal	Total (n=)	Percent (%)	Number with TAHRE signal	Total (n=)	Percent (%)	Number with TAHRE signal	Total (n=)	Percent (%)
Germ	0	60	0	0	93	0	0	45	0
I	0	60	0	0	93	0	0	45	0
II	0	60	0	0	93	0	0	45	0
III	0	60	0	15	93	15.1	0	45	0
IV	0	60	0	62	89	69.7	0	45	0
V	0	50	0	63	84	75	0	42	0
VI	3	72	4.2	54	62	87.1	4	36	11.1
VII	3	37	8.10	32	32	100	5	32	15.6

Table 3-1. Stage Specific quantification of TAHRE FISH signal in WT, $p53^{-}$, and p53Rescue ovaries

The table indicates the number of *Drosophila* ovaries with TAHRE signal, the total number assayed, and the percent positive for TAHRE signal in each stage of the ovariole. Genotypes are also indicated. Note that TAHRE signal is readily detected in $p53^{-}$ ovaries but rarely seen in wt or p53 rescue flies.

Genotype	Trial	Infertile (n=)	Total (n=)	Percent Infertile (%)
$p53^{-/-}$	1	15	129	11.6%
	2	16	164	9.8%
	Total	**31**	**293**	**10.6%**
p53Rescue; $p53^{-/-}$	1	7	152	4.6%
	2	12	207	5.8%
	Total	**19**	**359**	**5.3%**

Table 3-2. Elevated rates of infertility occur in $p53^{-/-}$ flies
The fertility of $p53^{-/-}$ and p53Rescue flies was assessed by single pair matings to *yw* males (see methods). To negate background influences, $p53^{-/-}$ and p53Rescue flies were backcrossed into the *yw* background ($p53^{-/-}$ 17 generations; p53Rescue 10 generations) before testing fertility. The table indicates number of infertile animals, the total number assayed, and the percent infertile. A modest but reproducible increase in congenital sterility was observed in the $p53^{-/-}$ genotype compared to controls. $p53^{-/-}$ infertility is significantly different from the p53Rescue (* p value =0.0381) when using an unpaired t-test at the 95% confidence level (see methods).

Increased expression in bam$^{-/-}$;p53$^{-/-}$ ovaries

Signal to Log Ratio	P-Value	Transposon
3.6	0.000002	Springer
2.5	0.000408	PPI251
2.1	0.000002	Quasimodo
1.9	0.000002	Blood
1.9	0.000002	Tart
1.7	0.000005	Invader 3
1.7	0.000004	Tart
1.5	0.000002	Copia
1.3	0.000003	Gypsy6
1.2	0.000002	Dm88

Decreased expression in bam$^{-/-}$;p53$^{-/-}$ ovaries

Signal to Log Ratio	P-Value	Transposon
-5.1	0.999998	Tirant
-4.1	0.999897	Gtwin
-3.9	0.999998	DMGYPF1A
-3.8	0.999998	1731
-2.7	0.999998	Tabor
-1.5	0.999998	H-element
-1.5	0.999998	Ivk
-1.4	0.999998	Transpac
-1.1	0.999998	R2-element

Table 3-3 Retroelement transcripts are dysregulated in p53$^{-/-}$ ovarian stem-like tumors in *Drosophila*

We performed microarray analysis on bam$^{-/-}$ and bam$^{-/-}$;p53$^{-/-}$ tumors (see methods in Chapter 2). The transposon transcripts that are altered by p53 status in bam$^{-/-}$ tumors are recorded. Listed on the top table are the retroelements whose abundance is directly or indirectly suppressed by p53. Listed on the bottom table are the transposon transcripts whose abundance is directly or indirectly induced by p53. The fold dysregulation (log2) is listed on the left, the p-value is listed in the middle, and the transposon identity is listed on the left. Note that the transposon transcripts that are elevated in the bam$^{-/-}$;p53$^{-/-}$ animal are signficiantly different from bam$^{-/-}$ animals. However transcripts that are decreased in the bam$^{-/-}$;p53$^{-/-}$ animals are not significant.

	Plasmid	EGFP+ (n=)	Total (n=)	Percent EGFP+ (%)
WT				
	pLRE3-*mEGFPI* TR1	28	58	48.3%
	pLRE3-*mEGFPI* TR2	27	48	56.2%
	pLRE3-*mEGFPI* TR3	14	27	51.8%
	pLRE3-*mEGFPI* TR4	25	32	68.7%
	pLRE3H230A-*mEGFPI* TR1	0	30	0%
	pLRE3H230A-*mEGFPI* TR2	0	119	0%
	Uninjected control TR1	0	51	0%
	Uninjected control TR2	0	37	0%
	Uninjected control TR3	0	121	0%
$p53^{-/-}$				
	pLRE3-*mEGFPI* TR1	59	96	61.4%
	pLRE3-*mEGFPI* TR2	64	106	60.3%
	pLRE3-*mEGFPI* TR3	20	33	60.6%
	pLRE3H230A-*mEGFPI* TR1	0	49	0%
	Uninjected control TR1	0	9	0%
	Uninjected control TR2	0	37	0%
	Uninjected control TR3	0	132	0%

Table 3-4. Quantification of LINE-1 reporter integration in WT and $p53^{-/-}$ zebrafish

The table quantifies the number of EGFP positive cells in parental wt and $p53^{-}$ zebrafish embryos injected with a LINE-1 movement reporter (pLRE3-*mEGFPI*). Different trials are designated as (TR1, etc). The number of EGFP+ embryos, the total number of embryos, and the percent EGFP+ embryos are indicated. The number of EGFP+ embryos include both class I and class II embryos. The number of EGFP+ cells per embryo are graphed in Figure 2C'. Note that EGFP+ cells were never observed with uninjected control animals or with a mutated version of the reporter (pLRE3H230A-*mEGFPI*). These studies were performed in collaboration with Jim Amatruda and John V. Moran.

Genotype	Trial	Unfertilized (n=)	Total (n=)	Percent Infertile (%)
$p53^{-/-}$	1	135	491	27.5%
	2	82	255	32.1%
	3	82	247	33.3
	Total	**299**	**993**	**30.1%**
WT(AB)	1	130	1108	11.7%
	2	10	243	4.1%
	3	41	576	7.1
	Total	**181**	**1927**	**9.4%**

Table 3-5. Elevated rates of infertility occur in $p53^{-/-}$ zebrafish
The fertility of $p53^{-/-}$ and WT zebrafish was assessed by scoring the number of unfertilized eggs after matings (see methods). The table indicates number of unfertilized embryos, the total number assayed, and the percent unfertilized. We observed a consistent three fold increase in the number of unfertilized embryos in the $p53^{-/-}$ fish when compared to the WT. $p53^{-/-}$ infertility is significantly different from the WT (* p value =0.0012) when using an unpaired t-test at the 99% confidence level (see methods). These studies were performed in collaboration with Jim Amatruda and John V. Moran.

Table 3-6: Primer and Probe sequences used in these studies:

Primer	Sequence
TAHRE Fwd	CTGTTGCACAAAGCCAAGAA
TAHRE Rev	GTTGGTAATGTTCGCGTCCT
Rp49 Fwd	ATGACCATCCGCCCAGCATACA
Rp49 Rev	CGTAACCGATGTTGGGCATCAGATACT
Idefix Fwd	AACAAAATCGTGGCAGGAAG
Idefix Rev	TCCATTTTTCGCGTTTACTG
Burdock Fwd	GCCATCCCAACAGCAAAATTC
Burdock Rev	TTTTGGCCCTGTAAACCTTG
HeT-A Fwd	TCCAACTTTGTAACTCCCAGC
HeT-A Rev	TTCTGGCTTTGGATTCCTCG
Gypsy Fwd	CCAGGTCGGGCTGTTATAGG
Gypsy Rev	GAACCGGTGTACTCAAGAGC
Flamenco Fwd1	CAGATTACCATTTGGCTATGAGGATCAGAC
Flamenco Rev1	TGGTGAAATACCAAAGTCTTGGGTCAA C
Flamenco Fwd 2	TCTGGAGGGTTTCCTCCTTT
Flamenco Rev 2	GGTGGTACGACCATCCAAAC

DDPCR Primer/Probe Sequence

Primer/Probe	Sequence	Dye/Quencher
TAHRE Fwd	CTGTTGCACAAAGCCAAGAA	
TAHRE Rev	GTTGGTAATGTTCGCGTCCT	
TAHRE Probe	TCACCAGAGCAGTTGACGCAGG	Fam/Zen/IBFQ
Rp49 Fwd	ATGACCATCCGCCCAGCATACA	

Rp49 Rev	CGTAACCGATGTTGGGCATCAGATACT	
Rp49 Probe	ATCGATCCGACTGGTGGCGGATGAAGTG CTTGGT	HEX/ZEN/IBFQ

TAHRE Stellaris Probe Sequence (Quasar 570 Dye)

gtgttggtgagtatgtgaga
tttctgcgcttatgtttgtg
actagtaatggccttcttga
tattttcttggttgtgttcc
tgaccatgaagcgtagcaac
aaatgtctggctttgggttt
cactatttccagtacggttg
tcttttggtgggggaaatg
gcagaagggcataacgaagc
gctgctgataaattcacctc
ggctcctggaagatgaatta
aaactcataggctgctcttc
gggtgctattatatctggac
aaagctagagcagtccagat
taggagtcgcacgtaatctt
aaacgggtgtaatgagcggg
tctacatctgtgttctgagg
caatttccctcacattgttg
gactcctgctgtataattca
gattttgttgtaggcagtca
aaaggaaaaccgttggcggt
aggtgtctgatgatgactcg
cgagcatggtgtggaatgat
attcgtcatgtttctagcga

cttcaaacattcgcatgggg
gagataattttgccatggct
tgtttttcctttcgatatcc
catgaatttttggagtgcct
tgcaacaggatgacaggtga
ccttgtacgcactaatatgc
tttcagtcttataagcgggg
tccttgattgtccttatttt
tcgtccatagttggtaatgt
ggaaagttgttgcgagaggg
tgaggagctaaatggtagcc
cttgcttcgtttctgttttg
aaagtcgtgggaggagaagc
gccatttattcagacgtttc
tttggagacgttgtcagagt
aggattgctcgtcatgttag
agcttttcctggaacatttc
cctgatgtttgtcttctttt
ggatgttgtcgtctatgatc
ttttgcgggttagagtatgt
cttttgctgtcgaagtcaga
atattttccactcgttgtgt
gtagactctttcgtggattc
ttaggaggtcatgaggtgtg

a

BIBLIOGRAPHY

This is an entry that is preformatted to have a hanging indent that will bring the second line of the bibliographic reference in about .5 inch. Apply the Reference Item style to produce this format.

1 Levine, A. J. & Oren, M. The first 30 years of p53: growing ever more complex. *Nat Rev Cancer* **9**, 749-758, doi:nrc2723 [pii]
10.1038/nrc2723 (2009).

2 Vousden, K. H. & Lane, D. P. p53 in health and disease. *Nat Rev Mol Cell Biol* **8**, 275-283 (2007).

3 Vousden, K. H. & Prives, C. Blinded by the Light: The Growing Complexity of p53. *Cell* **137**, 413-431, doi:S0092-8674(09)00459-0 [pii]
10.1016/j.cell.2009.04.037 (2009).

4 Jacks, T. *et al.* Tumor spectrum analysis in p53-mutant mice. *Current biology : CB* **4**, 1-7 (1994).

5 Martin-Caballero, J., Flores, J. M., Garcia-Palencia, P. & Serrano, M. Tumor susceptibility of p21(Waf1/Cip1)-deficient mice. *Cancer research* **61**, 6234-6238 (2001).

6 Villunger, A. *et al.* p53- and drug-induced apoptotic responses mediated by BH3-only proteins puma and noxa. *Science* **302**, 1036-1038 (2003).

7 Valente, L. J. *et al.* p53 Efficiently Suppresses Tumor Development in the Complete Absence of Its Cell-Cycle Inhibitory and Proapoptotic Effectors p21, Puma, and Noxa. *Cell reports*, doi:10.1016/j.celrep.2013.04.012 (2013).

8 Soussi, T. p53 alterations in human cancer: more questions than answers. *Oncogene* **26**, 2145-2156, doi:1210280 [pii]
10.1038/sj.onc.1210280 (2007).

9 Donehower, L. A. *et al.* Effects of genetic background on tumorigenesis in p53-deficient mice. *Mol Carcinog* **14**, 16-22 (1995).

10 Lang, G. A. *et al.* Gain of function of a p53 hot spot mutation in a mouse model of Li-Fraumeni syndrome. *Cell* **119**, 861-872, doi:S0092867404010487 [pii]
10.1016/j.cell.2004.11.006 (2004).

11 Olive, K. P. *et al.* Mutant p53 gain of function in two mouse models of Li-Fraumeni syndrome. *Cell* **119**, 847-860, doi:10.1016/j.cell.2004.11.004 (2004).

12 Lubin, R. *et al.* Serum p53 antibodies as early markers of lung cancer. *Nature medicine* **1**, 701-702 (1995).

13 King, N. *et al.* The genome of the choanoflagellate Monosiga brevicollis and the origin of metazoans. *Nature* **451**, 783-788, doi:nature06617 [pii]
10.1038/nature06617 (2008).

14 Lu, W. J., Amatruda, J. F. & Abrams, J. M. p53 ancestry: gazing through an evolutionary lens. *Nat Rev Cancer* **9**, 758-762 (2009).

15 Pankow, S. & Bamberger, C. The p53 tumor suppressor-like protein nvp63 mediates selective germ cell death in the sea anemone Nematostella vectensis. *PLoS One* **2**, e782, doi:10.1371/journal.pone.0000782 (2007).

16 Barker, C. M., Calvert, R. J., Walker, C. W. & Reinisch, C. L. Detection of mutant p53 in clam leukemia cells. *Exp Cell Res* **232**, 240-245, doi:10.1006/excr.1997.3513 (1997).

17 Brodsky, M. H. *et al.* Drosophila p53 binds a damage response element at the reaper locus. *Cell* **101**, 103-113 (2000).

18 Jin, S. *et al.* Identification and characterization of a p53 homologue in Drosophila melanogaster. *Proc Natl Acad Sci U S A* **97**, 7301-7306. (2000).

19 Ollmann, M. *et al.* Drosophila p53 is a structural and functional homolog of the tumor suppressor p53. *Cell* **101**, 91-101 (2000).

20 Bessard, A. C. *et al.* Regulation of the specific DNA binding activity of Xenopus laevis p53: evidence for conserved regulation through the carboxy-terminus of the protein. *Oncogene* **16**, 883-890, doi:10.1038/sj.onc.1201598 (1998).

21 Chen, J. *et al.* Loss of function of def selectively up-regulates Delta113p53 expression to arrest expansion growth of digestive organs in zebrafish. *Genes & development* **19**, 2900-2911, doi:10.1101/gad.1366405 (2005).

22 Oren, M. & Levine, A. J. Molecular cloning of a cDNA specific for the murine p53 cellular tumor antigen. *Proceedings of the National Academy of Sciences of the United States of America* **80**, 56-59 (1983).

23 Lu, W. J., Chapo, J., Roig, I. & Abrams, J. M. Meiotic recombination provokes functional activation of the p53 regulatory network. *Science* **328**, 1278-1281 (2010).

24 Hu, W., Feng, Z., Teresky, A. K. & Levine, A. J. p53 regulates maternal reproduction through LIF. *Nature* **450**, 721-724 (2007).

25 Rotter, V. *et al.* Mice with reduced levels of p53 protein exhibit the testicular giant-cell degenerative syndrome. *Proceedings of the National Academy of Sciences of the United States of America* **90**, 9075-9079 (1993).

26 Beumer, T. L. *et al.* The role of the tumor suppressor p53 in spermatogenesis. *Cell Death Differ* **5**, 669-677, doi:10.1038/sj.cdd.4400396 (1998).

27 Derry, W. B., Putzke, A. P. & Rothman, J. H. Caenorhabditis elegans p53: role in apoptosis, meiosis, and stress resistance. *Science* **294**, 591-595 (2001).

28 Schumacher, B. *et al.* C. elegans ced-13 can promote apoptosis and is induced in response to DNA damage. *Cell Death Differ* **12**, 153-161 (2005).

29 Derry, W. B. *et al.* Regulation of developmental rate and germ cell proliferation in Caenorhabditis elegans by the p53 gene network. *Cell Death Differ* **14**, 662-670 (2007).

30 Donehower, L. A. *et al.* Mice deficient for p53 are developmentally normal but susceptible to spontaneous tumours. *Nature* **356**, 215-221, doi:10.1038/356215a0 (1992).

31 Lee, J. H. *et al.* In vivo p53 function is indispensable for DNA damage-induced apoptotic signaling in Drosophila. *FEBS letters* **550**, 5-10 (2003).

32 Sogame, N., Kim, M. & Abrams, J. M. Drosophila p53 preserves genomic stability by regulating cell death. *Proc Natl Acad Sci U S A* **100**, 4696-4701 (2003).
33 Nordstrom, W. & Abrams, J. M. Guardian ancestry: fly p53 and damage-inducible apoptosis. *Cell Death & Differentiation* **7**, 1035-1038 (2000).
34 Aranda-Anzaldo, A. & Dent, M. A. Reassessing the role of p53 in cancer and ageing from an evolutionary perspective. *Mech Ageing Dev* **128**, 293-302, doi:S0047-6374(07)00016-4 [pii]
10.1016/j.mad.2007.01.001 (2007).
35 Cicalese, A. *et al.* The tumor suppressor p53 regulates polarity of self-renewing divisions in mammary stem cells. *Cell* **138**, 1083-1095, doi:S0092-8674(09)00840-X [pii]
10.1016/j.cell.2009.06.048 (2009).
36 Krizhanovsky, V. & Lowe, S. W. Stem cells: The promises and perils of p53. *Nature* **460**, 1085-1086, doi:10.1038/4601085a (2009).
37 Lin, T. *et al.* p53 induces differentiation of mouse embryonic stem cells by suppressing Nanog expression. *Nat Cell Biol* **7**, 165-171, doi:ncb1211 [pii]
10.1038/ncb1211 (2005).
38 Neveu, P. *et al.* MicroRNA profiling reveals two distinct p53-related human pluripotent stem cell states. *Cell Stem Cell* **7**, 671-681, doi:S1934-5909(10)00634-X [pii]
10.1016/j.stem.2010.11.012 (2010).
39 Zhao, T. & Xu, Y. p53 and stem cells: new developments and new concerns. *Trends Cell Biol* **20**, 170-175, doi:S0962-8924(09)00299-2 [pii]
10.1016/j.tcb.2009.12.004 (2010).
40 Pearson, B. J. & Sanchez Alvarado, A. A planarian p53 homolog regulates proliferation and self-renewal in adult stem cell lineages. *Development* **137**, 213-221, doi:137/2/213 [pii]
10.1242/dev.044297 (2010).
41 Eliazer, S., Shalaby, N. A. & Buszczak, M. Loss of lysine-specific demethylase 1 nonautonomously causes stem cell tumors in the Drosophila ovary. *Proc Natl Acad Sci U S A* **108**, 7064-7069, doi:10.1073/pnas.1015874108 (2011).
42 McKearin, D. & Ohlstein, B. A role for the Drosophila bag-of-marbles protein in the differentiation of cystoblasts from germline stem cells. *Development* **121**, 2937-2947 (1995).
43 Chen, D. & McKearin, D. M. A discrete transcriptional silencer in the bam gene determines asymmetric division of the Drosophila germline stem cell. *Development* **130**, 1159-1170 (2003).
44 Sykiotis, G. P. & Bohmann, D. Keap1/Nrf2 signaling regulates oxidative stress tolerance and lifespan in Drosophila. *Developmental cell* **14**, 76-85, doi:10.1016/j.devcel.2007.12.002 (2008).
45 Venken, K. J. *et al.* Versatile P[acman] BAC libraries for transgenesis studies in Drosophila melanogaster. *Nature methods* **6**, 431-434, doi:nmeth.1331 [pii]
10.1038/nmeth.1331 (2009).

46 Galindo, K. A., Lu, W. J., Park, J. H. & Abrams, J. M. The Bax/Bak ortholog in Drosophila, Debcl, exerts limited control over programmed cell death. *Development* **136**, 275-283, doi:dev.019042 [pii]
10.1242/dev.019042 (2009).
47 Rorth, P. Gal4 in the Drosophila female germline. *Mech Dev* **78**, 113-118 (1998).
48 Song, Y. H., Mirey, G., Betson, M., Haber, D. A. & Settleman, J. The Drosophila ATM ortholog, dATM, mediates the response to ionizing radiation and to spontaneous DNA damage during development. *Curr Biol* **14**, 1354-1359, doi:10.1016/j.cub.2004.06.064
S0960982204004762 [pii] (2004).
49 Seita, J. *et al.* Gene Expression Commons: an open platform for absolute gene expression profiling. *PloS one* **7**, e40321, doi:10.1371/journal.pone.0040321 (2012).
50 Ward, J. F. The complexity of DNA damage: relevance to biological consequences. *Int J Radiat Biol* **66**, 427-432 (1994).
51 Chen, Y., Pane, A. & Schupbach, T. Cutoff and aubergine mutations result in retrotransposon upregulation and checkpoint activation in Drosophila. *Curr Biol* **17**, 637-642, doi:10.1016/j.cub.2007.02.027 (2007).
52 Klattenhoff, C. *et al.* Drosophila rasiRNA pathway mutations disrupt embryonic axis specification through activation of an ATR/Chk2 DNA damage response. *Dev Cell* **12**, 45-55 (2007).
53 Mehrotra, S. & McKim, K. S. Temporal analysis of meiotic DNA double-strand break formation and repair in Drosophila females. *PLoS genetics* **2**, e200, doi:10.1371/journal.pgen.0020200 (2006).
54 Yu, T. W. & Anderson, D. Reactive oxygen species-induced DNA damage and its modification: a chemical investigation. *Mutation research* **379**, 201-210 (1997).
55 Lee, T., Feig, L. & Montell, D. J. Two distinct roles for Ras in a developmentally regulated cell migration. *Development* **122**, 409-418 (1996).
56 Joyce, E. F. *et al.* Drosophila ATM and ATR have distinct activities in the regulation of meiotic DNA damage and repair. *The Journal of cell biology* **195**, 359-367, doi:10.1083/jcb.201104121 (2011).
57 Lin, H., Yue, L. & Spradling, A. C. The Drosophila fusome, a germline-specific organelle, contains membrane skeletal proteins and functions in cyst formation. *Development* **120**, 947-956 (1994).
58 D'Brot, A. *Of apoptosomes and oncogenes: repurposing a death machine and deconstructing the action of p53 mutations* Ph.D. thesis, UT Southwestern Medical Center at Dallas, (2014).
59 Abdu, U., Brodsky, M. & Schupbach, T. Activation of a meiotic checkpoint during Drosophila oogenesis regulates the translation of Gurken through Chk2/Mnk. *Curr Biol* **12**, 1645-1651 (2002).
60 Deng, W. & Lin, H. Spectrosomes and fusomes anchor mitotic spindles during asymmetric germ cell divisions and facilitate the formation of a polarized microtubule array for oocyte specification in Drosophila. *Developmental biology* **189**, 79-94, doi:10.1006/dbio.1997.8669 (1997).

61 Mandal, P. K., Blanpain, C. & Rossi, D. J. DNA damage response in adult stem cells: pathways and consequences. *Nat Rev Mol Cell Biol* **12**, 198-202, doi:nrm3060 [pii]
10.1038/nrm3060 (2011).
62 Sperka, T., Wang, J. & Rudolph, K. L. DNA damage checkpoints in stem cells, ageing and cancer. *Nature reviews. Molecular cell biology* **13**, 579-590, doi:10.1038/nrm3420 (2012).
63 Drummond-Barbosa, D. & Spradling, A. C. Stem cells and their progeny respond to nutritional changes during Drosophila oogenesis. *Dev Biol* **231**, 265-278, doi:10.1006/dbio.2000.0135
S0012-1606(00)90135-0 [pii] (2001).
64 Wylie, A., Lu, W. J., D'Brot, A., Buszczak, M. & Abrams, J. M. p53 activity is selectively licensed in the Drosophila stem cell compartment. *Elife* **3**, e01530, doi:10.7554/eLife.01530 (2014).
65 Cordaux, R. & Batzer, M. A. The impact of retrotransposons on human genome evolution. *Nature reviews. Genetics* **10**, 691-703, doi:10.1038/nrg2640 (2009).
66 Beck, C. R. *et al.* LINE-1 retrotransposition activity in human genomes. *Cell* **141**, 1159-1170, doi:S0092-8674(10)00557-X [pii]
10.1016/j.cell.2010.05.021 (2010).
67 Carreira, P. E., Richardson, S. R. & Faulkner, G. J. L1 retrotransposons, cancer stem cells and oncogenesis. *FEBS J* **281**, 63-73, doi:10.1111/febs.12601 (2014).
68 Miki, Y. *et al.* Disruption of the APC gene by a retrotransposal insertion of L1 sequence in a colon cancer. *Cancer research* **52**, 643-645 (1992).
69 Khurana, J. S. & Theurkauf, W. piRNAs, transposon silencing, and Drosophila germline development. *J Cell Biol* **191**, 905-913, doi:jcb.201006034 [pii]
10.1083/jcb.201006034 (2010).
70 Czech, B., Preall, J. B., McGinn, J. & Hannon, G. J. A transcriptome-wide RNAi screen in the Drosophila ovary reveals factors of the germline piRNA pathway. *Mol Cell* **50**, 749-761, doi:10.1016/j.molcel.2013.04.007 (2013).
71 Soper, S. F. *et al.* Mouse maelstrom, a component of nuage, is essential for spermatogenesis and transposon repression in meiosis. *Dev Cell* **15**, 285-297, doi:10.1016/j.devcel.2008.05.015 (2008).
72 Nagarkar-Jaiswal, S. *et al.* A genetic toolkit for tagging intronic MiMIC containing genes. *eLife* **4**, doi:10.7554/eLife.08469 (2015).
73 Link, N., Kurtz, P., O'Neal, M., Garcia-Hughes, G. & Abrams, J. M. A p53 enhancer region regulates target genes through chromatin conformations in cis and in trans. *Genes Dev* **27**, 2433-2438, doi:10.1101/gad.225565.113 (2013).
74 Nishida, K. M. *et al.* Gene silencing mechanisms mediated by Aubergine piRNA complexes in Drosophila male gonad. *RNA* **13**, 1911-1922, doi:rna.744307 [pii]
10.1261/rna.744307 (2007).
75 Saito, K. *et al.* Roles for the Yb body components Armitage and Yb in primary piRNA biogenesis in Drosophila. *Genes Dev* **24**, 2493-2498, doi:gad.1989510 [pii]
10.1101/gad.1989510 (2010).

76 Klattenhoff, C. *et al.* The Drosophila HP1 homolog Rhino is required for transposon silencing and piRNA production by dual-strand clusters. *Cell* **138**, 1137-1149, doi:S0092-8674(09)00853-8 [pii]
10.1016/j.cell.2009.07.014 (2009).
77 Westerfield, M. *A guide for the laboratory use of zebrafish (Danio rerio)* 4th ed. edn, (University of Oregon Press; . , 2000).
78 Garcia-Perez, J. L. *et al.* Epigenetic silencing of engineered L1 retrotransposition events in human embryonic carcinoma cells. *Nature* **466**, 769-773, doi:nature09209 [pii]
10.1038/nature09209 (2010).
79 Coufal, N. G. *et al.* Ataxia telangiectasia mutated (ATM) modulates long interspersed element-1 (L1) retrotransposition in human neural stem cells. *Proc Natl Acad Sci U S A* **108**, 20382-20387, doi:1100273108 [pii]
10.1073/pnas.1100273108 (2011).
80 Coufal, N. G. *et al.* L1 retrotransposition in human neural progenitor cells. *Nature* **460**, 1127-1131, doi:10.1038/nature08248 (2009).
81 Rodic, N. *et al.* Long interspersed element-1 protein expression is a hallmark of many human cancers. *Am J Pathol* **184**, 1280-1286, doi:S0002-9440(14)00077-7 [pii]
10.1016/j.ajpath.2014.01.007 (2014).
82 Comerford, S. A., Schultz, N., Hinnant, E. A., Klapproth, S. & Hammer, R. E. Comparative analysis of SV40 17kT and LT function in vivo demonstrates that LT's C-terminus re-programs hepatic gene expression and is necessary for tumorigenesis in the liver. *Oncogenesis* **1**, e28, doi:10.1038/oncsis.2012.27 (2012).
83 Rakheja, D. *et al.* Somatic mutations in DROSHA and DICER1 impair microRNA biogenesis through distinct mechanisms in Wilms tumours. *Nat Commun* **2**, 4802, doi:ncomms5802 [pii]
10.1038/ncomms5802 (2014).
84 Shpiz, S. *et al.* Mechanism of the piRNA-mediated silencing of Drosophila telomeric retrotransposons. *Nucleic Acids Res* **39**, 8703-8711, doi:gkr552 [pii]
10.1093/nar/gkr552 (2011).
85 Illmensee, K. & Mahowald, A. P. Transplantation of posterior polar plasm in Drosophila. Induction of germ cells at the anterior pole of the egg. *Proceedings of the National Academy of Sciences of the United States of America* **71**, 1016-1020 (1974).
86 Lehmann, R. & Ephrussi, A. Germ plasm formation and germ cell determination in Drosophila. *Ciba Found Symp* **182**, 282-296; discussion 296-300 (1994).
87 Hu, W., Zheng, T. & Wang, J. Regulation of Fertility by the p53 Family Members. *Genes Cancer* **2**, 420-430, doi:10.1177/1947601911408892
10.1177_1947601911408892 [pii] (2011).
88 Peters, M. *et al.* Chk2 regulates irradiation-induced, p53-mediated apoptosis in Drosophila. *Proc Natl Acad Sci U S A* **99**, 11305-11310 (2002).

89 Brouha, B. *et al.* Evidence consistent with human L1 retrotransposition in maternal meiosis I. *American journal of human genetics* **71**, 327-336, doi:S0002-9297(07)60478-9 [pii]
10.1086/341722 (2002).
90 McKim, K. S. & Hayashi-Hagihara, A. mei-W68 in Drosophila melanogaster encodes a Spo11 homolog: evidence that the mechanism for initiating meiotic recombination is conserved. *Genes Dev* **12**, 2932-2942 (1998).
91 Fuller, A. M., Cook, E. G., Kelley, K. J. & Pardue, M. L. Gag proteins of Drosophila telomeric retrotransposons: collaborative targeting to chromosome ends. *Genetics* **184**, 629-636, doi:10.1534/genetics.109.109744 (2010).
92 McClintock, B. Induction of Instability at Selected Loci in Maize. *Genetics* **38**, 579-599 (1953).
93 Aravin, A. A., Hannon, G. J. & Brennecke, J. The Piwi-piRNA pathway provides an adaptive defense in the transposon arms race. *Science* **318**, 761-764 (2007).
94 Ross, R. J., Weiner, M. M. & Lin, H. PIWI proteins and PIWI-interacting RNAs in the soma. *Nature* **505**, 353-359, doi:10.1038/nature12987 (2014).
95 Siomi, M. C., Sato, K., Pezic, D. & Aravin, A. A. PIWI-interacting small RNAs: the vanguard of genome defence. *Nat Rev Mol Cell Biol* **12**, 246-258, doi:nrm3089 [pii]
10.1038/nrm3089 (2011).
96 Harris, A. N. & Macdonald, P. M. Aubergine encodes a Drosophila polar granule component required for pole cell formation and related to eIF2C. *Development* **128**, 2823-2832 (2001).
97 George, J. A., DeBaryshe, P. G., Traverse, K. L., Celniker, S. E. & Pardue, M. L. Genomic organization of the Drosophila telomere retrotransposable elements. *Genome research* **16**, 1231-1240, doi:10.1101/gr.5348806 (2006).
98 Ostertag, E. M., Prak, E. T., DeBerardinis, R. J., Moran, J. V. & Kazazian, H. H., Jr. Determination of L1 retrotransposition kinetics in cultured cells. *Nucleic Acids Res* **28**, 1418-1423 (2000).
99 Feng, Q., Moran, J. V., Kazazian, H. H., Jr. & Boeke, J. D. Human L1 retrotransposon encodes a conserved endonuclease required for retrotransposition. *Cell* **87**, 905-916, doi:S0092-8674(00)81997-2 [pii] (1996).
100 Wei, W. *et al.* Human L1 retrotransposition: cis preference versus trans complementation. *Mol Cell Biol* **21**, 1429-1439, doi:10.1128/MCB.21.4.1429-1439.2001 (2001).
101 Cole, L. K. & Ross, L. S. Apoptosis in the developing zebrafish embryo. *Dev Biol* **240**, 123-142, doi:10.1006/dbio.2001.0432
S0012-1606(01)90432-4 [pii] (2001).
102 Iskow, R. C. *et al.* Natural mutagenesis of human genomes by endogenous retrotransposons. *Cell* **141**, 1253-1261, doi:S0092-8674(10)00556-8 [pii]
10.1016/j.cell.2010.05.020 (2010).
103 Smit, A., Hubley, R. & Green, P. RepeatMasker Open-4.0. <***Error! Hyperlink reference not valid.***. (2013-2015).

104 Tubio, J. M. *et al.* Mobile DNA in cancer. Extensive transduction of nonrepetitive DNA mediated by L1 retrotransposition in cancer genomes. *Science* **345**, 1251343, doi:10.1126/science.1251343 (2014).

105 Beauregard, A., Curcio, M. J. & Belfort, M. The take and give between retrotransposable elements and their hosts. *Annual review of genetics* **42**, 587-617, doi:10.1146/annurev.genet.42.110807.091549 (2008).

106 Harris, C. R. *et al.* p53 responsive elements in human retrotransposons. *Oncogene* **28**, 3857-3865, doi:onc2009246 [pii]
10.1038/onc.2009.246 (2009).

107 Haase, A. D. *et al.* Probing the initiation and effector phases of the somatic piRNA pathway in Drosophila. *Genes Dev* **24**, 2499-2504, doi:10.1101/gad.1968110 (2010).

108 Vagin, V. V. *et al.* Minotaur is critical for primary piRNA biogenesis. *RNA* **19**, 1064-1077, doi:rna.039669.113 [pii]
10.1261/rna.039669.113 (2013).

109 Kirino, Y. *et al.* Arginine methylation of Aubergine mediates Tudor binding and germ plasm localization. *RNA* **16**, 70-78, doi:rna.1869710 [pii]
10.1261/rna.1869710 (2010).